

Chapter 1 Introduction

The consumption of energy all over the world has been growing during the past twenty years. According to British Petroleum (BP) Statistical Review of World Energy in 2004, the consumption of the primary energy is with the growth trend near 1 % (excluding China). This growth trend is shown in Figure 1.1.

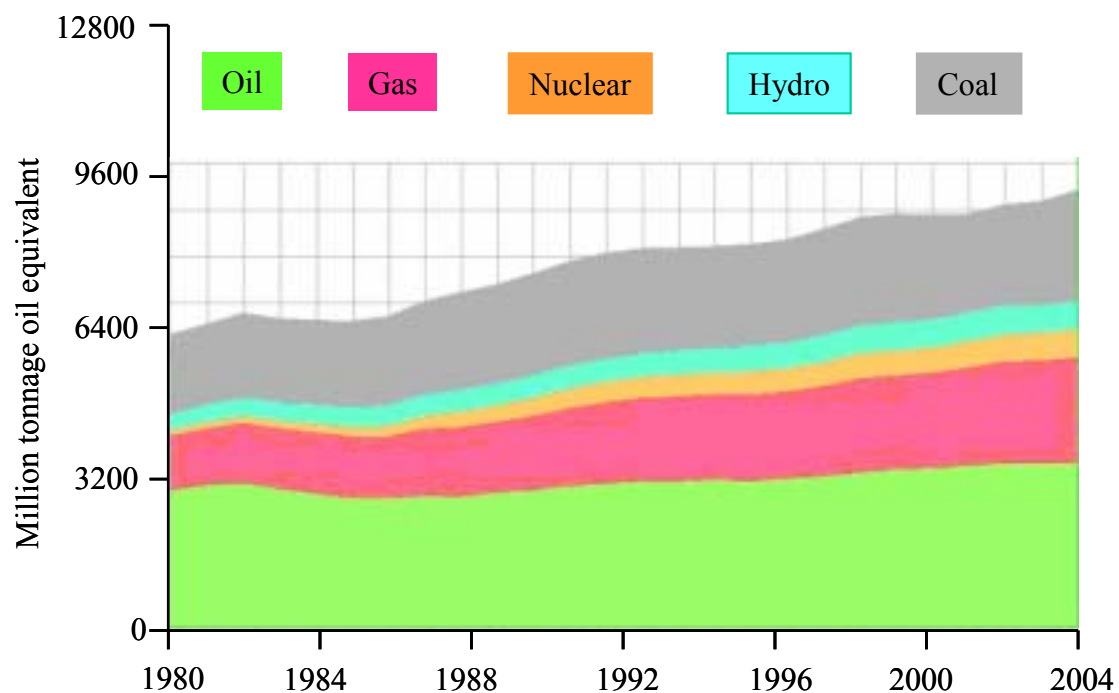


Figure 1.1 The trend of consumption of primary energy in the world

On the other hand the requirement of electric power capacity in 2030 in Europe will be expected to reach 800 GW as shown in Figure 1.2.

It is clear that the growing demand for electricity result in a corresponding increase in power generation and transmission in the developed countries. The electricity generation, transmission and distribution comprise the power system.

In recent years, high capacity synchronous generators (over 1800MVA) have been installed all over the world to supply the electricity. A large impact on the power

system will occur if such a high capacity generator is shut down. Blackouts will occur if the incident is a coincidence of more fragile operating conditions and serious damage (such as generator was shut down unpredictably) or many successive diverse hazardous occurrences far beyond those common events. In practice, those cases rarely occur, but the consequence may be very serious when they do. The long-term loss of energy in a power system results in the disruption of the economic activity in the area.

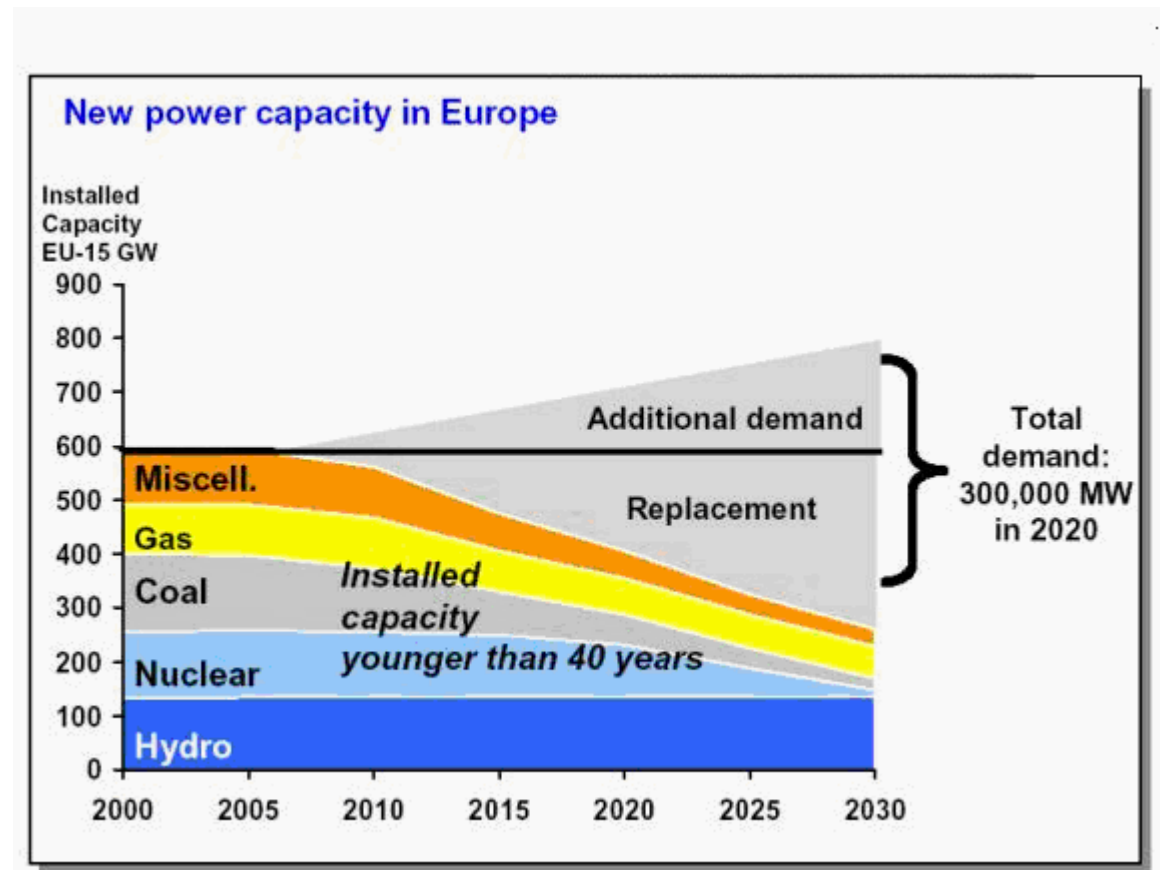


Figure 1.2 Anticipated requirement of new power capacity in Europe

There are already plenty of papers discussing the safety, reliability and stability of the power system from the point of view of whole systems [1, 2] or of each subsystem and its components [3, 4, 5].

O. Faucon and L. Dousset have described a coordinated defense plan to protect against transient instabilities so that blackouts in the large area of France or in the entire network can be prevented, or restoration of the full power can be accelerated [1]

when they occur.

E. Handschin, E. Ordunea and F. Garces have presented an Algorithmic-Knowledge-Based adaptive coordination in transmission protection [3]. In their paper a system for on line adaptive settling and coordination of protection relay in meshes networks was developed. When states of the network are changing, an expert system is used to perform detection and to propose the correction of erroneous settling of protection zones and miscoordination between relays at different stations. This expert system is tested on a network with 34 nodes, 55 branches and 110 relays. The result of test shows that using the on line adaptive can reduce operating time and the number of erroneous coordination settlings.

On the other hand, with the growth of electric power demand and the restriction on building new lines, Flexible AC Power Transmission System (FACTS) were used to provide a full dynamic control over active and reactive power flow on transmission system based on some key variables such as the impedance of transmission line, phase angle and voltage [6, 7-8]. FACTS is based on the use of reliable high-speed power electronics, advanced control technology, advanced microcomputer systems, and powerful analytical tools. The key feature is the availability of power electronic switching devices that can switch the electricity at megawatt levels (kV and kA levels). The use of FACTS results in the full utilization of the whole transmission system and relieving transmission line bottlenecks without building new lines [9].

The synchronous generator is the principal element of a power system. Its operational condition directly affects the reliability and stability of the whole power system.

IEEE committee has published several different exciter system structures, which are utilized for the computer simulation to study the stability of the generator systems [10, 11]. Those structures represent the characteristics of exciter, Automatic Voltage Regulator (AVR) and limiter.

The stability of great capacity synchronous generators can be investigated through the use of different control methods, such as root locus method, optimal control method, Bode plot and modern control theory [12-15]. But there are only few papers to discuss the Critical Fault Clearing Time (CFCT) of a synchronous generator (the definition of CFCT is defined by Stefan Kulig) for a short circuit on the transmission line or on the terminal of the generator itself. There were few papers to discuss the

detail behavior of main exciter winding current, auxiliary exciter winding current and rectifier current as the generator was impacted by the short circuit on transmission line and generator terminal.

In recent years, the artificial intelligence method has been utilized in various fields such as power system stabilizer, industrial control and so on [16-22]. Fuzzy logic method and neural network are two important development methods which are used for artificial intelligence. The major distinction compared to these and the traditional control design method is that it is not necessary to know the exact mathematical model of the controlled system. Engineer criticizes those methods as they were initially applied to industrial application. Nevertheless, it had been proven that artificial intelligence technology could be used successfully in industrial control.

A combination of the artificial intelligence method and traditional control structure for the generator terminal voltage control, which is published by IEEE committee, was discussed to a lesser extent in the published papers. The aim of this work is to investigate a controller structure with artificial intelligence such that the stability and reliability of the generator system can be improved and the CFCT of a generator system can be prolonged. A comparison will be made of the CFCT under the IEEE AC exciter model and its model combined with fuzzy neural network.

The simulation results show that the use of a Fuzzy Neural Network (FNN) in conjunction with an AVR improves the stability of the synchronous generator system suffered from small impact. However, the FNN compensator cannot maintain the terminal voltage constant as the system suffered from three-phase short circuit or two-phase short circuit on the generator terminal and transmission line. The simulation also shows that using FNN compensator prolongs the CFCT of a generator a little.

Chapter 2 Review

2.1 AVR research literature review

The investigation of the control over the terminal voltage of synchronous turbine generator is an important topic in power system research. In seeking a resolution of this problem we must ask, how we shall control the terminal voltage and what factors will affect its stability.

To answer these questions, the theorem of electric generator must be examined. The output power of generator is shown as equation (2.1):

$$P = \left(\frac{E V_t}{X_d} \right) \sin(\gamma) \quad (2.1)$$

Where P is the output power of the generator, E is the induced voltage at stator, V_t is the terminal voltage, γ is the loading angle between V_t and E . X_d is the impedance between E and V_t .

In equation (2.1), the exciter current i_F of a generator can directly control the induced voltage E . The output power P of the generator is decided by requirement of power system. Terminal voltage V_t is affected by the induced voltage E , the loading angle γ and the output power P .

If the output power P is fixed, then V_t is affected by the exciter current as well as the loading angle. This means that there are two controlled variables, terminal voltage V_t and the loading angle γ , but only one control variable, the exciter current i_F . Therefore to control the terminal voltage V_t , the effect of the loading angle must be eliminated.

To control the terminal voltage V_t , two algorithms can be used and described as following:

- Use the exciter current i_F to control the induced voltage E , then the induced voltage E will affect the terminal voltage V_t .

- Eliminate the effect of loading angle variations.

The second question is which factors will affect the stability of the terminal voltage.

Terminal voltage stability is disturbed by many factors, such as the load required from the generator, the structure of the transmission line connected to the generator, as well as the occurrence of a short circuit on transmission line or the transmission line being turned off. As these factors affect the dynamic behavior of the generator, a differential equation set with constant parameters cannot describe the system dynamic behavior perfectly. These factors mentioned above sometimes result in the instability of the system or the damage to the generator.

The purpose of Automatic Voltage Regulator (AVR) is to keep the terminal voltage constant and protect the generator from damage which is caused by short circuit in the system.

In 1968 and 1981, an IEEE Committee published several different excitation system models [10, 11], which can be used in generator system simulations on computers. These are type DC (direct current), type AC (alternate current) and type ST (static transformer) excitation systems. Each type is suited for a different exciter system produced by the manufacturers.

Type DC excitation systems utilize a direct current generator with a commutator as the source of the excitation system power. Type AC excitation systems utilize an alternator and either stationary or rotating rectifier to produce the direct current needed for generator field. In type ST excitation systems, the excitation power is supplied through transformers and rectifiers.

Conventional analog automatic voltage regulators are designed by using classical control theory, which employs linear model of synchronous generator with an infinite bus. The basic control structures for the excitation system block, which are published by IEEE Committee, are rate feedback controller. For AC model the voltage drop due to the rectifier regulation and the demagnetizing effect of load current is also considered.

F. P. Demello and C. Concordia [23] have presented a detailed analysis of the

stability problem for generator system using the linearized synchronous generator model. The type DC excitation system was used. He investigated the load-angle loop first. He found that automatic voltage regulator would attenuate the original damping ratio of the generator system. For the generator system with a sufficient damping, the generator system at steady-state needs a high gain controller, but the controller gain should be attenuated at transient state. This aim can be reached with a lead-lag network series with controller or alternately with a rate feedback from the exciter voltage.

Anderson and A. A. Fouad [12] had developed both a linear and a nonlinear generator model for system simulation purpose in their book. They also developed a simplified linear generator model for the analysis of a linear generator control system (it is the same model as that used by F. P. Demello and C. Concordia [23]). An AVR design procedure using root locus method was also presented, where the exciter and generator were considered as first-order system. The disadvantage of this analysis is that the generator model is too simple. It cannot display the influence of the terminal voltage due to the variation on the rotor angle.

M. S. Ghazizadeh and F. M. Hughes suggested a new form of auxiliary control loop for an AVR [24]. The purpose of this auxiliary control signal, which is fed to input of the main exciter, is to compensate dynamically the variation of load current of the generator, which is affected by the variation of loading. In this way, the dynamic response characteristics of the generator system can be improved. In the auxiliary control loop the currents of direct and quadrature axis of the generator, which is accounted for the influence of the loading, are adopted to feed the auxiliary control loop. The output signal of this auxiliary control loop is limited so that the unnecessary saturation of the excitation system can be avoided under large disturbance condition. A watch-out circuit is also incorporated so that the auxiliary control signal does not affect the excitation system at steady state.

The analysis method of this approach is based on the small-signal analysis of the generator system. The assumption of this approach is that the characteristics of both generator and exciter are always constant and linear during operation. However, a synchronous generator is a nonlinear system, and consequently, the control system design is based on the linearized model which is only valid under the chosen operating condition. The resulting fixed-gain AVR is therefore unable to response satisfactorily over the whole range of system.

P, PI, and PID controllers are the most widely used regulators in industrial process [25, 26]. The physical meaning of P, I and D can be easily understood by the engineer. The function of P is as an amplifier of the error, function I is as an accumulation of the error and function D is the differential of the error. Suitable tuning of PID parameters can execute good control in industrial system. Owing to the rapid development of computer science, computers are now widely used in industrial control applications. A digital PID controller has also been applied in different control fields.

Numerous papers about the tuning of the parameters of PID controllers had been published [27-29]. O. P. Malik, G. S. Hope and Badr have used a digital PID voltage regulator to control the terminal voltage [13]. In their papers, an alternative control structure is used. The inputs of the PID controller are the compromise between the error of terminal voltage and the differential of the rotor angle. These two signals are weighted by separated weighting factors and then they are added together as the input signal of the PID controller.

The benefit of this PID structure with the dynamic variation of weighting factors is that the differential of the rotor angle is taken into consideration. Therefore the effect of rotor angle variation can be compensated. The results of the simulation show that with this PID structure the damping of the rotor angle is enhanced and the settling time is shorter than that of the traditional PID controller; but the relative overshoot of the terminal voltage with this PID structure is greater.

V. H. Quitana [14] designed an AVR using optimal control theory. In this paper several different feedback controller structures are simulated. Those feedback signals fed to controller are the combination of several different output signals, such as the deviation of terminal voltage, the deviation of torque angle, the rate of deviation of load angle, the deviation of real power and the deviation of exciter voltage. The effectiveness of the various design controller structures had been studied by subjecting the system to two distinct types of disturbance: (a) -5 % reference voltage pulse of 0.1 sec. duration; and (b) three-phase-to-ground disturbance applied on one of two transmission lines.

Simulation results show that the combination of deviation of terminal voltage and the rate of deviation of load angle, which is connected to wash-out circuit, derive the best response.

The above mentioned methods have the hypothesis that the parameters of AVR are

fixed during the application of the generator system. The dynamic performance characteristics of a generator is changed by both the generator loading condition and the configuration of the power network. In many cases it is impossible to design a fixed parameter of AVR, which can be effective under all conditions. Several forms of adaptive control have been investigated to address the problem of performance variation [15, 30]; adaptive controller can improve the dynamic performance of a generator over wide range of operating conditions. The adaptive controller measures the input and output signals of the system in real time and identifies the system mode, then adapts the gain settling based on the identified model and adaptive rules. Although the adaptive controller can enhance generator damping, a major disadvantage of the adaptive controller is that it is computationally inefficient due to the requirement of identifying the system model in real time [31].

In 1989 A. S. Abraham presented the self-tuning AVR for a synchronous generator [32]. His design was based on Auto-Regressive Moving Average Models (ARMA). It is obtained by linearization of the system equation about the current operating point. He adapted two methods to tune the parameters of the controller, one is minimum-variance exciter controller, and the other is the pole-assignment exciter controller. The drawback of the latter is that computational load may become excessive. There is no systematic way of choosing the locations of the closed-loop eigenvalues which give the best response for the selected poles and zeros. The former uses a recursive least-square algorithm to estimate the parameters of the system. A possible problem is that the estimator may be divergent in some situations, such as short circuit at transmission line. Both of the two methods gave good responses for terminal voltage under the step change of reference voltage.

C. L. Brasca and M. A. Johnson have reported an investigation of a new generation of practical adaptive automatic voltage regulators for synchronous generator [33]. Due to the uncertainty of the parameters of synchronous generator affected by the network, which it feeds, the parameters of synchronous generator have the property of probability with the time. Therefore the treatment of AVR design is regarded as a stochastic process. In this paper, the positions of roots for the generator system are first shown by the root locus plot. It pointed out that at some situations the synchronous generator system is unstable.

A Multi-Input Multi-Output (MIMO) structure for a Linear Quadratic Gaussian (LQG) polynomial system is applied to design an AVR. In this method the input and output signals are combined with input disturbance signals and output disturbance

signals separately. A performance index with linear quadratic form is defined so that optimal control gain can be tuned by minimizing this index. In order to solve the minimization problem a Riccati equation must be used. The optimal control law indicates that for an optimum system to exist when the quadratic performance index is used, all state variables must be fed back. In practice, not all states of the system may be available for measurement. In order to synthesize the optimal control law, it is necessary to reconstruct the unavailable states. Therefore a state estimator must be established by using on-line recursive identification.

The simulation results show that LQG method can be used to design AVR system. In future using this LQG structure, an AVR of MIMO can be investigated. The disadvantage of this method is that LQG method is lack of robustness. Another disadvantage is that the solution of the Riccati equation and recursive identification must be done. This produces a heavy calculation burden upon the computer for on-line control. Nevertheless, the idea of using a stochastic system to design a self-optimal tuning AVR system is a new approach.

In recent years, several papers have proposed that artificial intelligence such as fuzzy logic technology and artificial neural networks have been applied on various areas [16-18, 34].

E. Handschin developed an excitation control system including the Power System Stabilizer (PSS) by using fuzzy logic theory [35]. In this paper three input variables, terminal voltage deviation, power deviation and power derivative, are fed to fuzzy controller as input signals. The first signal is devoted on controlling terminal voltage; the other two are served for damping voltage. Each of the input signals is mapped to three membership functions. The output signal of fuzzy controller, which is defuzzified by using Center Of Area (COA), is delivered to the excitation system.

Two testings with the following conditions are performed.

- A three-phase fault on the transmission line with duration of 0.1 s.
- The system load is increased by 50%.

In the first case, the simulation result indicates that the terminal voltage controlled by fuzzy controller and AVR shows a significant difference in the damping effect. The fuzzy controller devotes on more damping effect than AVR. In the second case, the simulation result shows that the terminal voltage controlled by the fuzzy controller will be stable after a short settling time, but on the other hand the terminal voltage has

a steady error by using AVR + PSS and has a longer settling time by using AVR. That is one of the reasons why even in well-designed power systems the power system stabilizer is inactive in industrial engineering. This paper demonstrates that fuzzy controller is superior to conventional controller for the purpose of terminal voltage control. One of weaknesses of this fuzzy controller is that all parameters require specific tuning; there is no systematic method to tune these parameters.

Recently the emergence of the neural network had made it feasible to integrate fuzzy logic controllers and neural network model for the development of control systems [36-37]. Fuzzy neural network systems, which combine the capability of fuzzy reasoning to handle uncertain information and the capability of artificial neural networks to learn from the process, deal with the nonlinear part and uncertainties of a control system.

R. B. Chedid, S. H. Karaki and El Chamali have investigated an Adaptive-Neural-Based Fuzzy Inference System (ANFIS) for a wind-diesel system, which contains a stall-regulated wind turbine with an induction generator connected to an AC bus-bar in parallel with a diesel generator [61]. In this paper, five-layers ANFIS is used to generate fuzzy membership functions and control rules for the controller. A Feedback Linearized Proportional Integral controller (FLPI) is used to provide the required expert knowledge. The input signals of the govern controller are frequency error and its integral. The terminal voltage and the deviation of frequency are the input signals of the automatic voltage regulator.

The design objective of this ANFIS is to learn and achieve the performance as good as the FLPI in the presence of disturbances and uncertainties. The design of membership functions is done based on the ANFIS batch learning technique. The ANFIS described in this paper has five layers, as follows:

1. Layer one is a membership function, which is normalized by a bell-shape function.
2. Layer two is the multiplication of incoming signals from layer one. The output signal in layer two is represented as the firing strength (or weight) of a rule.
3. Layer three is used to calculate the ratio of the *i*th rule's firing strength to the sum of all rules' firing strengths.
4. Layer four is the consequence part of this system.
5. Layer five is the sum of the incoming signals from layer four.

Parameters in ANFIS are updated using the gradient descent method and the least square estimation method. The simulation result shows that the ANFIS can be trained to have the same performance as FLPI controller in the wind-diesel weak power system.

Lin proved that Fuzzy Neural Network (FNN) is effective for on-line motor position control [36], A. Haririr and O.P. Malik applied FNN to power system stabilizers and it proved to work very well [37].

In this research, a fuzzy neural network will be applied to integrate with an automatic voltage regulator. The objective of this FNN is to compensate for wide changes in operating range and to prolong the CFCT of synchronous generator system, which suffered from large impacts.

2.2 The objective of the research

The objective of this research is to develop a new complementary compensator, which can work with the conventional controller. Under normal steady-state conditions, the conventional controller works very efficiently. The additional compensator is implemented by means of a fuzzy algorithm with self-tuning ability.

The purpose of this additional control signal is to compensate the nonlinear part of the generator system, the variation in the operating point of the system as well as the variation of rotor angle.

The development procedure of this controller will be divided into five parts as follows:

1. A linear generator system model will be studied.
2. The linear control theorem is used to design the conventional controller based on the linear synchronous generator system.
3. The complementary control signal is developed in accordance with the fuzzy neural network algorithm.
4. The conventional controller combined with the complementary control signal is simulated in Matlab software (software from the Mathworks).
5. The complete controller will be tested in NETOMAC software based on the

following different situations.

- Two-phase fault on the generator terminal.
- Three-phase fault on the generator terminal.
- Single-phase fault midway out on the transmission line.
- Two-phase fault midway out on the transmission line
- Three-phase fault midway out on the transmission line.

The simulation results for a controller designed by conventional control theory with an FNN compensator and without an FNN compensator will be compared. The simulation condition is divided into two parts. The first part is to test the effect of terminal voltage suffered due to variations of mechanical torque for controllers with an FNN compensator and without the compensator. The second part is to test the critical fault clearing time of a generator suffering a short circuit on network and on the generator terminal.

Finally an evaluation of the structure of conventional AVR integrated with an FNN will be made.

Chapter 3 Mathematical models of the system components

3.1 System description

Figure 3.1 is a turbine AC generator system that is combined with a turbine, exciter and generator. The generator is supplied with real power from a prime mover, usually a turbine, while the excitation current is provided by the excitation system.

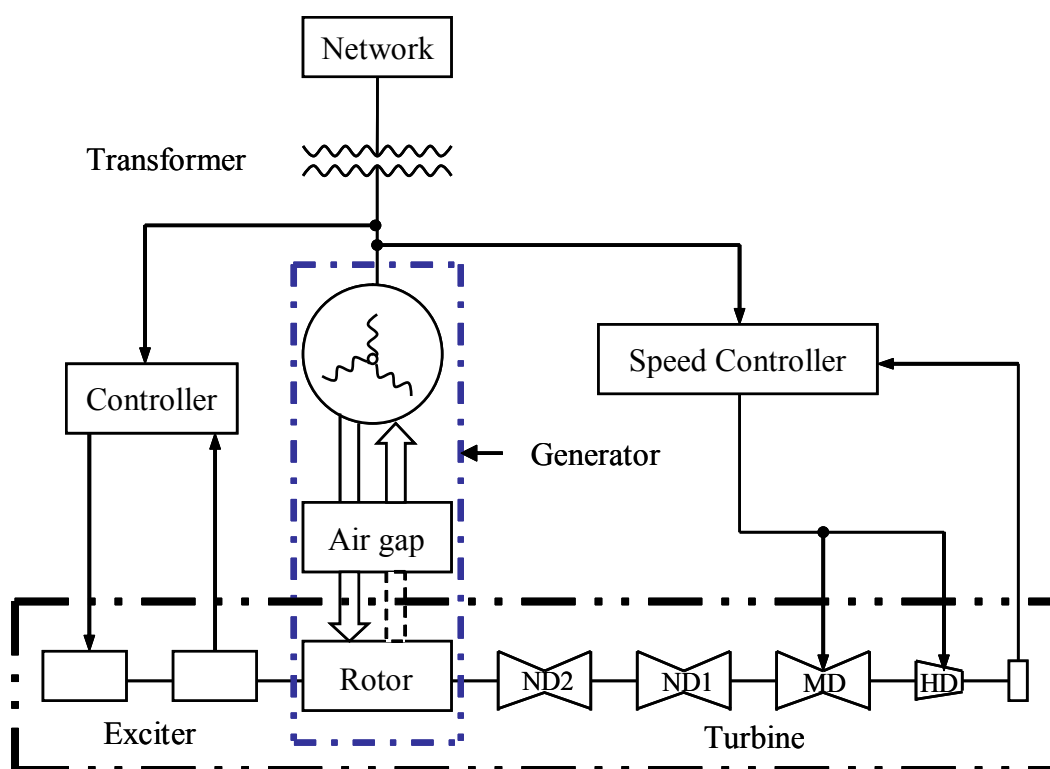


Figure 3.1 A complete generator system with turbine

The turbine system is composed of steam generator (boiler), high-, middle- and low-pressure turbines. The steam generator is used to transform the primary energy (such as oil and coal) into thermal energy. Under normal operating circumstances the fossil fuel is converted to the high temperature steam. The high-pressure steam is then conducted to the first part of the turbine, the high-pressure turbine (HD). The lower pressure steam exhausted from high-pressure turbine is led to the second part of

system, middle-pressure turbine (MD) again. The steam exhausted from this component of the system is then used to drive low-pressure turbine. Finally the exhausted steam is retrieved and returned to the boiler. A speed controller is employed to control turbine speed. The setting point of the speed controller is compared with the measured speed of turbine, and then the error signal is fed to speed controller to regulate the turbine speed. The output signal of speed controller is used to control the steam valve.

The generator system is composed of an AC synchronous generator, a main AC exciter and a Permanent Magnetic Generator (PMG). The power of the AC synchronous generator is 412 MVA, rotation frequency is 50 Hz and terminal voltage is 21 kV. The main AC exciter is a brushless exciter. It is a small AC generator with its field circuit mounted on the stator and the armature circuit mounted on the rotor shaft. The specifications of this brushless exciter are a power of 2.67 MVA, terminal voltage of 387 V and rotation frequency of 150 Hz. The PMG is a small AC generator with permanent magnets mounted on the rotor shaft and a three-phase winding on the stator. It produces the power for the field circuits of the main exciter. The PMG is mounted on the generator shaft. It does not require external electric power to run the generator. The specifications of this PMG are a power of 61 kVA, terminal voltage of 220 V and frequency of 400 Hz. An automatic voltage regulator sustains the terminal voltage constant. The output signal of AVR is fed to the main exciter to adjust the field current.

It is impossible to measure any field quantities of the generator directly since these components are always moving with the rotor. The three-phase output current of the main exciter is fed to rectifier diodes, which rectify the alternative current to direct current. It is fed to the rotor of AC synchronous generator directly. In order to control terminal voltage, a six-phase controlled rectifier power amplifier is added between the output of PMG and input of the main exciter. The complete detailed structure of the generator system is shown in Figure 3.2.

In Figure 3.2 the terminal voltage of the generator is measured and is fed directly into the controller as the input signal. The output signal of the controller, which is adjusted by the error signal between reference voltage (set point) and terminal voltage, will trigger the firing angle of the Silicon Controlled Rectifier (SCR) so that the suitable field current can be produced in the main exciter. A non-controlled six-phase

rectifier is connected on the output voltage of main exciter; this rectified voltage is then fed directly into the rotor winding of the AC synchronous generator.

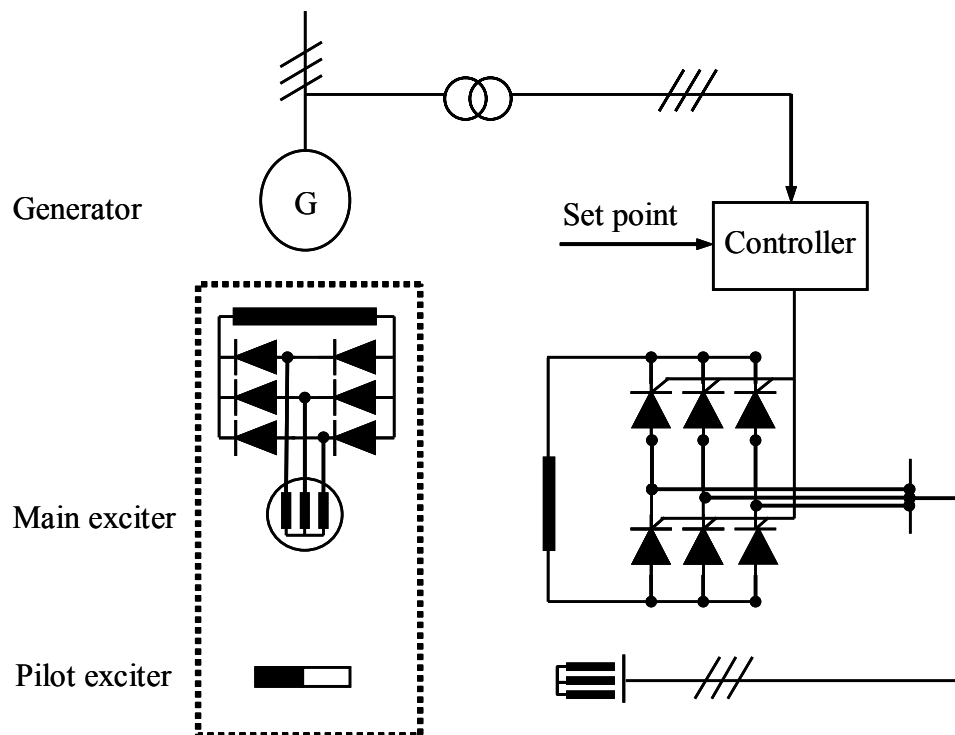


Figure 3.2 Brushless excitation system with the rotor rectifier

3.2 Synchronous machines

Physically, a three-phase synchronous generator consists of three windings on the stator, and one field winding on the rotor. There are several damper bars embedded in the rotor and connected together at the ends by either continuous rings or segments. Figure 3.3 schematically describes the three-phase generator from the circuit theory point of view. The windings on the stator are spatially distributed in the stator slots and each other by 120 degrees. In a cylindrical rotor generator, the rotor body is made of forged steel with uniformly spaced slots on the periphery in which the distributed field winding is placed. The field winding is excited by direct current, which establishes the main field winding flux along the direct axis.

In order to investigate the transient response of a generator, a set of equations,

which can describe the transient phenomenon of a generator, must be found. On fixed axis coordinates the solution of generator equations for obtaining the machine voltages, currents and flux linkages when expressed in v_a, v_b, v_c , etc. quantities are highly formidable due to the existence of the complicated time-varying coefficients in the governing equations. This is mainly due to the dependence of the machine inductances on the position of the rotor. All of the self and mutual inductances of the three stator windings and field winding are expressed as periodic functions of the rotor angle θ except self-inductance of the field winding.

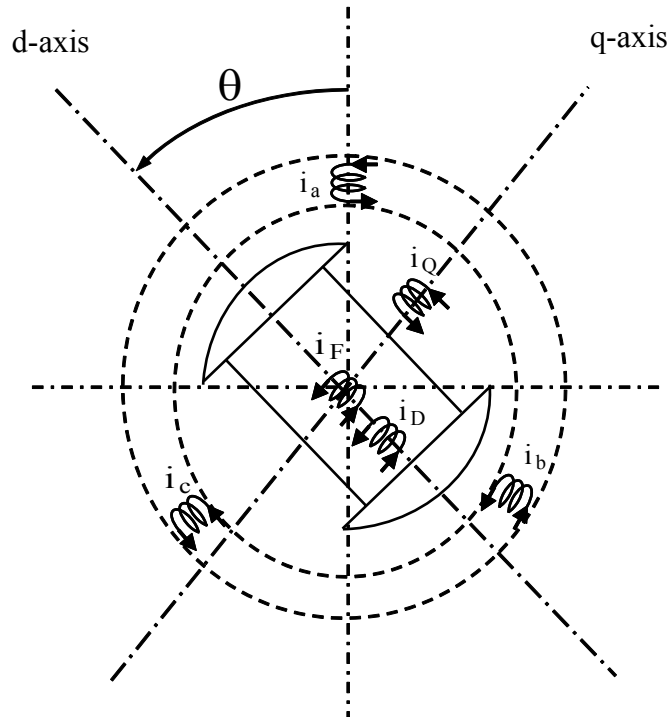


Figure 3.3 The winding of the generator

In steady-state operation the current shown in fig. 3.3 can be described as follows:

$$\begin{aligned} i_a &= i_{\max} \cos(\omega t + \theta) \\ i_b &= i_{\max} \cos\left(\omega t + \theta + \frac{2\pi}{3}\right) \\ i_c &= i_{\max} \cos\left(\omega t + \theta + \frac{2\pi}{3}\right) \end{aligned} \quad (3.1)$$

where θ is the angle between current i_a and reference axis in radians.

As shown in Figure 3.3, the axis of the phase a is chosen as a reference axis. The network is consisted of six coils which are coupled together. There are three phase winding, a, b, c; the fielding winding F; two damper winding, D and Q. The flux linkage equations of six circuits can be written as:

$$\begin{bmatrix} \Psi_a \\ \Psi_b \\ \Psi_c \\ \Psi_F \\ \Psi_D \\ \Psi_Q \end{bmatrix} = \begin{bmatrix} L_{aa} & L_{ab} & L_{ac} & L_{aF} & L_{aD} & L_{aQ} \\ L_{ba} & L_{bb} & L_{bc} & L_{bF} & L_{bD} & L_{bQ} \\ L_{ca} & L_{cb} & L_{cc} & L_{cF} & L_{cD} & L_{cQ} \\ L_{Fa} & L_{Fb} & L_{Fc} & L_{FF} & L_{FD} & L_{FQ} \\ L_{Da} & L_{Db} & L_{Dc} & L_{DF} & L_{DD} & L_{DQ} \\ L_{Qa} & L_{Qb} & L_{Qc} & L_{QF} & L_{QD} & L_{QQ} \end{bmatrix} \begin{bmatrix} i_a \\ i_b \\ i_c \\ i_F \\ i_D \\ i_Q \end{bmatrix} \quad (3.2)$$

where L_{jk} = self-inductance when $j = k$
= mutual-inductance when $j \neq k$

Equation (3.2) can also be abbreviated and represented in matrix form as follows:

$$\begin{bmatrix} \Psi_{abc} \\ \Psi_{FDQ} \end{bmatrix} = \begin{bmatrix} \mathbf{L}_{aa} & \mathbf{L}_{aR} \\ \mathbf{L}_{Ra} & \mathbf{L}_{RR} \end{bmatrix} \begin{bmatrix} \mathbf{I}_{abc} \\ \mathbf{I}_{FDQ} \end{bmatrix} \quad (3.3)$$

where

$$\mathbf{L}_{aa} = \begin{bmatrix} L_{aa} & L_{ab} & L_{ac} \\ L_{ba} & L_{bb} & L_{bc} \\ L_{ca} & L_{cb} & L_{cc} \end{bmatrix} ; \mathbf{L}_{aR} = \begin{bmatrix} L_{aF} & L_{aD} & L_{aQ} \\ L_{bF} & L_{bD} & L_{bQ} \\ L_{cF} & L_{cD} & L_{cQ} \end{bmatrix} ; \mathbf{L}_{RR} = \begin{bmatrix} L_{FF} & L_{FD} & L_{FQ} \\ L_{DF} & L_{DD} & L_{DQ} \\ L_{QF} & L_{QD} & L_{QQ} \end{bmatrix}$$

\mathbf{L}_{aa} = stator-stator inductance

\mathbf{L}_{aR} , \mathbf{L}_{Ra} = stator-rotor inductance

\mathbf{L}_{RR} = rotor-rotor inductance

All of the inductances L_{jk} are functions of the time due to the rotor movement.

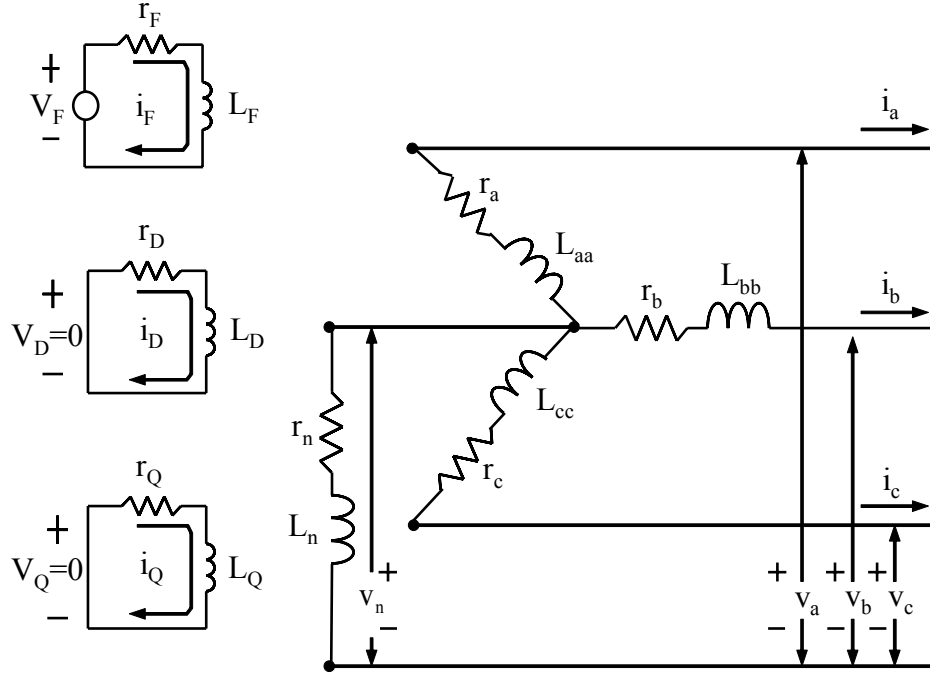


Figure 3.4 Schematic diagram of synchronous generator

Figure 3.4 is a schematic diagram of a synchronous machine in which the mutual inductances are not presented. There are a resistance r_n and an inductance L_n between neutral point and ground. In accordance with Figure 3.4 three-phase terminal voltage equations can be expressed as follows:

$$\begin{bmatrix} v_a \\ v_b \\ v_c \\ -v_F \\ v_D \\ v_Q \end{bmatrix} = - \begin{bmatrix} r_a & 0 & 0 & 0 & 0 & 0 \\ 0 & r_b & 0 & 0 & 0 & 0 \\ 0 & 0 & r_c & 0 & 0 & 0 \\ 0 & 0 & 0 & r_F & 0 & 0 \\ 0 & 0 & 0 & 0 & r_D & 0 \\ 0 & 0 & 0 & 0 & 0 & r_Q \end{bmatrix} \begin{bmatrix} i_a \\ i_b \\ i_c \\ i_F \\ i_D \\ i_Q \end{bmatrix} - \begin{bmatrix} \dot{\Psi}_a \\ \dot{\Psi}_b \\ \dot{\Psi}_c \\ \dot{\Psi}_F \\ \dot{\Psi}_D \\ \dot{\Psi}_Q \end{bmatrix} + \begin{bmatrix} \mathbf{V}_n \\ 0 \end{bmatrix} \quad (3.4)$$

where we define the neutral voltage contribution as:

$$\mathbf{V}_n = -r_n \begin{bmatrix} 1 & 1 & 1 \\ 1 & 1 & 1 \\ 1 & 1 & 1 \end{bmatrix} \begin{bmatrix} \dot{\mathbf{i}}_a \\ \dot{\mathbf{i}}_b \\ \dot{\mathbf{i}}_c \end{bmatrix} - L_n \begin{bmatrix} 1 & 1 & 1 \\ 1 & 1 & 1 \\ 1 & 1 & 1 \end{bmatrix} \begin{bmatrix} \dot{\mathbf{i}}_a \\ \dot{\mathbf{i}}_b \\ \dot{\mathbf{i}}_c \end{bmatrix}$$

$$= -\mathbf{R}_n \mathbf{I}_{abc} - \mathbf{L}_n \dot{\mathbf{I}}_{abc}$$

and

$$\mathbf{R}_n = r_n \begin{bmatrix} 1 & 1 & 1 \\ 1 & 1 & 1 \\ 1 & 1 & 1 \end{bmatrix} ; \quad \mathbf{L}_n = L_n \begin{bmatrix} 1 & 1 & 1 \\ 1 & 1 & 1 \\ 1 & 1 & 1 \end{bmatrix}$$

For the identical winding on the stator, the resistance on the coils is also the same.

therefore

$$r = r_a = r_b = r_c$$

A resistance matrix can be defined as:

$$\mathbf{R}_{abc} = r \begin{bmatrix} 1 & 0 & 0 \\ 0 & 1 & 0 \\ 0 & 0 & 1 \end{bmatrix} = r \mathbf{O}_3 ; \quad \mathbf{R}_{FDQ} = \begin{bmatrix} r_F & 0 & 0 \\ 0 & r_D & 0 \\ 0 & 0 & r_Q \end{bmatrix}$$

$$\mathbf{O}_3 = \begin{bmatrix} 1 & 0 & 0 \\ 0 & 1 & 0 \\ 0 & 0 & 1 \end{bmatrix} \text{ is a 3 multiplied by 3 unit matrix.}$$

Equation (3.4) can be written in form of matrix abbreviated:

$$\begin{bmatrix} \mathbf{V}_{abc} \\ \mathbf{V}_{FDQ} \end{bmatrix} = - \begin{bmatrix} \mathbf{R}_{abc} & 0 \\ 0 & \mathbf{R}_{FDQ} \end{bmatrix} \begin{bmatrix} \mathbf{I}_{abc} \\ \mathbf{I}_{FDQ} \end{bmatrix} - \begin{bmatrix} \dot{\Psi}_{abc} \\ \dot{\Psi}_{FDQ} \end{bmatrix} + \begin{bmatrix} \mathbf{V}_n \\ 0 \end{bmatrix} \quad (3.5)$$

Equation (3.3) and (3.5) are the primary equations of the generator.

There are several different mathematic models for synchronous machines. Most of these are based upon Park's model. The original Park's Model was published in 1929 and has been expanded over time [39].

T. S. Kulig proposed the ladder network model of synchronous machine, which can be simulated precisely [38].

In order to design a conventional automatic voltage regulator, a simplified linear mathematic model of synchronous generator is investigated. The equation (3.5) describes the behavior of a generator system in time domain. Most of the variables in this equation vary with time. The use of this equation to analyze a generator system presents difficulties. For simplifying the process of analysis, a Park transformation matrix is used to transform the equation based on the fixed-axis in the time domain into a two-axis system. In the following section the Park's model is derived first; then according to Park's model, the simplified linear mathematical model is also evolved.

3.2.1 Park's model of a synchronous machine

The synchronous machine under consideration is assumed to have three stator windings, one field winding and two damper windings. These six windings are magnetically coupled. The magnetic coupling between them is a function of the rotor position. The flux linkage in each winding is also a function of the rotor position. The synchronous generator model is shown in Figure 3.3.

A considerable simplification of the mathematical description of the synchronous machine is obtained if certain information of variable is performed. A transformation, which transforms these variables to new quantities, is usually called Park's transformation [39-40]. The new quantities are obtained from the projections of the actual variables along three axes; the first is along the direct axis of the rotor field winding, called the direct axis; the second along neutral axis of the field winding, called the quadrature axis; and the third on a stationary axis. The new coordinate odq are built on the frame of reference, which moves with the rotor. The detailed development of the equation can be found in the literature [39-40].

The current and voltage on stator winding on fixed axis coordinates will be converted to new quantities on the rotating frame by transformation matrix T . The

transformation of Park's model will be stated:

$$\begin{bmatrix} v_0 \\ v_d \\ v_q \end{bmatrix} = [\mathbf{T}] \begin{bmatrix} v_a \\ v_b \\ v_c \end{bmatrix} \quad (3.6)$$

$$\begin{bmatrix} i_0 \\ i_d \\ i_q \end{bmatrix} = [\mathbf{T}] \begin{bmatrix} i_a \\ i_b \\ i_c \end{bmatrix} \quad (3.7)$$

Under the power-invariance condition the transformation and inverse transformation of modified Park's matrix is shown as follows:

$$[\mathbf{T}] = \sqrt{\frac{2}{3}} \begin{bmatrix} \frac{1}{\sqrt{2}} & \frac{1}{\sqrt{2}} & \frac{1}{\sqrt{2}} \\ \cos \theta & \cos\left(\theta - \frac{2\pi}{3}\right) & \cos\left(\theta + \frac{2\pi}{3}\right) \\ \sin \theta & \sin\left(\theta - \frac{2\pi}{3}\right) & \sin\left(\theta + \frac{2\pi}{3}\right) \end{bmatrix}$$

$$[\mathbf{T}]^{-1} = \sqrt{\frac{2}{3}} \begin{bmatrix} \frac{1}{\sqrt{2}} & \cos \theta & \sin \theta \\ \frac{1}{\sqrt{2}} & \cos\left(\theta - \frac{2\pi}{3}\right) & \sin\left(\theta - \frac{2\pi}{3}\right) \\ \frac{1}{\sqrt{2}} & \cos\left(\theta + \frac{2\pi}{3}\right) & \sin\left(\theta + \frac{2\pi}{3}\right) \end{bmatrix} \quad (3.8)$$

and we note that $[\mathbf{T}]^{-1} = [\mathbf{T}]^T$, which means the transformation \mathbf{T} is orthogonal.

After using the modified Park's transformation the power in the stationary coordinates $v_a i_a + v_b i_b + v_c i_c$ is the same as the power in the rotating frame $v_d i_d + v_q i_q + v_0 i_0$.

In the previous section, the generator equation was developed in the fixed coordinates soon. Based on equations (3.3) and (3.5), the Park's transformation about flux linkage and voltage can be executed.

First, the flux linkage will be transformed from the fixed coordinates to the rotating coordinates.

$$\begin{aligned}
\begin{bmatrix} \Psi_{odq} \\ \Psi_{FDQ} \end{bmatrix} &= \begin{bmatrix} \mathbf{T} & 0 \\ 0 & \mathbf{O}_3 \end{bmatrix} \begin{bmatrix} \Psi_{abc} \\ \Psi_{FDQ} \end{bmatrix} \\
&= \begin{bmatrix} \mathbf{T} & 0 \\ 0 & \mathbf{O}_3 \end{bmatrix} \begin{bmatrix} \mathbf{L}_{aa} & \mathbf{L}_{aR} \\ \mathbf{L}_{Ra} & \mathbf{L}_{RR} \end{bmatrix} \begin{bmatrix} \mathbf{T}^{-1} & 0 \\ 0 & \mathbf{O}_3 \end{bmatrix} \begin{bmatrix} \mathbf{T} & 0 \\ 0 & \mathbf{O}_3 \end{bmatrix} \begin{bmatrix} \mathbf{I}_{abc} \\ \mathbf{I}_{FDQ} \end{bmatrix} \\
&= \begin{bmatrix} \mathbf{T} & 0 \\ 0 & \mathbf{O}_3 \end{bmatrix} \begin{bmatrix} \mathbf{L}_{aa} & \mathbf{L}_{aR} \\ \mathbf{L}_{Ra} & \mathbf{L}_{RR} \end{bmatrix} \begin{bmatrix} \mathbf{T}^{-1} & 0 \\ 0 & \mathbf{O}_3 \end{bmatrix} \begin{bmatrix} \mathbf{I}_{odq} \\ \mathbf{I}_{FDQ} \end{bmatrix} \tag{3.9}
\end{aligned}$$

Then the Park's transformation of the voltage can be stated as:

$$\begin{aligned}
\begin{bmatrix} \mathbf{V}_{odq} \\ \mathbf{V}_{FDQ} \end{bmatrix} &= \begin{bmatrix} \mathbf{T} & 0 \\ 0 & \mathbf{O}_3 \end{bmatrix} \begin{bmatrix} \mathbf{V}_{abc} \\ \mathbf{V}_{FDQ} \end{bmatrix} \\
&= - \begin{bmatrix} \mathbf{R}_{abc} & 0 \\ 0 & \mathbf{R}_{FDQ} \end{bmatrix} \begin{bmatrix} \mathbf{I}_{odq} \\ \mathbf{I}_{FDQ} \end{bmatrix} - \begin{bmatrix} \dot{\Psi}_{odq} \\ \dot{\Psi}_{FDQ} \end{bmatrix} + \begin{bmatrix} \mathbf{T}\mathbf{T}^{-1}\Psi_{odq} \\ 0 \end{bmatrix} + \begin{bmatrix} \mathbf{n}_{odq} \\ 0 \end{bmatrix} \tag{3.10}
\end{aligned}$$

where

$$\begin{aligned}
\mathbf{T}\dot{\Psi}_{abc} &= \dot{\Psi}_{odq} - \dot{\mathbf{T}}\Psi_{abc} \\
\dot{\mathbf{T}}\mathbf{T}^{-1}\Psi_{odq} &= \begin{bmatrix} 0 \\ -\omega\Psi_q \\ \omega\Psi_d \end{bmatrix} \\
\mathbf{n}_{odq} = \mathbf{T}\mathbf{V}_n &= - \begin{bmatrix} 3r_n i_o \\ 0 \\ 0 \end{bmatrix} - \begin{bmatrix} 3L_n \dot{i}_o \\ 0 \\ 0 \end{bmatrix}
\end{aligned}$$

For balancing conditions, the zero-sequence voltage is zero because the current i_o is zero.

Equations (3.9) and (3.10) can be presented by per unit system (p.u.). The voltage equations of generator on the odq axis are:

$$V_0 = -R_a i_0 - \frac{d\Psi_0}{dt} \quad (3.11)$$

$$V_d = -R_a i_d - \frac{d\Psi_d}{dt} - \omega \Psi_q \quad (3.12)$$

$$V_q = -R_a i_q - \frac{d\Psi_q}{dt} + \omega \Psi_d \quad (3.13)$$

$$V_f = R_f i_f + \frac{d\Psi_f}{dt} \quad (3.14)$$

$$0 = R_{Dd} i_{Dd} + \frac{d\Psi_{Dd}}{dt} \quad (3.15)$$

$$0 = R_{Dq} i_{Dq} + \frac{d\Psi_{Dq}}{dt} \quad (3.16)$$

where flux linkages are defined as:

$$\Psi_0 = L_{a\sigma} i_0 \quad (3.17)$$

$$\Psi_d = L_d i_d + L_{hd} i_f + L_{hd} i_{Dd} \quad (3.18)$$

$$\Psi_q = L_q i_q + L_{hq} i_{Dq} \quad (3.19)$$

$$\Psi_f = L_f i_f + L_{hd} i_d + L_{hd} i_{Dd} \quad (3.20)$$

$$\Psi_{Dd} = L_{Dd} i_{Dd} + L_{hd} i_d + L_{hd} i_f \quad (3.21)$$

$$\Psi_{Dq} = L_{Dq} i_{Dq} + L_{hq} i_q \quad (3.22)$$

The swing equation (3.23) governs the motion of the machine rotor. It depends on the moment of inertial J , mechanical damping D and the resultant of the mechanical and electrical torques on the rotor.

$$J \frac{d^2\theta}{dt^2} + D \frac{d\theta}{dt} = T_m - T_e \quad (3.23)$$

$$T_e = (\Psi_d i_q - \Psi_q i_d) \quad (3.24)$$

Equations (3.11) to (3.24) describe the behavior of a synchronous machine in stationary and dynamic situation. The equivalent circuit of synchronous generator is shown in Figure 3.5.

Figure 3.5 is an equivalent circuit of synchronous generator according to Park's

model. This model is a seven order differential equations, including the damping circuit. There are two equivalent circuits, corresponding to the two axes d and q.

On the d-axis there are three coupled coils, namely, armature d-coil, field winding F, and damper winding D. All the quantities are referred to the armature side. In Figure 3.5, all the reactances are expressed per unit. $L_{a\sigma}$ is the armature leakage reactance. L_{fd} and L_{Dd} can be viewed as the leakage reactance of the field and the damper winding, respectively. L_{hd} is the main mutual reactance between the windings on stator and on rotor on the d-axis.

On the q-axis L_{hq} is the main mutual reactance and L_{Dq} is the linkage reactance of the damper.

An expanded equivalent circuit of synchronous generator was developed by Canay. It is shown in Figure 3.6. In Canay's model, the mutual inductance between field winding and damper coiling is considered. Therefore the main reactance of the field winding and the damp winding is $L_{hd} + L_{fc}$

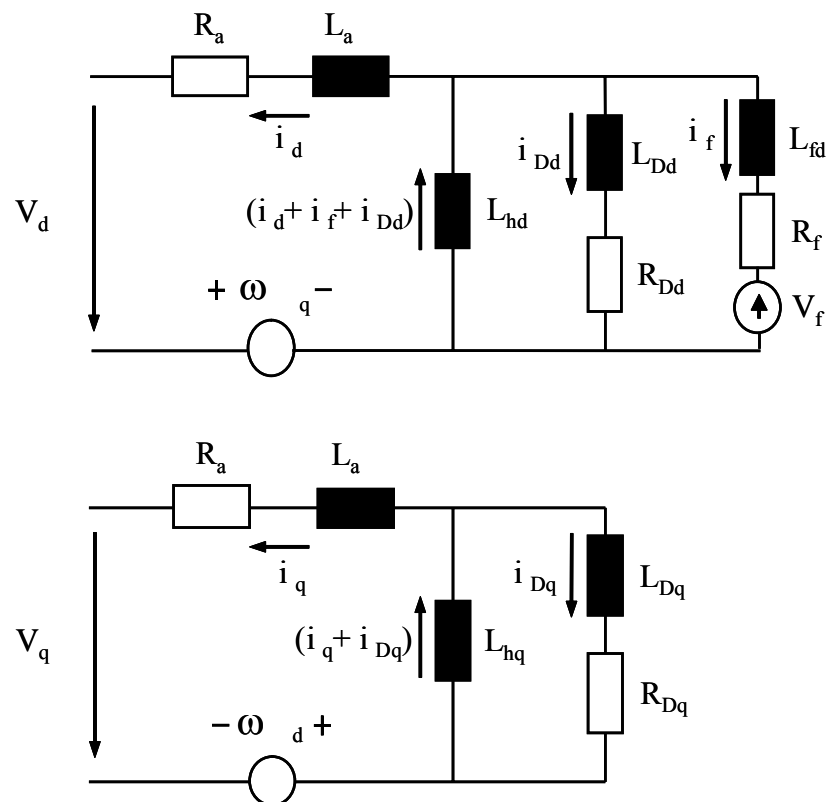


Figure 3.5 Equivalent circuit of synchronous generator

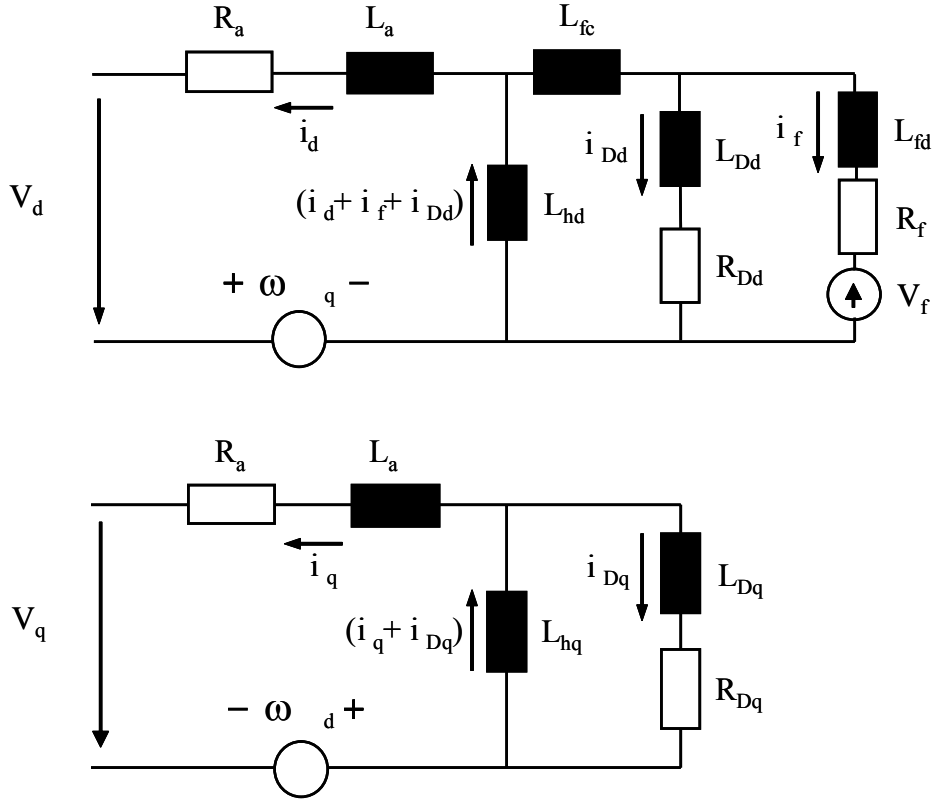


Figure 3.6 An expanded equivalent circuit of a synchronous generator

3.2.2 Linear model of a synchronous generator system

3.2.2.1 A linear equation of a synchronous generator system

When a system is subjected to a small load change, it tends to reach a new operating state. If the two states are such that all the state variables change only slightly, i.e., the variable x_i changes from x_{i0} to $x_{i0} + x_i$ where x_i is a small change in x_i , the system is operating near the initial state. To examine the behavior of the system when it is perturbed such that the new and old equilibrium states are nearly equal, the system equations are linearized about the quiescent operation condition.

Let the state-space vector \mathbf{X} have an initial state \mathbf{X}_0 at time $t = t_0$, at the occurrence of a small disturbance, i.e., after $t = t_0^+$, the states will change slightly from their positions or values, thus

$$\mathbf{X} = \mathbf{X}_0 + \mathbf{X}_\Delta \quad (3.25)$$

\mathbf{X}_0 is not necessary for a constant, but it need to be known. \mathbf{X}_Δ is a very small variation from \mathbf{X}_0 .

The state-space model is in the form:

$$\dot{\mathbf{X}} = \mathbf{f}(\mathbf{X}, t) \quad (3.26)$$

Using (3.25), equation (3.26) is reduced to:

$$\dot{\mathbf{X}}_0 + \dot{\mathbf{X}}_\Delta = \mathbf{f}(\mathbf{X}_0 + \mathbf{X}_\Delta, t) \quad (3.27)$$

In expanding (3.26), all second-order terms are neglected; i.e., terms of the form $\mathbf{X}_{i\Delta}\mathbf{X}_{j\Delta}$ are assumed to be negligibly small, therefore, the equation (3.27) becomes:

$$\dot{\mathbf{X}}_0 + \dot{\mathbf{X}}_\Delta \cong \mathbf{f}(\mathbf{X}_0, t) + \mathbf{A}(\mathbf{X}_0)\mathbf{X}_\Delta + \mathbf{B}(\mathbf{X}_0)\mathbf{U} \quad (3.28)$$

from which we obtain the linearized state-space equation:

$$\dot{\mathbf{X}}_\Delta = \mathbf{A}(\mathbf{X}_0)\mathbf{X}_\Delta + \mathbf{B}(\mathbf{X}_0)\mathbf{U}$$

The elements of the \mathbf{A} matrix depend upon the initial values of the state vector \mathbf{X}_0 . \mathbf{U} is an input matrix.

By linearizing equation (3.12) with the negligence of all the second-order terms, the d-axis voltage can be written as:

$$\begin{aligned}
V_d &= V_{d0} + V_{d\Delta} \\
&= -R_a (\dot{i}_{d0} + \dot{i}_{d\Delta}) - (\omega_0 + \omega_\Delta) L_{hq} (\dot{i}_{Dq0} + \dot{i}_{Dq\Delta}) - (\omega_0 + \omega_\Delta) L_q (\dot{i}_{q0} + \dot{i}_{q\Delta}) \\
&\quad - L_d \left(\dot{i}_{d0} + \dot{i}_{d\Delta} \right) - L_{hd} \left(\dot{i}_{Dd0} + \dot{i}_{Dd\Delta} \right) - L_{hd} \left(\dot{i}_{f0} + \dot{i}_{f\Delta} \right) \\
&= \left(-R_a \dot{i}_{d0} - \omega_0 L_q \dot{i}_{q0} - \omega_0 L_{hq} \dot{i}_{Dq0} - L_d \dot{i}_{d0} - L_{hd} \dot{i}_{f0} - L_{hd} \dot{i}_{Dd0} \right) \\
&\quad - R_a \dot{i}_{d\Delta} - \omega_0 L_q \dot{i}_{q\Delta} - \omega_0 L_{hq} \dot{i}_{Dq\Delta} - \omega_\Delta L_q \dot{i}_{q0} - \omega_\Delta L_{hq} \dot{i}_{Dq0} - L_d \dot{i}_{d\Delta} - L_{hd} \dot{i}_{f\Delta} - L_{hd} \dot{i}_{Dd\Delta}
\end{aligned} \tag{3.29}$$

The quantity in parenthesis on the right side is exactly equal to V_{d0} . Rearrange the remaining quantities, then

$$\begin{aligned}
V_{d\Delta} &= -R_a \dot{i}_{d\Delta} - \omega_0 L_q \dot{i}_{q\Delta} - \omega_0 L_{hq} \dot{i}_{Dq\Delta} - \omega_\Delta L_q \dot{i}_{q0} - \omega_\Delta L_{hq} \dot{i}_{Dq0} - L_d \dot{i}_{d\Delta} \\
&\quad - L_{hd} \dot{i}_{f\Delta} - L_{hd} \dot{i}_{Dd\Delta}
\end{aligned} \tag{3.30}$$

Similarly, for the q-axis voltage we can write as:

$$\begin{aligned}
V_{q\Delta} &= -R_a \dot{i}_{q\Delta} - L_q \dot{i}_{q\Delta} - L_{hq} \dot{i}_{Dq\Delta} + \omega_0 L_d \dot{i}_{d\Delta} + \omega_0 L_{hd} \dot{i}_{f\Delta} + \omega_0 L_{hd} \dot{i}_{Dd\Delta} \\
&\quad + \omega_\Delta (L_d \dot{i}_{d0} + L_{hd} \dot{i}_{f0} + L_{hd} \dot{i}_{Dd0})
\end{aligned} \tag{3.31}$$

For the field winding we compute as:

$$V_{f\Delta} = R_f \dot{i}_{f\Delta} + L_f \dot{i}_{f\Delta} + L_{hd} \dot{i}_{d\Delta} + L_{hd} \dot{i}_{Dd\Delta} \tag{3.32}$$

The linearized damper-winding equations are given by:

$$0 = R_{Dd} \dot{i}_{Dd\Delta} + L_{Dd} \ddot{i}_{Dd\Delta} + L_{hd} \left(\ddot{i}_{d\Delta} + \ddot{i}_{f\Delta} \right) \quad (3.33)$$

$$0 = R_{Dq} \dot{i}_{Dq\Delta} + L_{Dq} \ddot{i}_{Dq\Delta} + L_{hq} \ddot{i}_{q0}$$

The linearized torque equation derived from equation (3.23) and (3.24) can be established as:

$$\begin{aligned} & J \left(\ddot{\omega}_0 + \ddot{\omega}_\Delta \right) + D \left(\omega_0 + \omega_\Delta \right) \\ &= (T_{m0} + T_{m\Delta}) - \left((\Psi_{d0} + \Psi_{d\Delta})(i_{q0} + i_{q\Delta}) - (\Psi_{q0} + \Psi_{q\Delta})(i_{d0} + i_{d\Delta}) \right) \end{aligned}$$

then

$$\begin{aligned} & \left(J \ddot{\omega}_0 + D \omega_0 \right) + \left(J \ddot{\omega}_\Delta + D \omega_\Delta \right) \\ &= (T_{m0} - \Psi_{d0} i_{q0} + \Psi_{q0} i_{d0}) + T_{m\Delta} - \left[(\Psi_{d\Delta} i_{q0} + \Psi_{d0} i_{q\Delta}) - (\Psi_{q0} i_{d\Delta} + \Psi_{q\Delta} i_{d0}) \right] \end{aligned} \quad (3.34)$$

Rearranging equation (3.34)

$$\begin{aligned} J \ddot{\omega}_\Delta &= T_{m\Delta} - D \omega_\Delta - \left(L_d i_{q0} - (L_q i_{q0} + L_{hq} i_{Dq0}) \right) i_{d\Delta} \\ &\quad - \left[(L_d i_{d0} + L_{hd} (i_{f0} + i_{Dd0})) - i_{d0} L_q \right] i_{q\Delta} \\ &\quad - L_{hd} i_{q0} i_{f\Delta} - L_{hd} i_{q0} i_{Dd\Delta} + L_{hd} i_{d0} i_{Dq\Delta} \end{aligned} \quad (3.35)$$

Finally, the load angle equation may be written as:

$$\ddot{\delta}_\Delta = \omega_\Delta \quad (3.36)$$

Equation (3.31)~(3.36) describe linear model for a synchronous machine, If the Δ subscript is dropped, since all variables are now small displacements, then these equations may be written in the following matrix form:

$$\begin{bmatrix} V_d \\ -V_f \\ 0 \\ V_q \\ 0 \\ T_m \\ 0 \end{bmatrix} = - \begin{bmatrix} R_a & 0 & 0 & \omega_0 L_q & \omega_0 L_{hq} & \Psi_{q0} & 0 \\ 0 & R_f & 0 & 0 & 0 & 0 & 0 \\ 0 & 0 & R_{Dd} & 0 & 0 & 0 & 0 \\ -\omega_0 L_d & -\omega_0 L_{hd} & -\omega_0 L_{hd} & R_a & 0 & -\Psi_{d0} & 0 \\ 0 & 0 & 0 & 0 & R_q & 0 & 0 \\ -L_d i_{q0} + \Psi_{q0} & -L_{hd} i_{q0} & -L_{hd} i_{q0} & -\Psi_{d0} + L_q i_{d0} & L_{hd} i_{q0} & -D & 0 \\ 0 & 0 & 0 & 0 & 0 & -1 & 0 \end{bmatrix} \begin{bmatrix} i_d \\ i_f \\ i_{Dd} \\ i_q \\ i_{Dq} \\ \omega \\ \delta \end{bmatrix}$$

$$- \begin{bmatrix} L_d & L_{hd} & L_{hd} & 0 & 0 & 0 & 0 \\ L_{hd} & L_f & L_{hd} & 0 & 0 & 0 & 0 \\ L_{hd} & L_{hd} & L_{Dd} & 0 & 0 & 0 & 0 \\ 0 & 0 & 0 & L_q & L_{hq} & 0 & 0 \\ 0 & 0 & 0 & L_{Dq} & L_{hq} & 0 & 0 \\ 0 & 0 & 0 & 0 & 0 & -J & 0 \\ 0 & 0 & 0 & 0 & 0 & 0 & 1 \end{bmatrix} \left(\frac{d}{dt} \begin{bmatrix} i_d \\ i_f \\ i_{Dd} \\ i_q \\ i_{Dq} \\ \omega \\ \delta \end{bmatrix} \right)$$

(3.37)

If the synchronous machine is connected to an infinite bus voltage V_∞ through the transmission line with resistance R_{inf} and inductance L_{inf} , then equation (3.37) must be modified and expressed by equation (3.38):

$$\begin{bmatrix} 0 \\ -V_f \\ 0 \\ 0 \\ 0 \\ T_m \\ 0 \end{bmatrix} = - \begin{bmatrix} \hat{R} & 0 & 0 & \omega_0 \hat{L}_q & \omega_0 L_{hq} & \hat{\Psi}_{q0} & -\sqrt{3}V_\infty \cos(\delta_0 - \alpha) \\ 0 & R_f & 0 & 0 & 0 & 0 & 0 \\ 0 & 0 & R_{Dd} & 0 & 0 & 0 & 0 \\ -\omega_0 \hat{L}_d & -\omega_0 L_{hd} & -\omega_0 L_{hd} & \hat{R} & 0 & -\hat{\Psi}_{d0} & -\sqrt{3}V_\infty \sin(\delta_0 - \alpha) \\ 0 & 0 & 0 & 0 & R_0 & 0 & 0 \\ -\hat{L}_d i_{q0} + \Psi_{q0} & -L_{hd} i_{q0} & -L_{hd} i_{q0} & -\Psi_{d0} + \hat{L}_q i_{d0} & L_{hd} i_{q0} & -D & 0 \\ 0 & 0 & 0 & 0 & 0 & -1 & 0 \end{bmatrix} \begin{bmatrix} i_d \\ i_f \\ i_{Dd} \\ i_q \\ i_{Dq} \\ \omega \\ \delta \end{bmatrix}$$

$$- \begin{bmatrix} \hat{L}_d & L_{hd} & L_{hd} & 0 & 0 & 0 & 0 \\ L_{hd} & L_F & L_{hd} & 0 & 0 & 0 & 0 \\ L_{hd} & L_{hd} & L_D & 0 & 0 & 0 & 0 \\ 0 & 0 & 0 & \hat{L}_q & L_{hq} & 0 & 0 \\ 0 & 0 & 0 & L_{hd} & L_Q & 0 & 0 \\ 0 & 0 & 0 & 0 & 0 & -J & 0 \\ 0 & 0 & 0 & 0 & 0 & 0 & 1 \end{bmatrix} \left(\frac{d}{dt} \begin{bmatrix} i_d \\ i_f \\ i_{Dd} \\ i_q \\ i_{Dq} \\ \omega \\ \delta \end{bmatrix} \right)$$

(3.38)

where

$$\hat{L}_d = L_d + L_{inf} \quad ; \quad \hat{L}_q = L_q + L_{inf} \quad ; \quad \hat{R} = R_{inf} + R_a$$

$$\hat{\Psi}_{d0} = \Psi_{d0} + L_{inf} i_d \quad ; \quad \hat{\Psi}_{q0} = \Psi_{q0} + L_{inf} i_q$$

Equation (3.38) describes the linear model of generator.

3.2.2.2 A simplified linear model of synchronous machine

A simplified linear model for a synchronous machine connected to an infinite bus through a transmission line having resistance R_{inf} and inductance L_{inf} is adapted in [11-12].

In this simplified model the following assumptions shall be made:

- Damper winding effect are neglected.
- Stator winding resistance is neglected.
- $\dot{\Psi}_d$ and $\dot{\Psi}_q$ are neglected compared to the speed voltage $\omega\Psi_d$ and $\omega\Psi_q$.
- Balanced conditions are assumed and saturation effect is neglected.

From the equation (3.14) and (3.20) the field equations are given by

$$V_f = R_f i_f + \dot{\Psi}_f \quad \Psi_f = L_f i_f + L_{hd} i_d \quad (3.39)$$

Eliminating i_f , we get:

$$V_f = \left(\frac{R_f}{L_f} \right) \Psi_f + \dot{\Psi}_f - \left(\frac{R_f}{L_f} \right) L_{hd} i_d \quad (3.40)$$

Let E_q be the stator EMF which is proportional to the main winding flux linkage to stator:

$$E_q = \omega L_{hd} \frac{\Psi_f}{L_f} \quad (3.41)$$

where ω is the angular velocity of the rotor.

Also let E_{FD} be the stator EMF that is produced by the field current and correspond to the field voltage V_f , i.e.,

$$E_{FD} = \omega L_{hd} \frac{V_f}{R_f} \quad (3.42)$$

The d-axis open circuit time constant is defined as:

$$\tau'_{d0} = \frac{L_f}{R_f} \quad (3.43)$$

Substituting equation (3.41) to equation (3.43) into equation (3.40), and then obtain the following result from equation (3.40) in the s-domain.

$$E_{FD} = (1 + \tau'_{d0} s) E_q - (X_d - X'_d) i_d \quad (3.44)$$

where

$$L'_d = L_d - \frac{L_{hd}^2}{L_f}, \quad X'_d = \omega \left(L_d - \frac{L_{hd}^2}{L_f} \right)$$

L'_d is the d-axis transient inductance.

The second part of equation (3.39) and equation (3.41) are arranged as:

$$E_q = \omega L_{hd} i_f + (X_d - X'_d) i_d = E + (X_d - X'_d) i_d \quad (3.45)$$

E is the stator EMF that is produced by the field current.

$$E = \omega L_{hd} i_f \quad (3.46)$$

Under the assumption of a simplified linear generator system, the generator is connected to infinite bus. The voltage V_d and V_q for infinite bus loading in equation (3.12) and (3.13) can be modified as [12]:

$$V_d = -\omega L_q i_q = -\sqrt{3} V_\infty \sin(\delta - \alpha) + R_{inf} i_d + \omega L_{inf} i_q \quad (3.47)$$

$$V_q = \omega L_d i_d + \omega L_{hd} i_f = \sqrt{3} V_\infty \cos(\delta - \alpha) + R_{inf} i_q - \omega L_{inf} i_d$$

Linearizing (3.47)

$$0 = -R_{inf} i_{d\Delta} - (X_q + X_{inf}) i_{q\Delta} + \left[\sqrt{3} V_\infty \cos(\delta_0 - \alpha) \right] \delta_\Delta \quad (3.48)$$

$$0 = -R_{inf} i_{q\Delta} + (X_d + X_{inf}) i_{d\Delta} + \omega_R L_{hd} i_{f\Delta} + \left[\sqrt{3} V_\infty \sin(\delta_0 - \alpha) \right] \delta_\Delta$$

where V_∞ is the infinite bus voltage to ground. Substituting equation (3.45) into (3.48) and solving (3.48) for $I_{d\Delta}$ and $I_{q\Delta}$. It can be got as following:

$$\begin{bmatrix} i_{d\Delta} \\ i_{q\Delta} \end{bmatrix} = K_I \begin{bmatrix} -(X_q + X_{inf}) & R_{inf} \cos(\delta_0 - \alpha) - (X_q + X_{inf}) \sin(\delta_0 - \alpha) \\ R_{inf} & (X_d' + X_{inf}) \cos(\delta_0 - \alpha) + R_{inf} \sin(\delta_0 - \alpha) \end{bmatrix} \begin{bmatrix} E_{q\Delta} \\ \sqrt{3} V_\infty \delta_\Delta \end{bmatrix} \quad (3.49)$$

where

$$K_I = \frac{1}{[R_{inf}^2 + (X_q + X_{inf})(X_d' + X_{inf})]} \quad (3.50)$$

Now I_d in equation (3.49) is substituted for an incremental version of equation (3.44). The result in s-domain can be expressed as:

$$E_{FD\Delta} = \left(\frac{1}{K_3} + \tau'_{d0} s \right) E_{q\Delta} + K_4 \delta_\Delta \quad (3.51)$$

where

$$\begin{aligned} \frac{1}{K_3} &= 1 + K_I (X_d - X_d') (X_q + X_{inf}) \\ K_4 &= \sqrt{3} V_\infty K_I (X_d - X_d') [(X_q + X_{inf}) \sin(\delta_0 - \alpha) - R_{inf} \cos(\delta_0 - \alpha)] \end{aligned} \quad (3.52)$$

The electrical moment T_e in p.u. is numerically equal to three-phase power. therefore:

$$T_e = (V_d i_d + V_q i_q) \quad , \text{ and } V_d = -X_q i_q \quad , \quad V_q = X_d i_d + \omega L_{hd} i_f \quad (3.53)$$

Using equation (3.45) in the second equation of (3.53), then

$$V_d = -X_q i_q \quad V_q = X'_d i_d + E_q \quad (3.54)$$

and T_e can be written as:

$$T_e = [E_q - (X_q - X'_d) i_d] i_q \quad (3.55)$$

Linearizing (3.55), T_e can be obtained as:

$$T_{e\Delta} = i_{q0} E_{q\Delta} + E_{qa0} i_{q\Delta} - (X_q - X'_d) i_{q0} i_{d\Delta} \quad (3.56)$$

where E_{qa} (as shown in Figure (3.21)) is defined as:

$$E_{qa} = E + (X_d - X_q) i_d \quad (3.57)$$

Therefore rearrange equation (3.57) and (3.45) at the initial condition:

$$\begin{aligned} E_{qa0} &= E_0 + (X_d - X_q) i_{d0} \\ &= E_{q0} - (X_d - X'_d) i_{d0} + (X_d - X_q) i_{d0} \\ &= E_{q0} - (X_q - X'_d) i_{d0} \end{aligned} \quad (3.58)$$

Substituting (3.49) and (3.50) into (3.56), the increment of moment is

$$\begin{aligned} T_{e\Delta} &= \sqrt{3} K_I V_\infty \left\{ E_{qa0} [R_{inf} \sin(\delta_0 - \alpha) + (X'_d + X_{inf}) \cos(\delta_0 - \alpha)] \right. \\ &\quad \left. + i_{q0} (X_q - X'_d) [(X_q + X_{inf}) \sin(\delta_0 - \alpha) - R_{inf} \cos(\delta_0 - \alpha)] \right\} \delta_0 \\ &\quad + K_I \left\{ i_{q0} [R_{inf}^2 + (X_q + X_{inf})^2] + E_{qa0} R_{inf} \right\} E_{q\Delta} \\ &= K_1 \delta_\Delta + K_2 E_{q\Delta} \end{aligned} \quad (3.59)$$

where

$$\begin{aligned}
K_1 &= \left. \frac{T_{e\Delta}}{\delta_\Delta} \right|_{E_q=E_{q0}} \\
&= \sqrt{3} K_I V_\infty \left\{ [R_{\text{inf}} \sin(\delta_0 - \alpha) + (X'_d + X_{\text{inf}}) \cos(\delta_0 - \alpha)] E_{q\Delta 0} \right. \\
&\quad \left. + i_{q0} (X_q - X'_d) [(X_{\text{inf}} + X_q) \sin(\delta_0 - \alpha) - R_{\text{inf}} \cos(\delta_0 - \alpha)] \right\}
\end{aligned} \tag{3.60}$$

$$K_2 = K_I \left\{ R_{\text{inf}} E_{q\Delta 0} + i_{q0} [R_{\text{inf}}^2 + (X_q + X_{\text{inf}})^2] \right\}$$

The terminal voltage V_t of the synchronous generator is given by

$$V_t^2 = V_d^2 + V_q^2 \tag{3.61}$$

This equation is linearized to obtain:

$$V_{t\Delta} = -\left(\frac{V_{d0}}{V_{t0}}\right) X_q i_{q\Delta} + \left(\frac{V_{q0}}{V_{t0}}\right) (X'_d i_{d\Delta} + E_{q\Delta}) \tag{3.62}$$

Substituting for i_d and i_q from equation (3.49)

$$\begin{aligned}
V_{t\Delta} &= \left\{ \left(\sqrt{3} K_I V_\infty X'_d \frac{V_{q0}}{V_{t0}} \right) [R_{\text{inf}} \cos(\delta_0 - \alpha) - (X_q + X_{\text{inf}}) \sin(\delta_0 - \alpha)] \right. \\
&\quad \left. - \left(\sqrt{3} K_I V_\infty X_q \frac{V_{d0}}{V_{t0}} \right) [(X'_d + X_{\text{inf}}) \cos(\delta_0 - \alpha) + R_{\text{inf}} \sin(\delta_0 - \alpha)] \right\} \delta_0 \\
&\quad + \left\{ \left(\frac{V_{q0}}{V_{t0}} \right) [1 - K_I X'_d (X_q + X_{\text{inf}})] - \left(\frac{V_{d0}}{V_{t0}} \right) K_I X_q R_{\text{inf}} \right\} E_{q\Delta} \\
&= K_5 \delta_\Delta + K_6 E_{q\Delta}
\end{aligned} \tag{3.63}$$

K_5 is the change in the terminal voltage V_t for a small change in rotor angle at constant d-axis flux linkage. K_6 is the change in terminal voltage V_t for a small change in the d-axis flux linkage at a constant rotor angle.

Finally, according to equation (3.51), (3.59) and (3.63), the simplified linear equations for synchronous machine can be written as follows:

$$\begin{aligned} E_{q\Delta} &= \frac{K_3}{1 + K_3 \tau'_{d0} s} E_{FD\Delta} - \frac{K_3 K_4}{1 + K_3 \tau'_{d0} s} \delta_{\Delta} \\ T_{e\Delta} &= K_1 \delta_{\Delta} + K_2 E_{q\Delta} \\ V_{t\Delta} &= K_5 \delta_{\Delta} + K_6 E_{q\Delta} \end{aligned} \quad (3.64)$$

To complete the model, the linear swing equation is used.

$$J \dot{\omega}_{\Delta} = T_{m\Delta} - T_{e\Delta} \quad (3.65)$$

then

$$\dot{\omega}_{\Delta} = -\left(\frac{K_2}{J}\right) E_{q\Delta} - \left(\frac{K_1}{J}\right) \delta_{\Delta} + \left(\frac{1}{J}\right) T_{m\Delta} \quad (3.66)$$

$$\dot{\delta}_{\Delta} = \omega_{\Delta} \quad (3.67)$$

where

$$K_1 = \left. \frac{T_{e\Delta}}{\delta_{\Delta}} \right|_{E_q = E_{q0}} \quad \text{Change in electrical torque for a change in rotor angle with constant flux linkages in the d - axis}$$

$$K_2 = \left. \frac{T_{e\Delta}}{E_{q\Delta}} \right|_{\delta = \delta_0} \quad \text{Change in electrical torque for a change in the main winding flux linkages with constant rotor angle}$$

$$K_3 = \frac{1}{[1 + K_I (X_d - X'_d) (X_q + X_{inf})]} \quad \text{Impedance factor}$$

$$K_1 = \frac{1}{[R_{inf}^2 + (X_q + X_{inf})(X'_d + X_{inf})]}$$

$$K_4 = \frac{1}{K_3} \frac{E_{q\Delta}}{\delta_\Delta} \Big|_{E_{FD} = \text{const}}$$

Demagnetizing effect
of a change in rotor angle

$$K_5 = \frac{V_{t\Delta}}{\delta_\Delta} \Big|_{E_q = E_{q_0}}$$

Change in terminal voltage with
change in rotor angle for a constant
d - axis flux linkage

$$K_6 = \frac{V_{t\Delta}}{E_{q\Delta}} \Big|_{\delta = \delta_0}$$

Change in terminal voltage with
change in main winding flux linkage
for constant rotor angel

The function block of the simplified linearized model of a synchronous generator is shown in Figure 3.7.

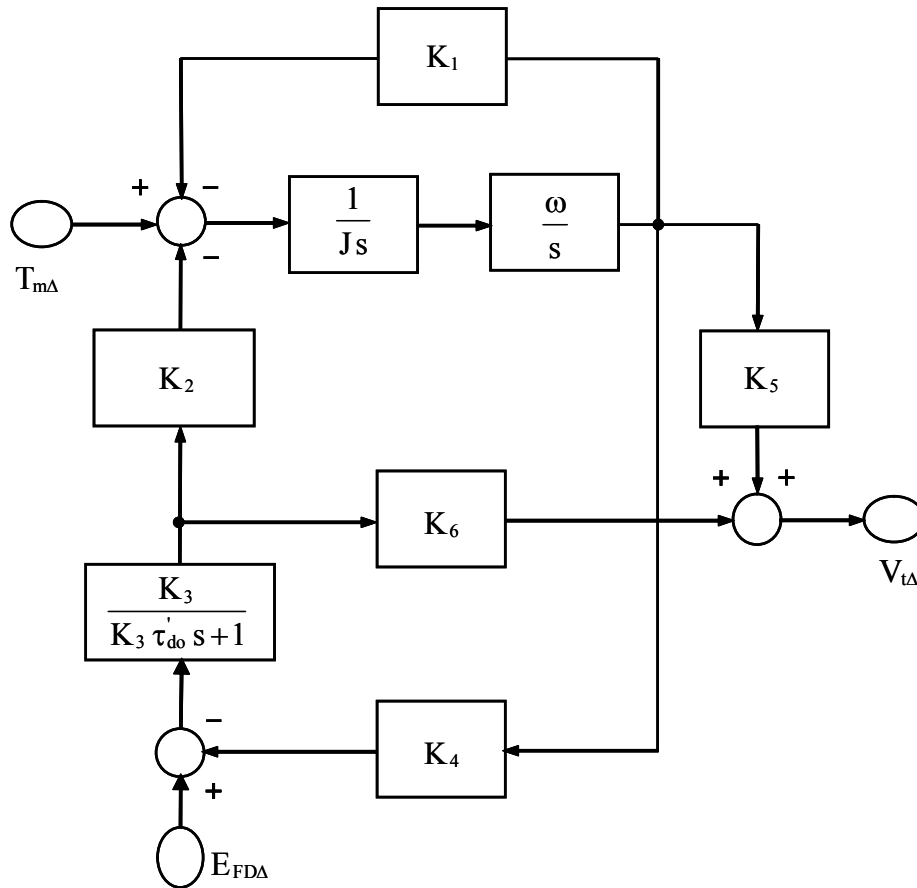


Figure 3.7 The function block of a linearized synchronous generator

In Figure 3.7, the output voltage $V_{t\Delta}$ is affected by the variation of mechanical Torque $T_{m\Delta}$ and the variation of $E_{FD\Delta}$. The angle δ_{Δ} is also affected by the variation in mechanical Torque $T_{m\Delta}$ and $E_{FD\Delta}$. The parameters K_1 to K_6 are dependent on the specifications of the generator and the load of the generator.

3.2.2.3 Linearized mechanical torque and angle relation

The relationship between mechanical torque and angle in Figure 3.7 is investigated first. For the purpose of simplification, we consider the constant flux linkage, i.e. $E_{q\Delta}=0$. A block diagram of linear generator model in Figure 3.7 can be simplified, as shown in Figure 3.8.

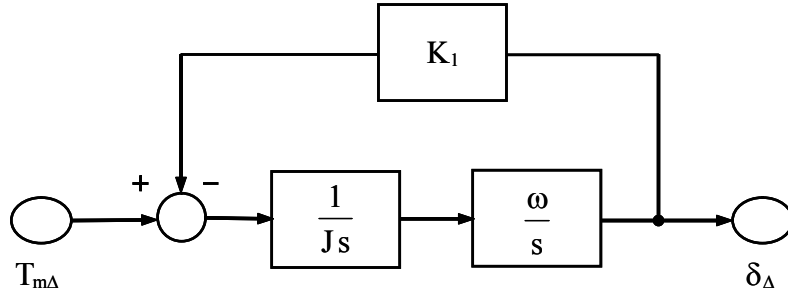


Figure 3.8 Linearized torque-angle relations

The transfer function in this block is expressed as:

$$\frac{\delta_{\Delta}}{T_{m\Delta}} = \frac{\omega}{Js^2 + \omega K_1} \quad (3.68)$$

where the output signal is δ_{Δ} and the input signal is $T_{m\Delta}$.

The nature frequency in equation (3.68) is $\sqrt{\omega K_1/J}$ and damping coefficient is zero. For conceivable range of inertia, impedance and loading value, the frequency of oscillation will be in the neighborhood of 0.5 to 2 HZ with the possibility of extreme values up to 4 Hz at the high end and 0.1 Hz at the low end [23]. It is important to

recognize that the response in Figure 3.8 is like an oscillator. Therefore, a braking torque in this system is needed. The braking torque is developed in phase with the rotor angle or with the machine rotor speed. The former are termed as synchronizing torque and the latter as damping torque.

3.2.2.4 Linearized torque and angle relation with the demagnetized effect

In Figure 3.9 we consider another feedback route with the transfer function

$$\frac{T_{e\Delta}}{\delta_{\Delta}} = \frac{-(K_2 K_3 K_4)}{(K_3 \tau'_{do} s + 1)} \quad (3.69)$$

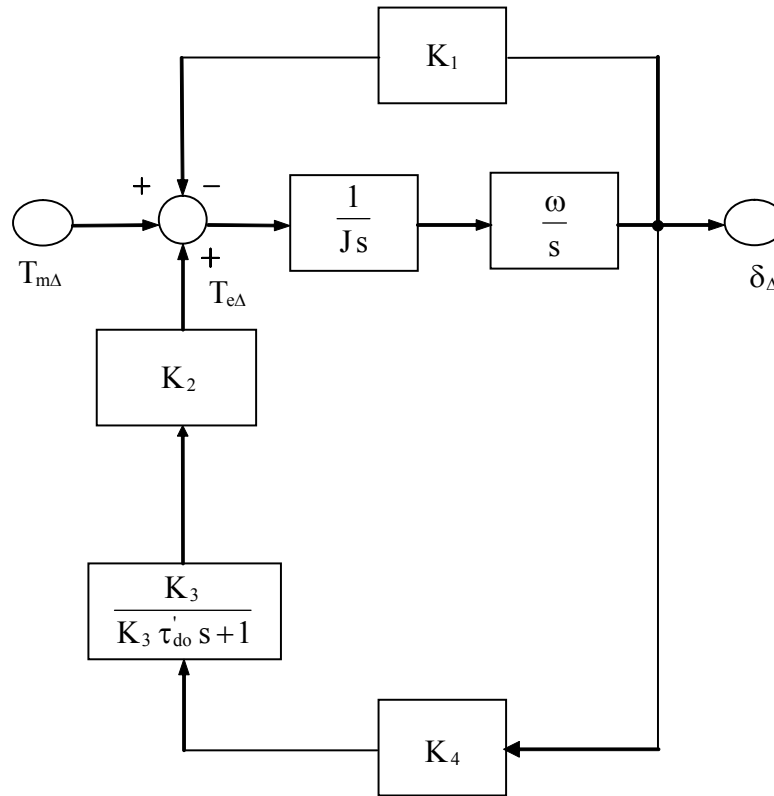
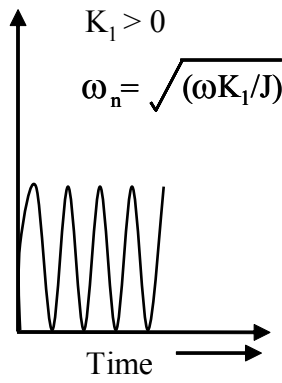


Figure. 3.9 Torque-angle loop including demagnetizing effect

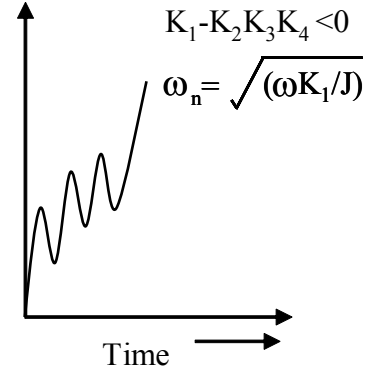
The complete closed loop transfer function in Figure 3.9 will then take the following form:

$$\frac{\delta_{\Delta}}{T_{m\Delta}} = \frac{H(s)}{((As^2 + Bs + C)(Ds + E))} \quad (3.70)$$

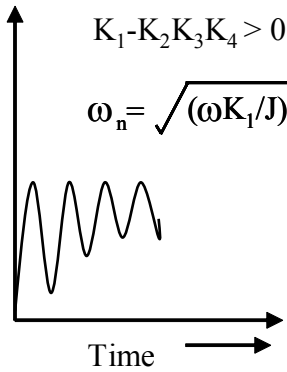
This form is comprised of a second-order differential system and a first-order differential equation.



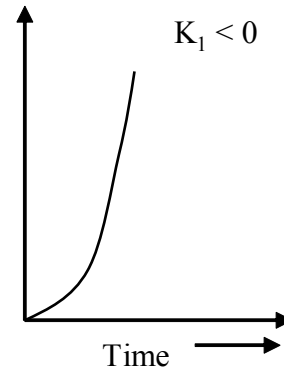
(a) $E_q = \text{constant}$



(c) $E_{FD} = \text{constant}$



(b) $E_{FD} = \text{constant}$



(d) $E_q = \text{constant}$

Figure 3.10 Typical response of rotor angle

The response of Figure 3.8 is shown in Figure 3.10 (a) and (d). It shows the time response of the rotor angle under a small variation in mechanical torque with flux linkage constant. It can be seen in Figure 3.10(d) that K_1 is less than zero and the system will be divergent. If K_1 is larger than zero, then the system will oscillate always.

A simulation of the torque-angle loop of Figure 3.9 is shown in Figure 3.10 (b) and (c). It shows the result of the time response of the rotor angle under a small variation in mechanical torque as the voltage of field winding is constant. The variation in rotor angle will affect the damping effect. The system will be stable, as shown in Figure 3.10 (c), when $K_1 - K_2 K_3 K_4$ is less than zero. It will be unstable when $K_1 - K_2 K_3 K_4$ is greater than zero.

3.2.3 Ladder networks model of synchronous machine

Park's model and the extended Park's model have a frequency limitation from 0 Hz to 100 Hz. It means that this model can be simulated at the situation, which the flux changes slowly. If the flux changes very rapidly, the Park's model cannot reflect the transient response of the system accurately.

The details and correct modeling of turbine generator are difficult, as currents are flowing during transients not only in the field and damper winding; but also in the solid rotor iron. To model this effect especially at high frequencies a new model structures is needed.

H. Bissig, K. Reichert and T. S. Kulig [38] establish a new model structures for turbo generator, called ladder-networks, to simulate this effect. Their parameters in this new modeling structure are identified by combining the Standstill Frequency Response (SSFR) measurements with the result of the standardized three-phase no-load short-circuit test.

A comparison between the standard model (Park's model) and ladder networks indicated that with respect to severe electrical faults both models yield only slight differences. On the other hands, the improvement becomes especially evident for ladder-circuit model if the disturbances are simulated whereby the currents include the frequencies f_0 (main rotation frequency) and $2f_0$ as well as low frequency swings. In such cases, the differing reactions of the real rotor with all its damper models and frequency dependent eddy current loss can be far better reflected by the ladder-circuit model than by the standard model.

The d-axis of ladder-circuit generator model shown in Figure 3.11 represents the field common to the field-windings and the damper (copper and iron) circuits of the

rotor by means of the inductances L_{ad} , L_{fd1} and L_{fd2} , where a part of the damper-currents is flowing in the resistor R_{1d} . The linkage fields as well as the eddy currents of the two circuits are independent from each other and modeled by two separate branches attached to the network common point (see Figure 3.11). The elements L_{3d} , R_{3d} etc. represent the damper circuit equivalent. The elements L_{fd1} , R_{fd1} , L_{fd2} and R_{fd2} describe the leakage field and the internal complex resistance of the field windings. For q-axis L_{1q} , R_{1q} , etc. are represented the damping circuit on q-axis.

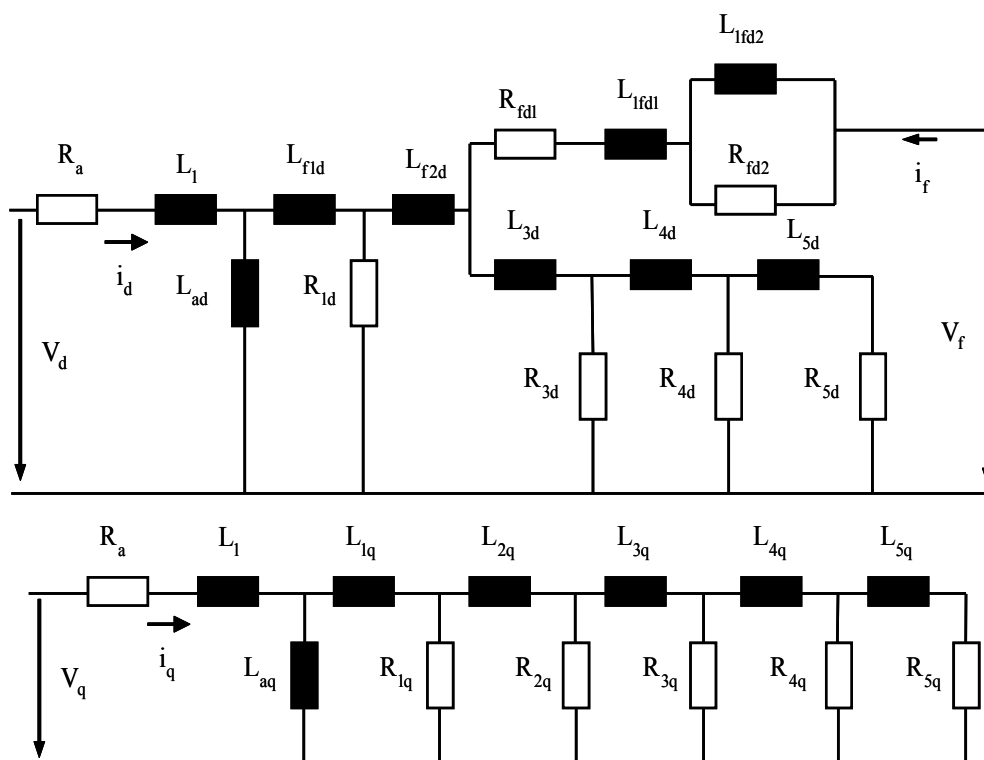


Figure 3.11 Equivalent networks of the synchronous machine with dq-axis

The basic scheme for frequency response measurement at standstill is shown in Figure 3.12. To obtain the d-impedance, the transfer impedance and current transfer function of the d-axis [41], the rotor is positioned such that the field winding gets maximum flux. To identify the impedance of the q-axis, the rotor must be turned until the field winding receives no flux.

After the standstill frequency response test for the d-impedance, the transfer impedance and current transfer function of the d-axis, the least square approximation is used to identify the parameters of the networks.

To check the usefulness of this unsaturated ladder network model, a no-load symmetrical terminal short-circuit test at 20 % rated voltage is simulated. The result is not fully satisfactory. The armature currents can be determined quite accurate, but ac-part of the field-winding current from the simulation is considerably larger than measured value.

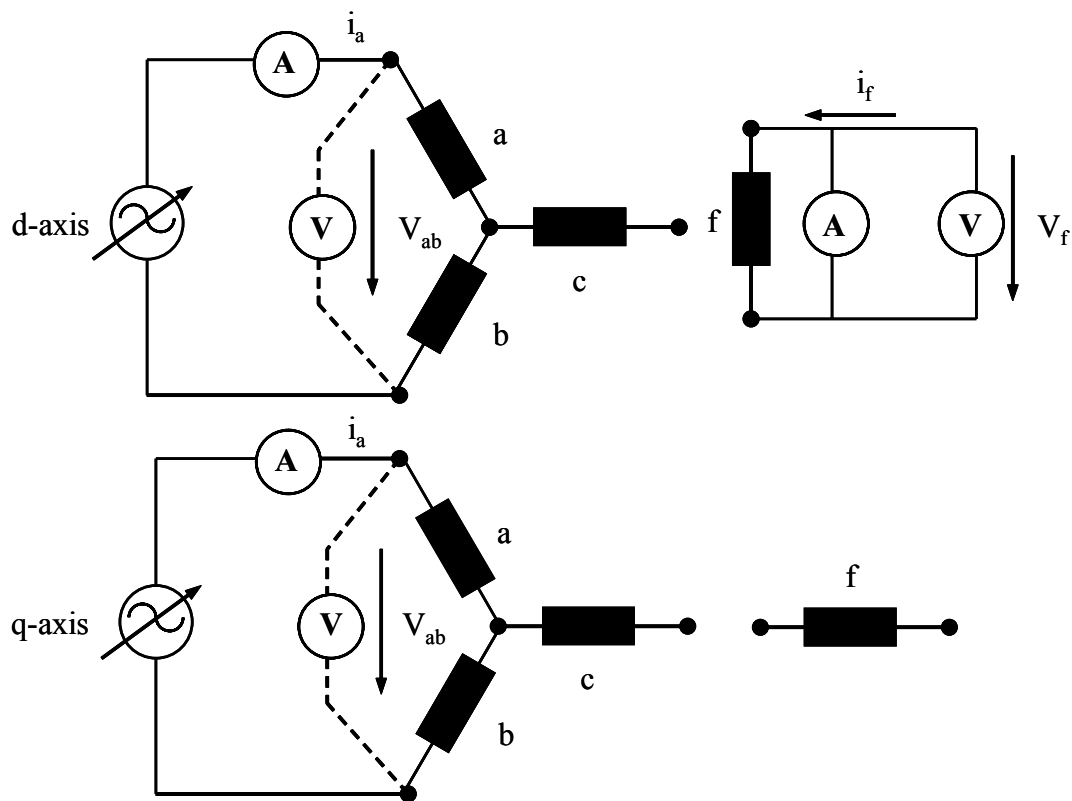


Figure 3.12 Principle test-set-up for standstill frequency response measurements

Information about the field-current during the no-load short-circuit test corrects the current transfer function. The current transfer function is multiplied by a correction function, which reduces the values for high frequencies. A simulation for the corrected ladder-network model is made and the result is compared with measured value. It shows that the current transfer function simulated by the new model can match the measured value testes in the SSFR method.

By means of the new ladder-networks, it is now possible to simulate the generator more precisely than was the case using the standard model. With this new model, an

additional extensive measurements and SSFR-frequency tests on real-life unit must be paid.

3.2.4 Three-machine system model

The voltage controller and excitation system had been represented by the diagram blocks discussed in [10]. Under fault conditions, the detailed reaction of component such as controlled and uncontrolled bridge rectifiers in the generator system cannot be measured. In order to research detailed behavior of each component in the generator system, a more precise generator system model is needed. N. Ataei [42] had developed a precise model for the Three-Machine System (TMS).

As shown in Figure 3.13, the three respective synchronous machines have different voltages, frequencies and powers ratings. These are normalized to different reference voltages and frequencies. For this reason, it is impossible to connect the generator field winding on the d-axis with the output of rotating bridge rectifier of the main excitation synchronous machine. The same reason is valid for the network connection between the field winding of the main excitation system and the thyristor bridge output, which rectifies the current of the auxiliary synchronous machine to DC and regulated by AVR. To solve this problem, an interface, consisting of a potential-free transformer, is added to the generator system. The equivalent supplementary circuit model in TMS is showed in Figure 3.13.

The benefit of this model is that the rotating rectifier bridge and thyristor, which cannot be directly measured in brushless generator system, can be simulated on a computer to know the transient reaction. The character of rotating rectifier bridge and the thyristor can be exactly checked during simulations of the generator system. Three-machine system thus gives a detailed response for each element of the generator system.

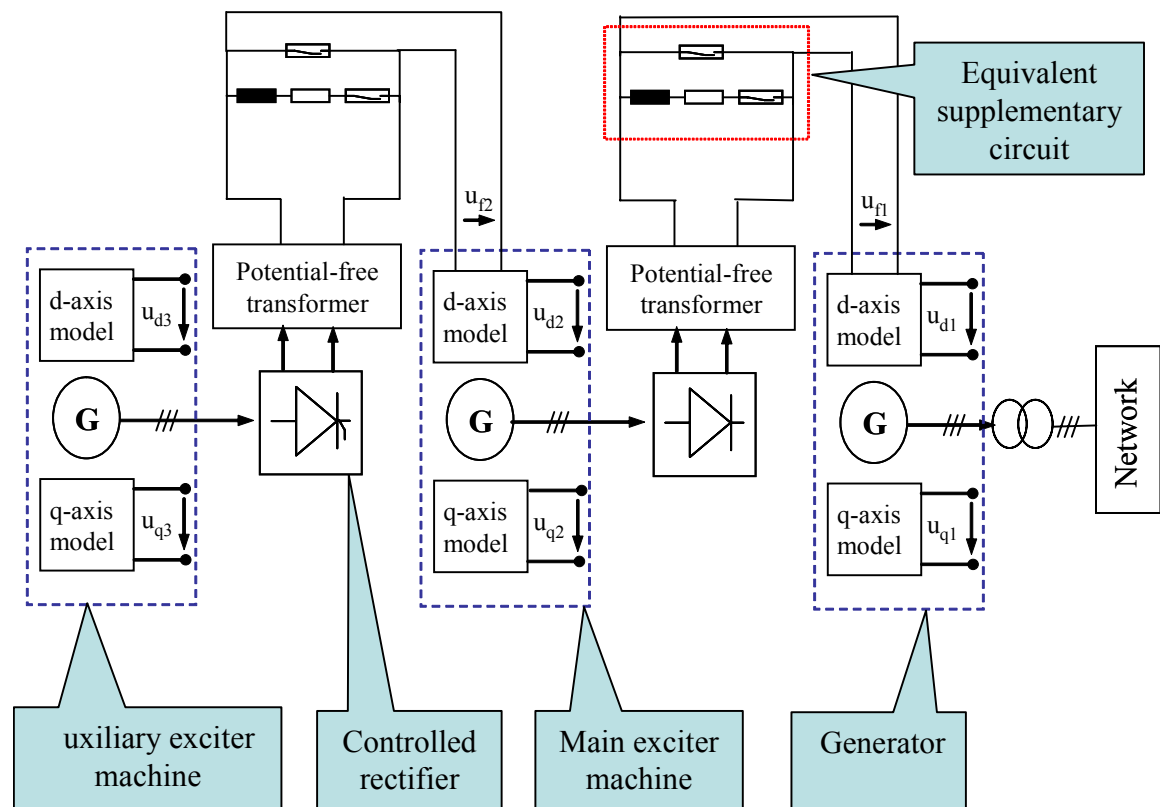


Figure 3.13 The equivalent supplementary circuit model of three-machine system

3.3 Automatic voltage controller

In 1981, the Power Committee of the IEEE Power Engineering Society recommended three distinctive types of excitation systems for the representation of the generator excitation in power system studies. These are the Direct Current (type DC), Alternative Current (type AC) and Static Transformer (type ST) excitation systems. Each type is suited to different generator systems produced by various manufacturers.

- Type DC excitation systems utilize a direct current generator with a commutator as a source of the excitation system power.
- Type AC excitation systems that utilize an alternator and either stationary or rotating rectifier to produce the direct current needed for generator field.

- Type ST excitation systems that the excitation power is supplied through transformers and rectifiers.

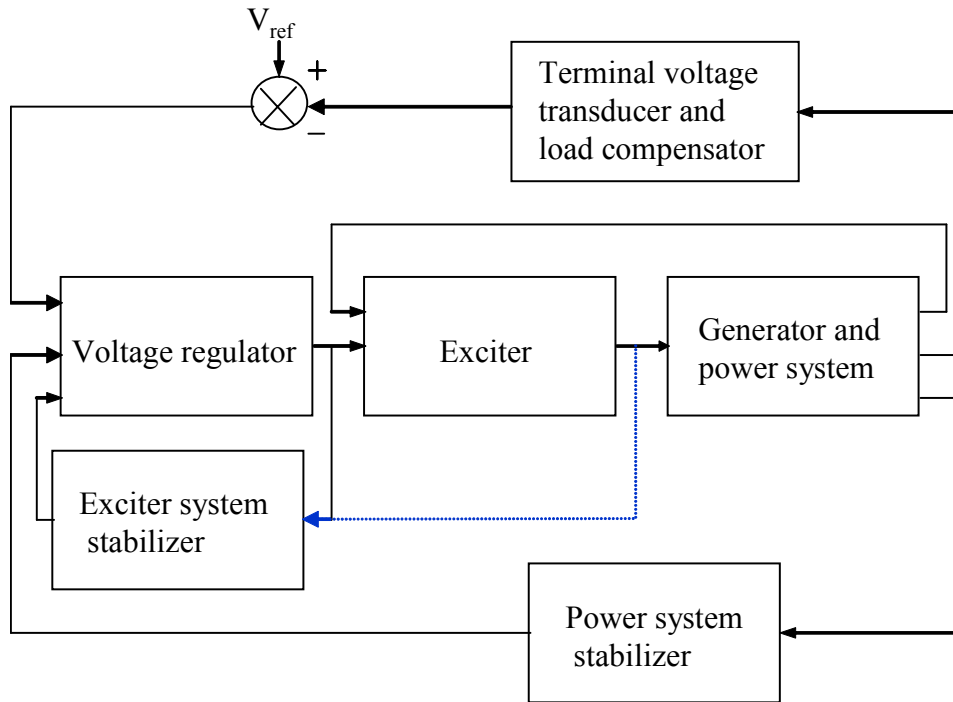


Figure 3.14 Generalized excitation control system

Figure 3.14 is the generalized excitation control system, where a voltage regulator is used to control the terminal voltage of generator. The controller functions as an amplifier. Excitation system stabilizer, which has a transfer function including the derivative element, adjusts the damping of the exciter. The power system stabilizer compensates for variation in the terminal voltage, which is affected by corresponding changes in the generator speed. We will analyze the DC excitation system model first. The AC excitation system model has the same function as the DC excitation system model except that extra consideration is given to the influence of rectifier-bridge and loading effect in the system. Therefore, understanding gained from an examination of the DC excitation system may be easily expanded into familiarity with the AC excitation system.

3.3.1 The standard DC excitation system

The standard DC excitation system model is represented in Figure 3.15

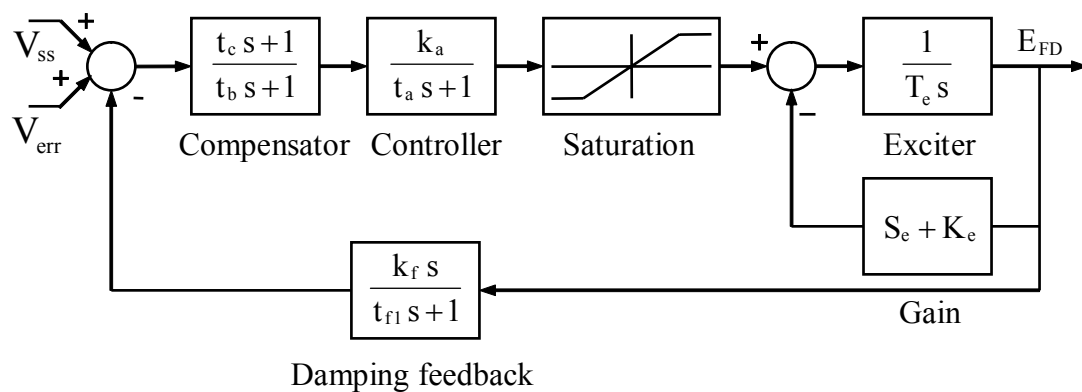


Figure 3.15 Field controlled DC commutator exciters with continuously acting voltage regulators

In this function block the main exciter is represented by transfer function $1/(T_e s)$ and a feedback path with $K_e + S_e$, where S_e represents the exciter saturation whose value is a function of exciter output voltage. The major controller is an amplifier with a gain k_a and a time constant t_a . The transfer function block $(t_c s + 1)/(t_b s + 1)$ is usually set to unity.

This system has a feedback loop with the transfer function $(k_f s)/(t_{f1} s + 1)$, which is composed of the differential component s and first-order time delay function $1/(t_{f1} s + 1)$. The power system stabilizing signal V_{ss} is added to error signals V_{err} . At the steady state, the output signals of the damping feedback and power system stabilizer V_{ss} are zero. The error signal V_{err} , between reference signal and terminal voltage, is amplified by k_a and is fed to exciter system.

3.3.2 The standard AC excitation system

This type of excitation system uses an AC alternator and stationary or rotating rectifiers to produce the direct current needed for the generator field. Loading effect in such exciters is significant and the use of the generator field current as an input to the model allows these effects to be represented accurately. Figure 3.16 represents the field controlled alternator-rectifier excitation system. This system consists of an alternator main exciter with uncontrolled rectifiers. The demagnetizing effect of loading current is represented by generator field current, i_{FD} , multiplied by a constant k_d [43].

The exciter output voltage drop due to rectifier regulation is simulated by inclusion of a constant k_c and a rectifier regulation curve FEX [44]. In this model, a signal i_{fe} is derived from the summation of the signals from exciter output voltage V_e multiplied by $K_e + S_e$ (where S_e represents the saturation of exciter) and i_{FD} multiplied by the demagnetization term k_d . The exciter field current signal i_{fe} is used as the input to damping feedback block.

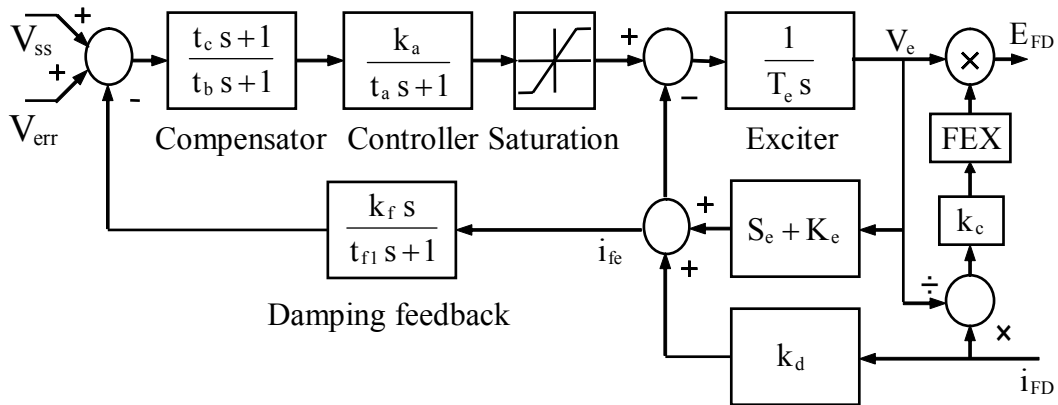


Figure 3.16 Alternator rectifier excitation system

There is also a simple model for the brushless excitation system. It is shown in Figure 3.17, unlike AC model in Figure 3.16, Figure 3.17 is the same as the diagram of the DC excitation system model. Because this model has been widely implemented by the power industry, it is sometimes used to represent other type of system when

either detailed data for them are not available or simplified models are required.

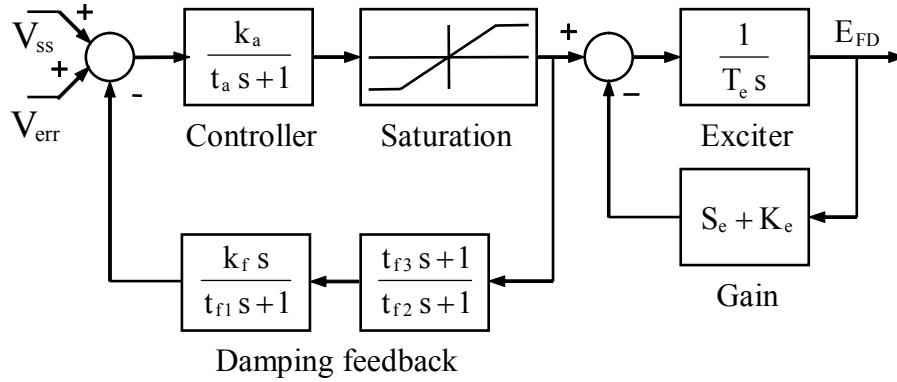


Figure 3.17 Representation of a simplified rotating rectifier excitation system

3.3.3 The ST type excitation system

The ST type excitation system can be seen as a form of self-excitation of the main AC synchronous machine. One of the type ST systems shown in Figure 3.18 represents a system, in which excitation power is supplied through a transformer from generator terminals, regulated by a controlled rectifier.

In this type of system, the inherent exciter time constants are very small; response to the main excitation system is almost instantaneous. The parameters of the exciter shown in Figure 3.15 is set $T_e = 0$, $K_e = 1$ and $S_e = 0$, the result is shown in Figure 3.18.

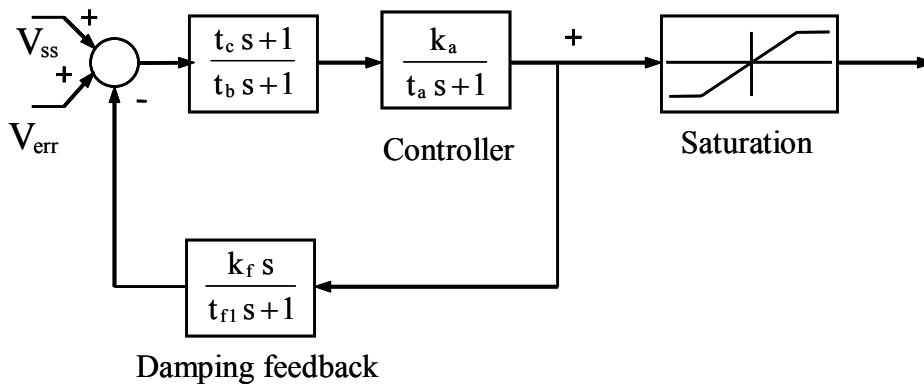


Figure 3.18 Type 1S controlled rectifier system with the terminal potential

3.4 Fuzzy neural controller

Fuzzy networks can be used for many different tasks within intelligent control systems because they represent general nonlinear relationships. Fuzzy networks have been used as plant models in predictive control algorithms as nonlinear estimators [45].

In this research, the fuzzy neural system is used to compensate for the variation in operating condition, which is influenced by loading, and achieves nonlinear compensation owing to the nonlinear characteristics of synchronous generator system itself.

A reference model is given so that a fuzzy neural system with self-learning ability can be trained and compensates for the external disturbance of the system. Therefore a combination of conventional controller and fuzzy neural controller will be used in this research to increase the system reliability. The testing of such a controller will be made under the normal conditions and fault conditions.

The detailed description of the fuzzy neural controller and learning algorithm will be provided in the next chapter.

3.5 Network

Normally, a synchronous machine connects with a large network, which is a combination of many generators, and loads. It is difficult to establish such a huge system in laboratory for research purpose. Therefore, a simplified equivalent network is required.

Figure 3.19 is single machine infinite bus model. A generator connects to an infinite bus through a transmission line having equivalent resistance R_{inf} and inductance L_{inf} . This transmission line model, which represents the transformer and transmission line, will be used for developing the generator controller.

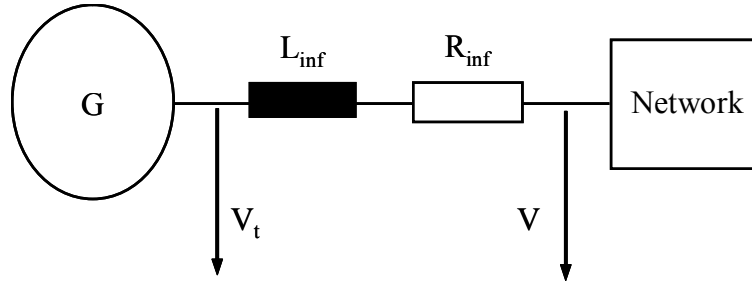


Figure 3.19 Generator connected with infinite bus

For the purpose of studying the dynamic response of generator system, the initial conditions of the system are required. These include all the currents, flux linkages, and voltages for the different machine circuits. The initial position of the rotor with respect to the system reference axis must also be known. The phasor diagram of Figure 3.19 under steady-state condition is represented in Figure 3.20

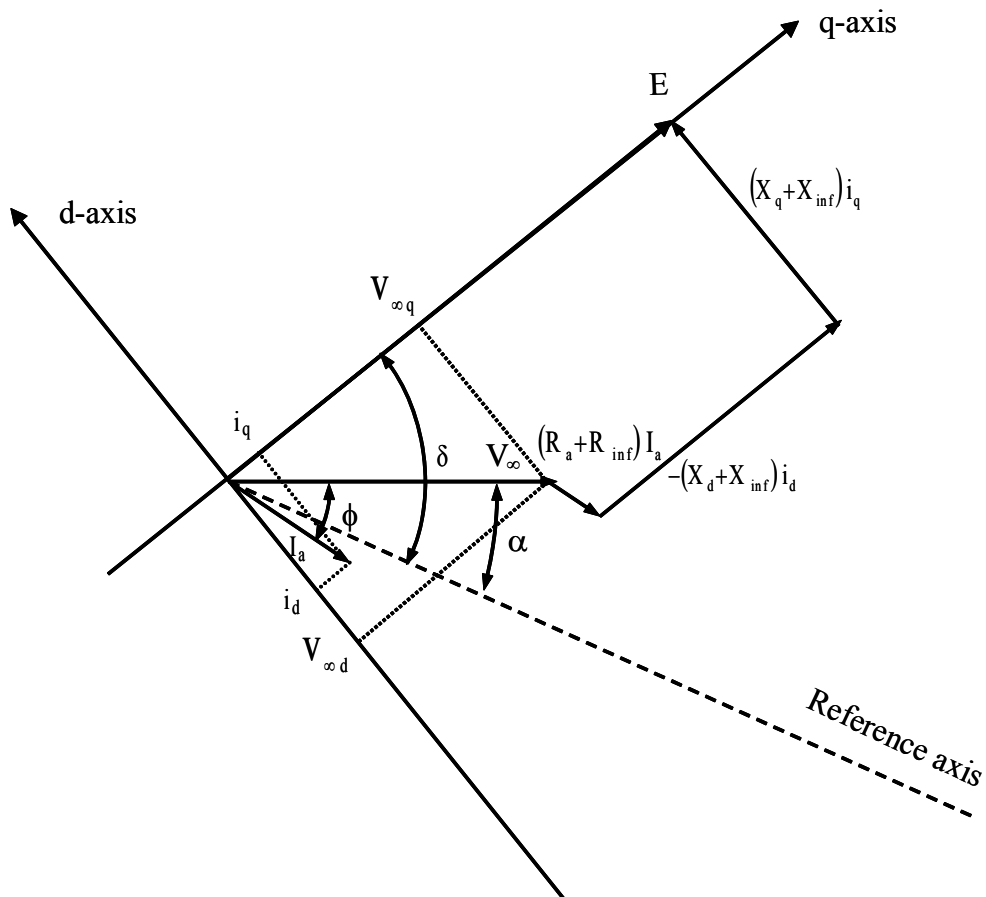


Figure 3.20 Phasor diagram of generator with infinite voltage

Note that V_d and V_q in Figure 3.20 are the projections of V along the d- and q-axis. i_d and i_q are also the projections of current along d- and q- axis. E is the induced voltage along the q-axis in the phasor diagram of Figure 3.20

The voltage equation along d-axis and q-axis can be written as:

$$\begin{aligned} E &= V_{\infty} \cos(\delta - \alpha) + (R_a + R_{inf}) i_q - (X_d + X_{inf}) i_d \\ 0 &= -V_{\infty} \sin(\delta - \alpha) + (R_a + R_{inf}) i_d + (X_d + X_{inf}) i_q \end{aligned} \quad (3.71)$$

where $X_{inf} = \omega L_{inf}$

Equation 3.71 represents the components of the voltage along the q- and d- axes respectively. Currents and flux linkages on the machine can be calculated by using equation 3.17 to 3.24 and 3.46.

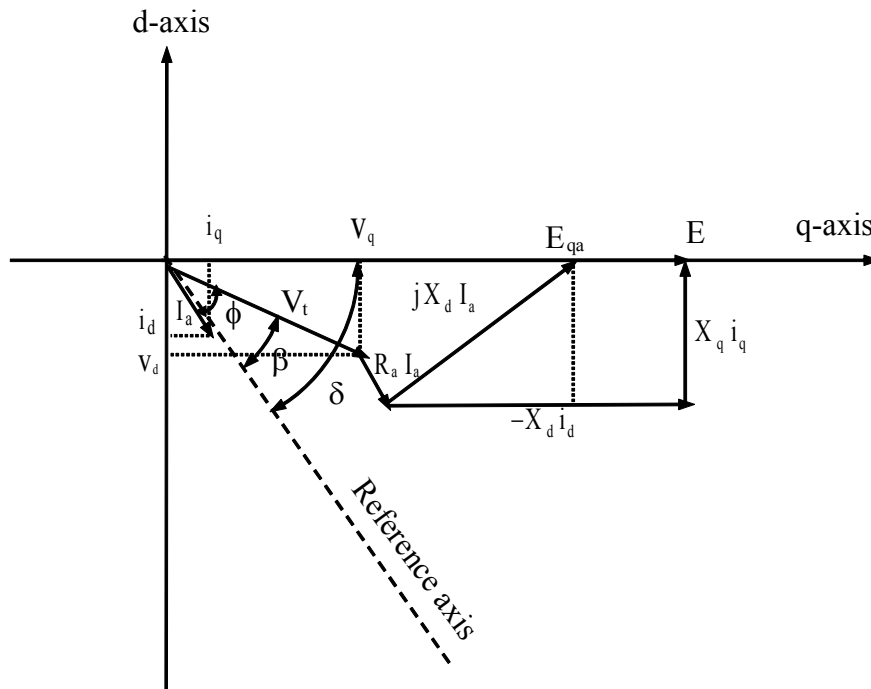


Figure 3.21 Alternate phasor diagram of the generator system

But in many cases the position of the q-axis is not available. Only the terminal conditions of the machine are given (i.e. V_t , I_a and the angle between them are known).

An alternate phasor diagram, as shown in Figure 3.21 is required.

The relationship shown in Figure 3.21 is:

$$\begin{aligned}
 \mathbf{E}_{qa} &= \mathbf{V}_t + \mathbf{R}_a \mathbf{I}_a + j \mathbf{X}_q \mathbf{I}_a \\
 &= \mathbf{V}_t + \mathbf{R}_a (\mathbf{I}_r + j \mathbf{I}_x) + j \mathbf{X}_q (\mathbf{I}_r + j \mathbf{I}_x) \\
 &= (\mathbf{V}_t - \mathbf{X}_q \mathbf{I}_x + \mathbf{R}_a \mathbf{I}_r) + j (\mathbf{X}_q \mathbf{I}_r + \mathbf{R}_a \mathbf{I}_x)
 \end{aligned} \tag{3.72}$$

\mathbf{I}_a is resolved into components with \mathbf{V}_t as a reference axis.

$$\mathbf{I}_a = \mathbf{I}_r + j \mathbf{I}_x$$

where \mathbf{I}_r is the component of \mathbf{I}_a in phase with \mathbf{V}_t , \mathbf{I}_x is the quadrature component of \mathbf{I}_a in the phase with \mathbf{V}_t .

The angle between the q-axis and the terminal voltage \mathbf{V}_t is given by:

$$\delta - \beta = \tan^{-1} \left(\frac{\mathbf{X}_q \mathbf{I}_r + \mathbf{R}_a \mathbf{I}_x}{(\mathbf{V}_t + \mathbf{R}_a \mathbf{I}_r - \mathbf{X}_q \mathbf{I}_x)} \right) \tag{3.73}$$

We consider a machine connected with infinite bus, where $V_\infty = 1.0$ and $V_t = 1.17$; a transmission line with impedance $Z_{inf} = R_{inf} + j X_{inf} = 0.02 + j 0.4$ p.u.. Using the machine data attached in appendix A, the initial conditions of the generator are calculated in p.u. as following:

$$\begin{array}{ll}
 i_d = -0.94 & \Psi_d = 3.08 \\
 i_q = 0.35 & \Psi_q = 0.72 \\
 i_f = 2.61 & \Psi_f = 3.55 \\
 V_d = -0.72 & \\
 V_q = 0.92 & \\
 E = 2.94 &
 \end{array}$$

3.6 The complete simplified linear model of generator system

In order to design the terminal voltage controller of the generator, a linearized equation had been developed in previous sections. In accordance with the simplified linear model introduced in the previous section, we can calculate each of the parameters of the linear generator model.

3.6.1 Calculation of the parameters of simplified linear model of a generator

In this section, we calculate the linear system model of a generator connected to an infinite bus with equivalent impedance $0.02 + j 0.4$ p.u. and the infinite bus voltage is 1.0 p.u.. The generator data is listed in Appendix A.

In the linear model which we developed above, six parameters from K_1 to K_6 are obtained as following:

$$K_1 = 1.173, \quad K_2 = 1.436, \quad K_3 = 0.280$$

$$K_4 = 2.531, \quad K_5 = -0.100, \quad K_6 = 0.340$$

3.6.2 Calculation of the parameters for the main exciter

In Appendix C, the exciter test data represents the relationship between the exciter output voltage and the exciter input current. This data shows that the exciter system has not saturation effect. The exciter voltage V_f and E_{FD} in p.u. are the same, therefore the transfer function of the exciter can be expressed as follows:

$$G_E(s) = \frac{E_{FD}}{E_{FE}} = \frac{1}{1 + s T_e} \quad \text{and} \quad T_e = \frac{L_{FE}}{R_{FE}} \quad (3.74)$$

In Appendix A the value of exciter is $R_{FE} = 0.00112$ p.u. , $X_{fd} = 0.55$ p.u. ,

$X_{hd} = 2.18 \text{ p.u.}$, $f_r = 150 \text{ Hz}$ and $L_{FE} = (X_{fd} + X_{hd}) / (2\pi f_r)$.

therefore

$$G_E(s) = \frac{E_{FD}}{E_{FE}} = \frac{1}{1 + 0.98s} \quad (3.75)$$

The time constant of exciter is modified by the loading current.

3.6.3 The block diagram of the complete simplified generator system

The linear models of generator, exciter, and controller as discussed in previous sections can be combined to form a complete generator system, as shown in Figure 3.22.

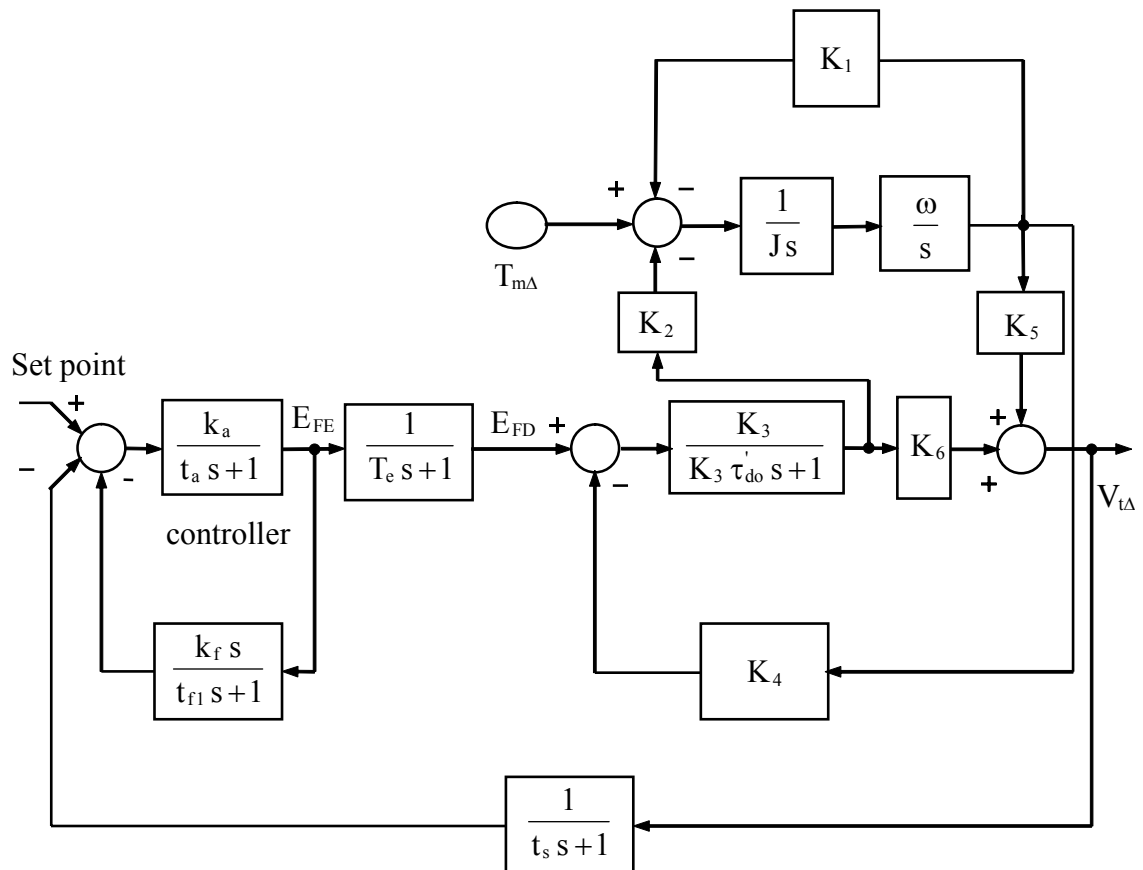


Figure 3.22 The complete linear generator system

Chapter 4 Controller of a synchronous generator

4.1 Introduction

Until now fuzzy systems and neural networks are two of major methods of artificial intelligence. Fuzzy modeling or fuzzy identification, first explored systematically by Takagi and Sugeno [46], has found numerous practical applications in control [45], and forecasting [47]. Fuzzy systems have proved to be very effective in applications to various areas without employing precise quantitative analyses. However, we should note that there are no standard methods for transforming human knowledge or experience into rules of a fuzzy inference system. On the other hand, neural networks have two major functions, learning and recalling. They have been applied to many areas such as image identification [48], representation of system model and control [49-51], and so on. For control engineering, neural networks are attractive in several aspects. They have processing capability for nonlinear plant modeling, can handle large amounts of sensory information and have learning ability. Neural controllers are high dimensional nonlinear controllers, with the capability to provide desired performance, but difficult for suitable tuning by trail and error method.

Fuzzy systems and neural networks are powerful design tools with their own strengths and weaknesses. Neural networks require computational effort, they lack an easy way to verify and optimize a solution, and the solution itself remains a “black box”. On the other hand, fuzzy systems are inherently approximate systems, lacking a general solution to the tuning problem. To overcome these deficiencies the neural-fuzzy approach has been developed based on fuzzy associative memories [46].

In this chapter, the root locus design method is introduced first, then fuzzy operation and neural networks are presented, and finally, the combined fuzzy neural network will be introduced in detail.

4.2 Root locus design method

To design a control system it is always necessary to know the system specification. According to this specification the system performance is also decided. Since the roots of the characteristic equation plays an important role in the dynamic behavior of a linear system, an important problem in linear control systems theory is the investigation of the locus of the root of the characteristic equation. If roots of the characteristic equation are known, then the transient response and stability of the system can be determined.

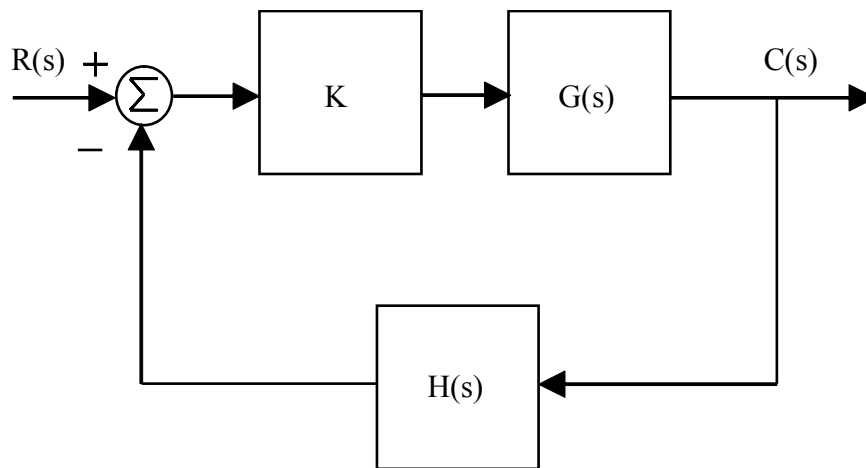


Figure 4.1 The basic control block

Considering Figure 4.1, the closed-loop transfer function of a control system is given as equation (4.1):

$$\frac{C(s)}{R(s)} = \frac{K G(s)}{1 + K G(s) H(s)} \quad (4.1)$$

where $G(s)$ is the transfer function of the process, $R(s)$ is the input signal, $C(s)$ is the output signal, $H(s)$ is the feedback transfer function and K is a variable constant. The characteristic equation is obtained by setting the denominator of $1 + K G(s) H(s)$ in equation (4.1) to zero. The characteristic equation is represented as equation (4.2):

$$1 + KG(s)H(s) = 0 \quad (4.2)$$

The transfer function $KG(s)H(s)$ can be expressed in pole-zero form, as shown in equation (4.3).

$$KG(s)H(s) = \frac{K(s + z_1)(s + z_2) \cdots (s + z_m)}{(s + p_1)(s + p_2) \cdots (s + p_n)} \quad (4.3)$$

where K is a constant, z_1, z_2, \dots, z_m are zeros of $G(s)H(s)$ and p_1, p_2, \dots, p_n are poles of $G(s)H(s)$.

Equation (4.2) can be rewritten as:

$$G(s)H(s) = -\frac{1}{K} \quad (4.4)$$

To satisfy this equation, the magnitude and phase in equation (4.4) must be met simultaneously.

$$|G(s)H(s)| = \frac{1}{|K|} \quad -\infty < K < \infty \quad (4.5)$$

$$\angle G(s)H(s) = (2k + 1)\pi \quad K \geq 0 \quad (4.6)$$

$$\angle G(s)H(s) = 2k\pi \quad K < 0 \quad (4.7)$$

If equation (4.3) is substituted for equation (4.2), then equation (4.5), (4.6) and (4.7) can be modified as:

$$\frac{\prod_{i=1}^m |s + z_i|}{\prod_{j=1}^n |s + p_j|} = \frac{1}{|K|} \quad -\infty < K < \infty \quad (4.8)$$

$$\angle G(s)H(s) = \sum_{i=1}^m \angle s + z_i - \sum_{j=1}^n \angle s + p_j = (2k + 1)\pi \quad K \geq 0 \quad (4.9)$$

$$\angle G(s)H(s) = \sum_{i=1}^m \angle s + z_i - \sum_{j=1}^n \angle s + p_j = 2k\pi \quad K < 0 \quad (4.10)$$

Equation (4.8), (4.9), and (4.10) may be used for the construction of the complete root locus in the s-plane. The relationship is interested between the position of roots on locus plot and the time domain response solution. A simple second-order system shown in equation (4.11) is investigated to display the relationship between the root locus and time response.

$$\frac{C(s)}{R(s)} = \frac{K}{s^2 + 2\xi\omega_n s + \omega_n^2} \quad (4.11)$$

ξ , ω_n are the damping ratio and natural frequency respectively. The transient response to a step input in equation (4.11) is:

$$c(t) = c_1 e^{s_1 t} + c_2 e^{s_2 t} \quad (4.12)$$

where the roots of this characteristic equation are:

$$\begin{aligned} s_1 &= -\xi\omega_n + j\omega_n \sqrt{1-\xi^2} = \sigma + j\omega_d \quad \xi < 1 \\ s_2 &= -\xi\omega_n - j\omega_n \sqrt{1-\xi^2} = \sigma - j\omega_d \end{aligned} \quad (4.13)$$

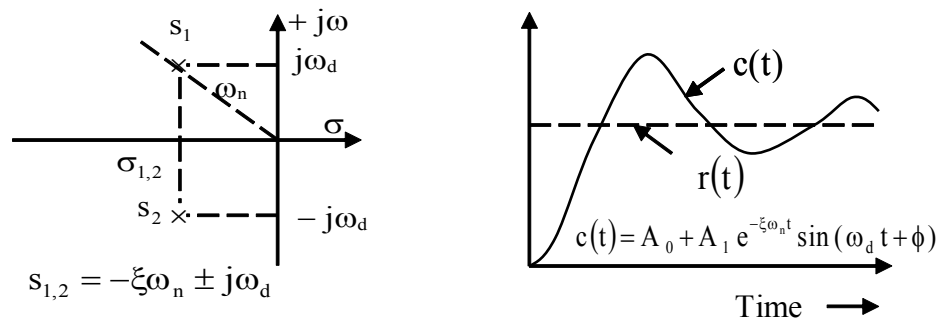
Thus

$$c(t) = Ae^{\sigma t} \sin(\omega_d t + \phi) \quad (4.14)$$

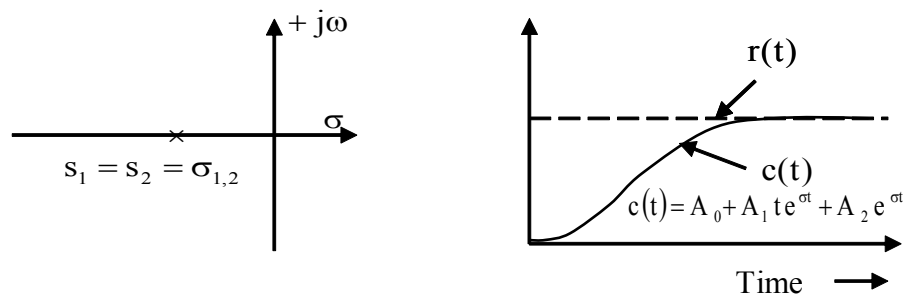
In Figure 4.2 six different cases are tested to show both the locations of the roots and the corresponding transient response plots. As shown in Figure 4.2, in the case of $\xi=0$ the roots lie on the $j\omega$ axis (plot D in Figure 4.2) and the time response has sustained oscillation. When $\xi\omega_n$ is negative, it means that the location of the root is in the right plane and it will result in unstable response. This is shown in Figure 4.2 (E) and (F). Therefore, it is necessary in a stable system that $\xi\omega_n$ is positive or the roots of characteristic equation must lie on left-half plane for a stable system. Figure 4.2 (A), (B) and (C) depict three different time responses due to different location of roots of the characteristic equation on the left-half plane. Figure 4.2 (A) indicates that the

damping ratio ξ is between 0 and 1 and the system has oscillation. Figure 4.2 (B) shows that damping ratio ξ is 1 and the system response likes a first-order system response with the same time constant.

(A)



(B)



(C)

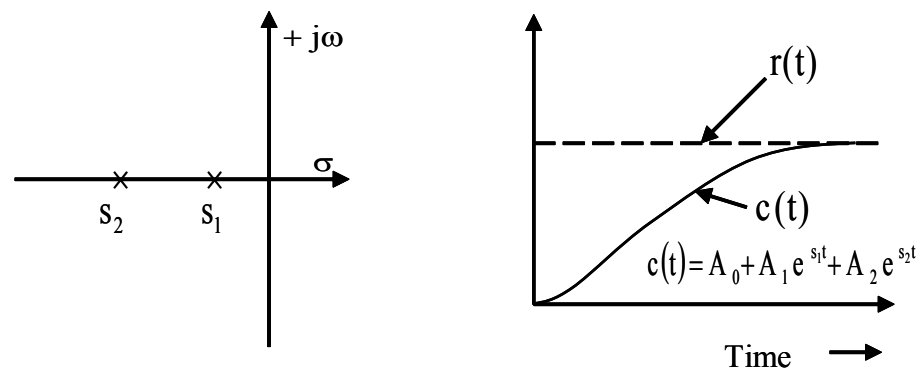
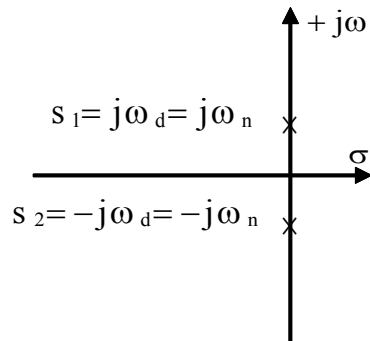
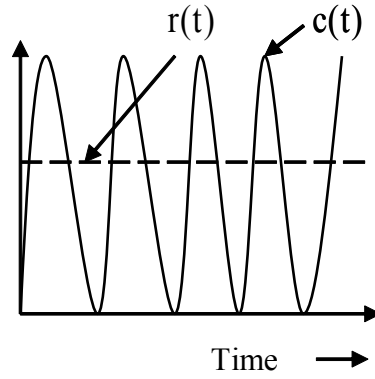


Figure 4.2 Plot of the roots of a second order characteristic equation in the s-plane and their correlation to the transient response in the time domain

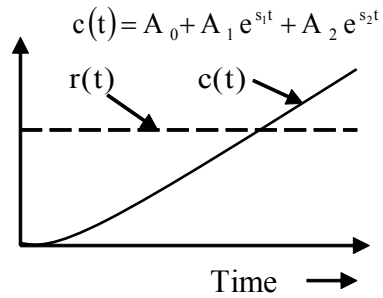
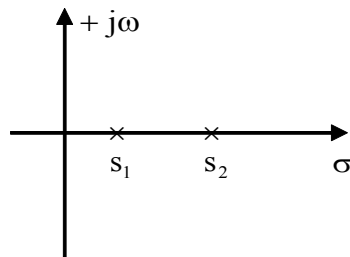
(D)



$$c(t) = A_0 + A_1 \sin(\omega_d t + \phi)$$



(E)



(F)

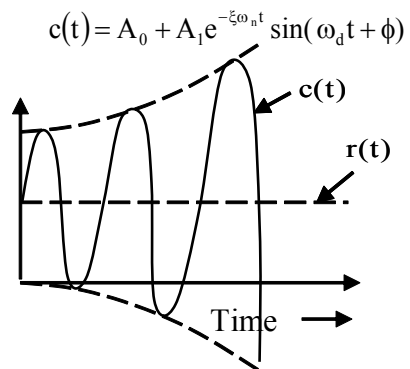
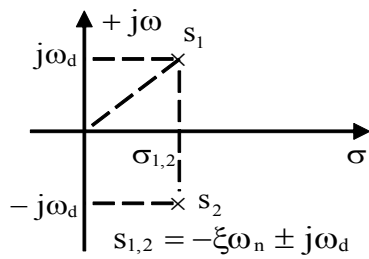


Figure 4.2 Plot of the roots of a second order characteristic equation in the s-plane and their correlation to the transient response in the time domain

Figure 4.2 (C) shows that damping ratio ξ is 1 and the system response of Figure 4.2 (C) is the cascade of two first-order systems with different time constant.

Figure 3.8 is a linearized torque-angle relation. The root locus plot for Figure 3.8 is shown in Figure 4.3 and the time response is shown in Figure 4.4, where the inertial moment J is 7 s, $\omega_n = 7.25$, $K=1$ and K_1 is 1.173. The roots in Figure 4.3 lie on an imaginary axis; therefore, the step response of this system is a sustained oscillation.

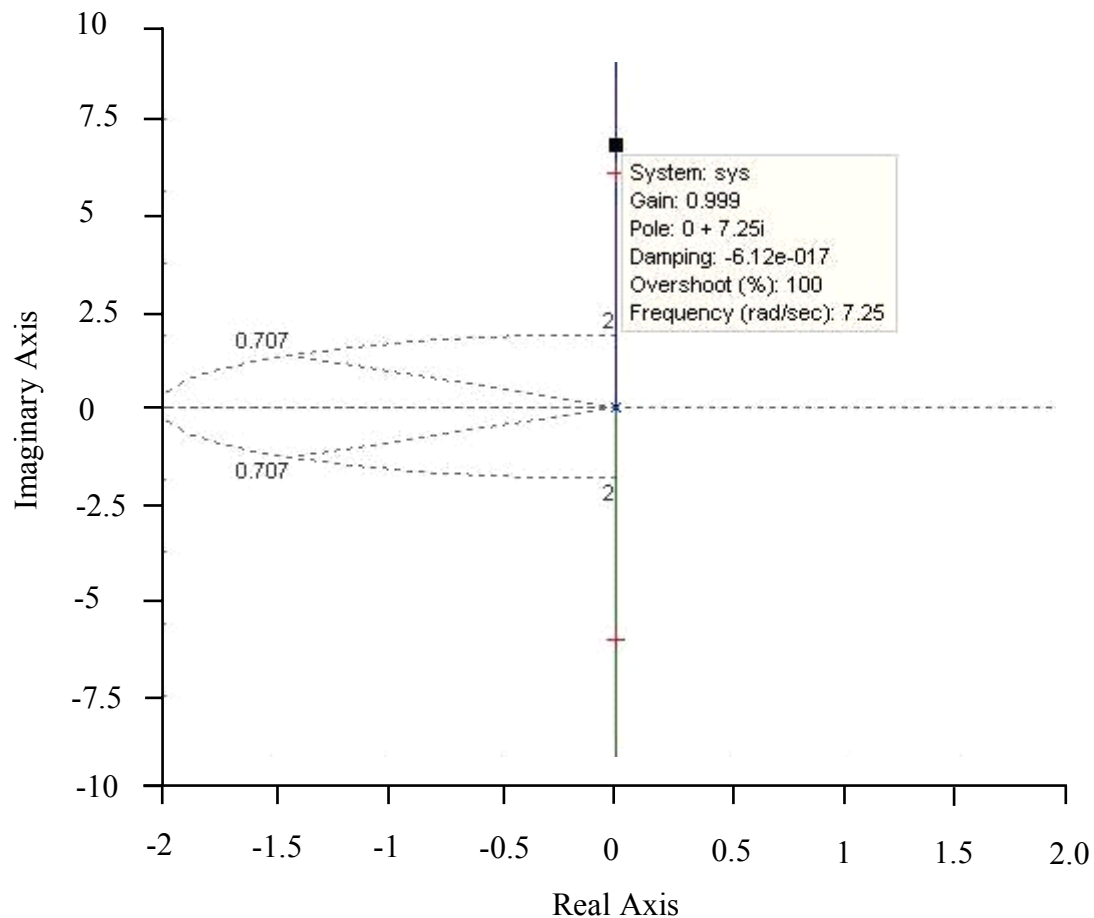


Figure 4.3 The root locus plot for linearized mechanical torque and rotor angle relation

Figure 3.9 is a linearized torque and angle relationship with a demagnetized effect. The root locus plot for Figure 3.9 is shown in Figure 4.5, where the roots of the characteristic equation are $-0.138 \pm j7.17$ and -4.26 . The time response for the output of the angle of rotor responding to a step input into a mechanical input is shown in Figure 4.6, where

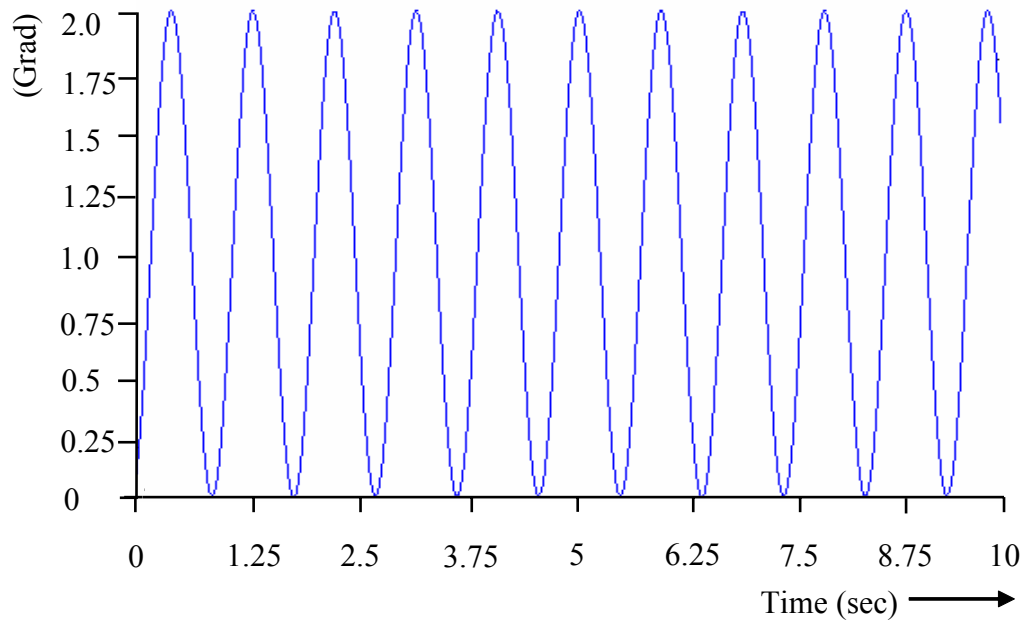


Figure 4.4 The time response of the rotor angle suffered from step mechanical torque input

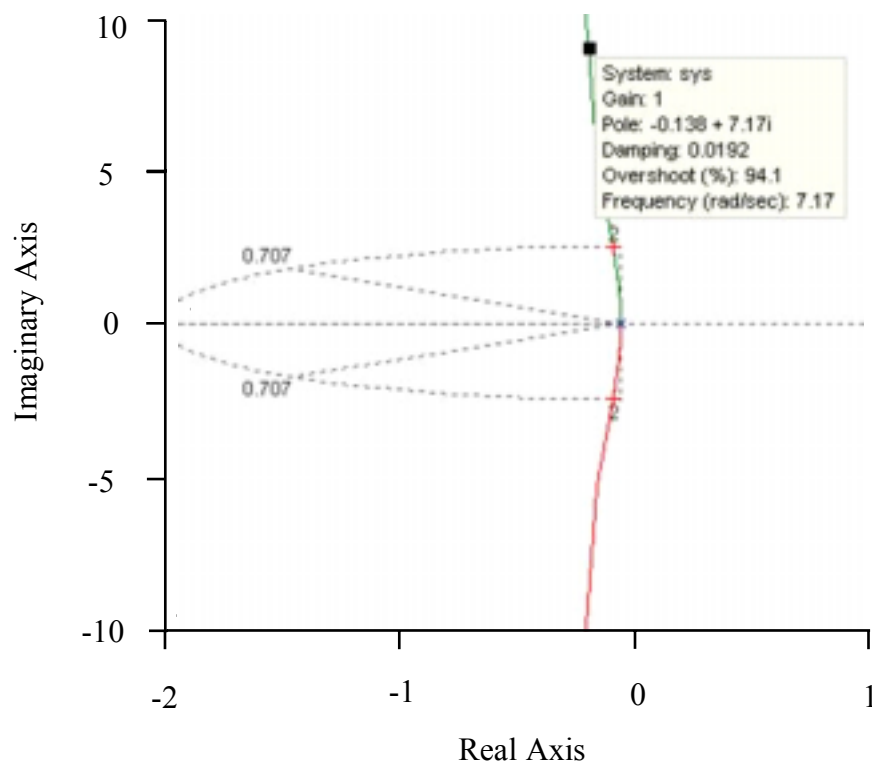


Figure 4.5 The root locus plot for linearized torque and the rotor angle relation with demagnetized effect

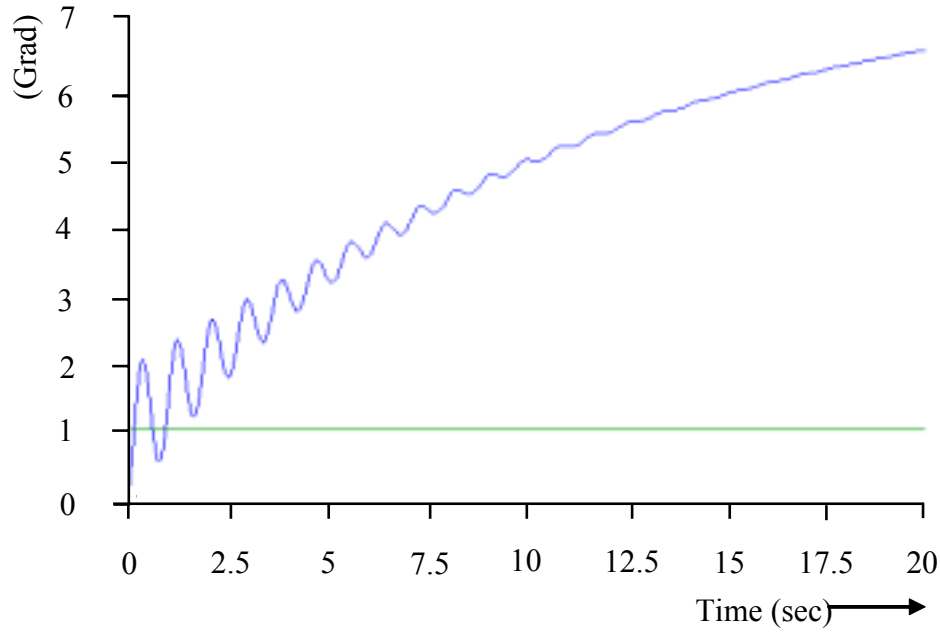


Figure 4.6 The time response of rotor angle for linearized torque and rotor angle relation with demagnetized effect

K_2 , K_3 and K_4 are calculated as shown in section 3.6. Figure 4.6 shows that the demagnetized effect supplied a small quantity of damping.

4.3 Fuzzy system

The idea of fuzzy sets was born in July 1964. Professor A. Zadeh, who worked in the department of electrical engineering and computer science at the University of California, Berkeley, believed that all real-world problems could not be solved with efficient and analytical methods. He felt that traditional systems analysis techniques were too precise for many complex real-world problems. A different kind of mathematics, in which fuzzy or imprecise quantities could be described, was needed.

4.3.1 Fuzzy logic

In 1976 Blue Circle Cement and SIRA in Denmark developed the first industrial application of fuzzy logic [66]. After that many different applications of fuzzy sets on industrial control were successfully developed.

The core technique of fuzzy logic is based on the following basic structures

1. Fuzzy set: sets with smooth boundaries.
2. Linguistic variable: variables whose values are both qualitatively and quantitatively described by a fuzzy set.
3. Possibility: constraints on the value of a linguistic variable imposed by assigning it to a fuzzy set.
4. Fuzzy IF-THEN rules: a knowledge representation scheme for describing a functional mapping or a logic formula that generalizes an implication in two-value logic.

4.3.2 Fuzzy set

A fuzzy set is a set with a smooth (unsharp) boundary. Fuzzy sets generalize the classical set theory to allow partial membership. A set in classical set theory always has a sharp boundary, but a fuzzy set directly addresses this limitation by allowing membership in a set to be a matter of degree. The degree of the membership function in a set is expressed by a number between 0 and 1; 0 means entirely not in the set, 1 means completely in the set, and a number in between means partially in the set. A fuzzy set is thus defined by a function that maps objects in a domain of concern to their membership value in the set. Such a function is called a membership function. Figure 4.7(a) and (b) illustrate membership functions of high temperature distribution for classical and fuzzy sets, respectively.

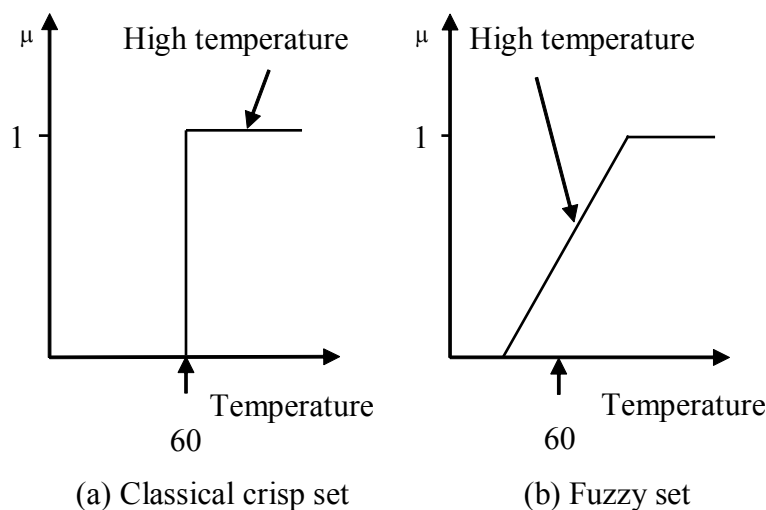


Figure 4.7 Membership functions for high temperature distribution

In Figure 4.7 (a) the temperature exactly over 60 is called high temperature, and (b) is the high temperature gradually transitive.

The purpose of a membership function is that it provides a gradual transition from regions completely outside a set to regions completely in the set. The membership function can be designed in three ways:

1. Interview those who are familiar with the underlying concept and later adjust it based on a tuning strategy.
2. Construct it automatically from data.
3. Learn it based on the feedback from the system performance.

In the early day the first approach was the main approach used by fuzzy logic research and engineer. Due to a lack of systematic tuning strategies in those days, most fuzzy systems were tuned through a trial-and-error process. This has become one of the main criticisms of fuzzy logic technology. Fortunately, many techniques in the second two categories have been developed using statistical techniques, neural networks and genetic algorithms.

There exist numerous types of membership functions, such as triangular, trapezoidal, Gaussian, bell-shaped membership function and so on. Most practitioners have found that triangular and trapezoidal membership functions are sufficient for developing good approximate solutions for the problem they wish to solve. Membership functions that are differentiable have certain advantages in their application to the neuro-fuzzy-system. Gaussian membership function has been a popular choice for this.

Three different membership function distributions are shown on Figure 4.8: (a) is the triangular function, (b) is the trapezoidal function and (c) is the Gaussian function.

A triangular membership function is specified by three parameters $\{a, b, c\}$ as follows:

$$\text{Triangle (x: a, b, c)} = \begin{cases} 0 & x < a \\ \frac{(x-a)}{(b-a)} & a \leq x \leq b \\ \frac{(c-x)}{(c-b)} & b \leq x \leq c \\ 0 & x > c \end{cases} \quad (4.15)$$

A trapezoidal membership function is specified by four parameters {a, b, c, d} as follows:

$$\text{Trapezoid (x: a, b, c, d)} = \begin{cases} 0 & x < a \\ \frac{(x-a)}{(b-a)} & a \leq x < b \\ 1 & b \leq x < c \\ \frac{(d-x)}{(d-c)} & c \leq x < d \\ 0 & x > d \end{cases} \quad (4.16)$$

A Gaussian membership function is specified by two parameters {m, } as follows:

$$\text{Gaussian (x: m,)} = \exp\left(-\frac{(x-m)^2}{\sigma^2}\right) \quad (4.17)$$

where m, σ denote the mean value and standard deviation of the function.

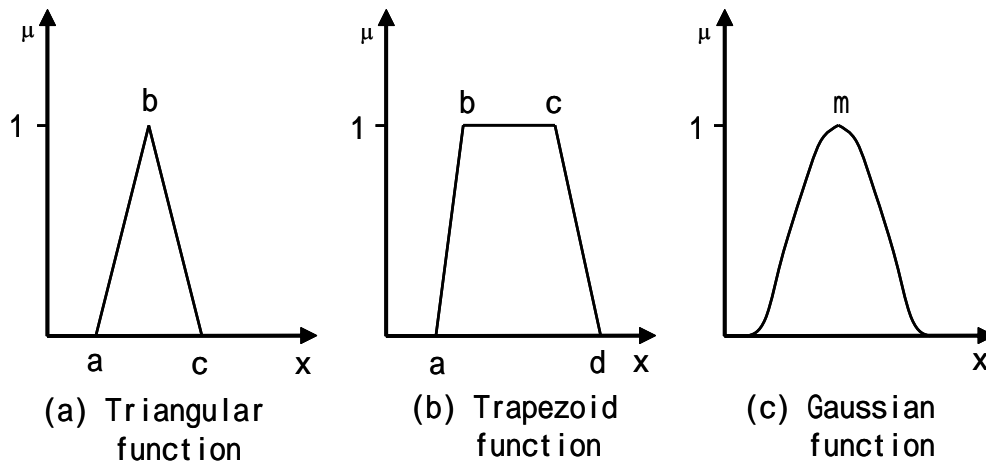


Figure 4.8 Three different membership function

4.3.3 Fuzzy IF-THEN rules

A fuzzy rule is the basic unit for capturing knowledge in fuzzy systems. A fuzzy rule has two components: an IF-part (referred to as the antecedent) and a THEN-part (also referred to as the consequent). The basic format of the fuzzy rule is:

IF < antecedent > THEN < consequent >

The antecedent describes the condition, and the consequent describes the conclusion that can be applied when the condition holds. The structure of a fuzzy rule is identical to that of a conventional rule in artificial intelligence. The main difference lies in the content of the rule's antecedent - the antecedent of a fuzzy rule describes an elastic condition while the antecedent of a conventional rule describes a rigid condition.

The consequent of a fuzzy rule can be classified as being of any of three types:

- Crisp consequent: IF ... THEN $y = a$
where a is a nonfuzzy numeric value or symbolic value.
- Fuzzy consequent: IF ... THEN $y = A$
where A is a fuzzy set.
- Functional consequent:
IF x_1 is A_1 AND x_2 is A_2 AND ... AND x_n is A_n
THEN $y = a_0 + \sum_{i=1}^n a_i x_i$
where a_0, a_1, \dots, a_n are constants.

Each type of rule consequent has its merit. Generally speaking, a fuzzy rule with a crisp consequent can be processed more efficiently. A rule with fuzzy consequent is easier to understand and more suitable for capturing imprecise human expertise. Finally, rules with a functional consequent can be used to approximate complex nonlinear models using only a small number of rules.

4.3.4 Fuzzy rule-based inference

The algorithm of a fuzzy rule-based inference consists of four basic steps:

1. Fuzzy Matching: Calculates the degree to which the input data match the condition of the fuzzy rules.
2. Inference: Calculates the rule's conclusion based on its matching degree.
3. Combination: Combines the conclusion inferred by all fuzzy rules into a final conclusion.
4. Defuzzification: This step transforms the fuzzy result of the inference into a crisp output.

An example for the terminal voltage control of a synchronous generator is used to explain the fuzzy-rules inference system. Two parameters must be detected to decide the control signal of the exciter. They are error (the difference between setting voltage and terminal voltage) and error derivative.

The quantity of error and error derivative are described with the fuzzy set. Figure 4.9 is the membership function of error. It is divided into five categories; there are Negative Big (NB), Negative Middle (NM), Zero (Z), Positive Middle (PM) and Positive Big (PB).

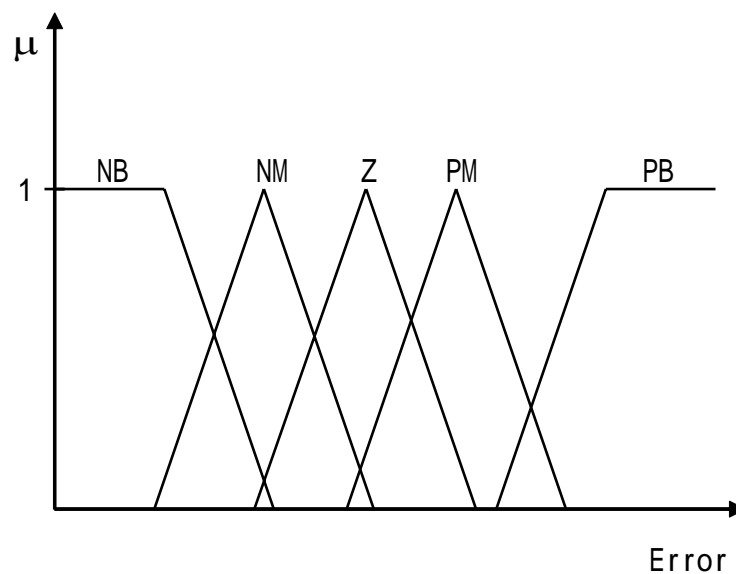


Figure 4.9 Membership function of error for terminal voltage control

Figure 4.10 shows the membership function for error derivative. It is divided into three categories; Negative (N), Zero (Z) and Positive (P). Figure 4.11 displays the membership function for fuzzy decisions related to the input of the exciter. It is divided into five categories; these are Negative Big (NB), Negative Middle (NM), Zero (Z), Positive Middle (PM) and Positive Big (PB). Each of the membership functions in Figure 4.9 to 4.11 is represented by a triangular function.

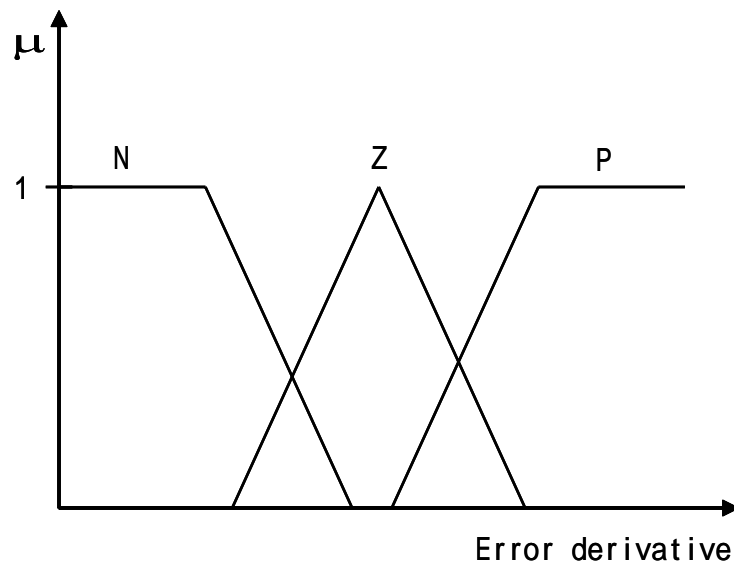


Figure 4.10 Membership function for error derivative

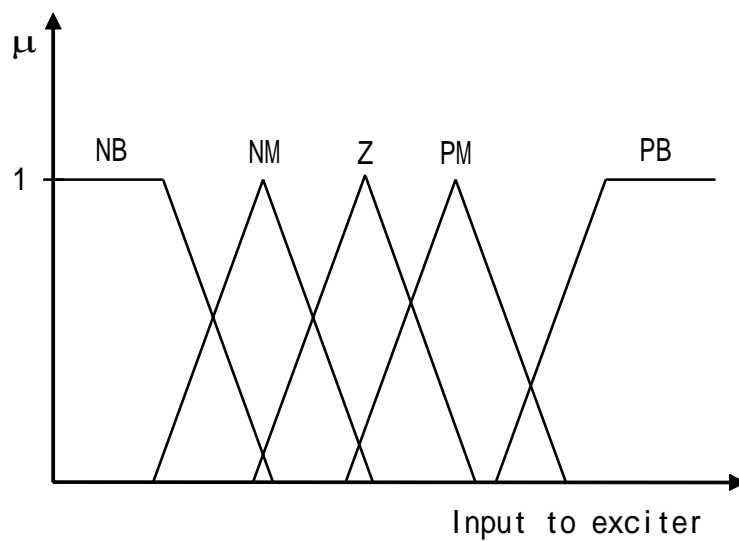


Figure 4.11 Membership function for input of exciter

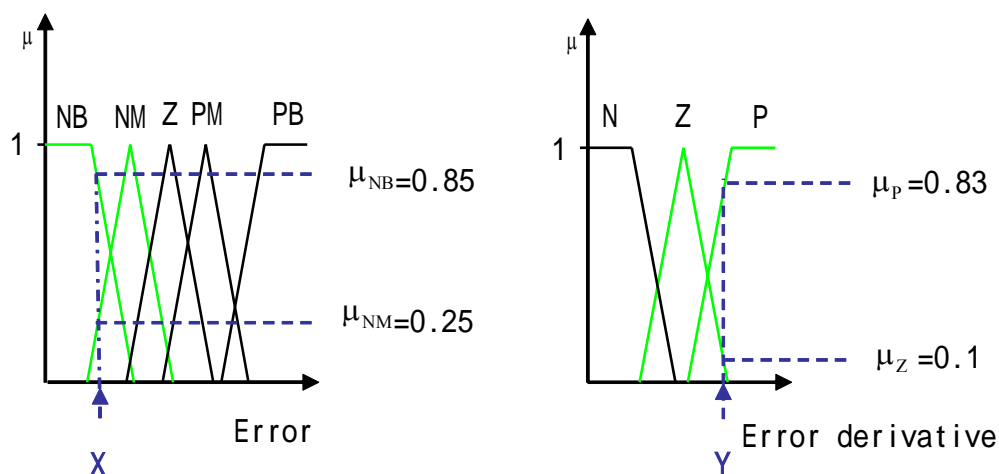
For the terminal voltage control, rules should combine conditions on error quantity and error derivative using conjunction (AND). Two rules for selecting output of exciter are listed below:

- R1: IF error is Negative Big AND error derivative is Positive
THEN the output of exciter is Positive Big
- R2: IF error is Negative Middle AND error derivative is Zero
THEN the output of exciter is Positive Middle

4.3.4.1 Fuzzy matching

Fuzzy matching is used to calculate the degree to which the input data match the antecedent conditions of the fuzzy rules. Let X is a value for error detected by a sensor and Y is a value of error derivative. The value X shown in Figure 4.12 (a) belongs to the fuzzy set “Negative Big” and “Negative Middle”. The degree matching fuzzy set “Negative Big” is 0.85 of membership function μ_{NB} and the degree matching to fuzzy set “Negative Middle” is 0.25 of membership function μ_{NM} .

The value Y shown in Figure 4.12 (b) belong to fuzzy sets “Positive” and “Zero”. The degree matching fuzzy set “Positive” is 0.83 of membership function μ_P and the degree matching to fuzzy set “Zero” is 0.1 of membership function μ_Z .



(a) Matching degree for error

(b) Matching degree for error derivative

Figure 4.12 Fuzzy matching degree for the antecedent part of fuzzy rule for the terminal voltage control

4.3.4.2 Inference

After the fuzzy matching step, a fuzzy inference step is invoked for each of the relevant rules to produce a conclusion based on their matching degree. When a rule has multiple conditions combined using the operator AND (conjunction) in the antecedent part, the fuzzy conjunction operator can be used to combine the matching degree of each condition. One of the most commonly used fuzzy conjunction operators is the MIN operator. The function of operator “MIN” is to get the minimum value from all matching values in the antecedent part of one rule. Another fuzzy conjunction operator used for this purpose is the product (i.e. multiplication) operator. Figure 4.13 illustrated the use of the MIN operator for combining the matching degree in the antecedent part. For the first rule R1 in Figure 4.13 the condition “error is Negative Big” matches the sensor input (X) 0.85; and the second condition “error derivative is Positive” matches the sensor input (Y) 0.83. Combining the two matching degrees using MIN, 0.83 is obtained as the degree to which the input data match the antecedent of the rule R1. Similarly, we can find the degree matching second rule R2 to be 0.1.

The membership function in the consequent part can be produced by suppressing the membership function of the consequent part using the matching degree of the antecedent part in the fuzzy rule. In Figure 4.14 (a) the inferred conclusion “Positive Big” by rule one (R1) is shown by diagonal line. Also in Figure 4.14 (b) show the inferred conclusion “Positive Middle” by rule two (R2).

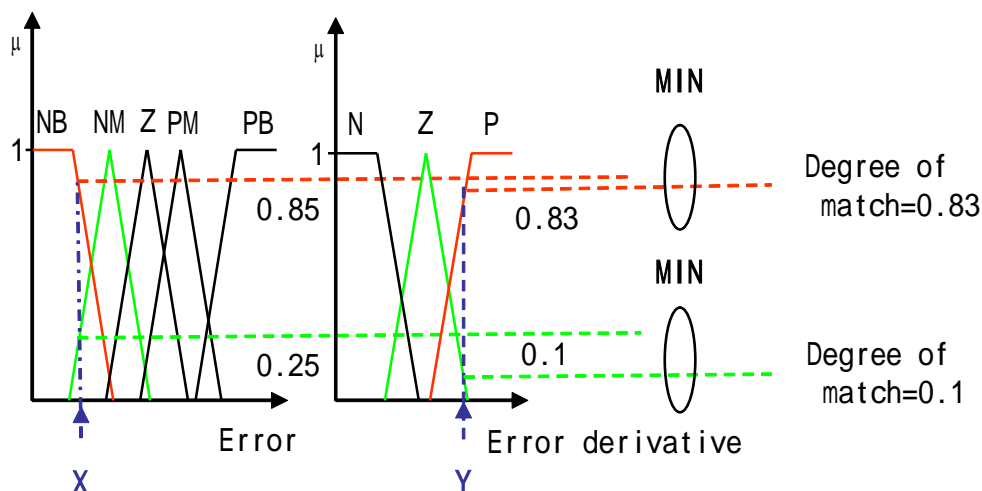


Figure 4.13 Fuzzy matching for conjunctive conditions using ‘MIN’ operator

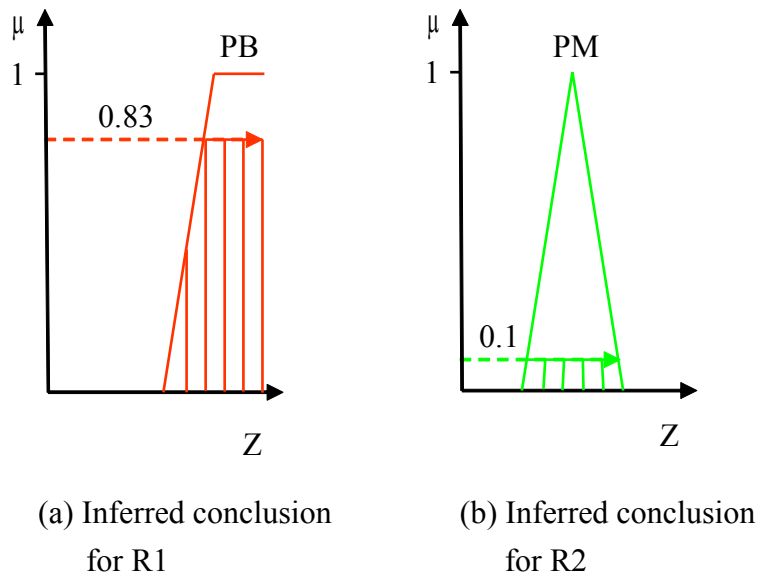


Figure 4.14 Inferred conclusions for rules R1 and R2

4.3.4.3 Combination of the conclusions

The two steps described in the last sections enable each fuzzy rule to infer a fuzzy statement about the value of the consequent variable. Because a fuzzy rule-based system consists of a set of fuzzy rules with partially overlapping conditions, a particular input to the system often triggers multiple fuzzy rules; therefore it is necessary to combine the inference results of these rules. This is accomplished, typically, by superimposing all fuzzy conclusions about a variable. Figure 4.15 is the combination of the two conclusions shown in Figure 4.14.

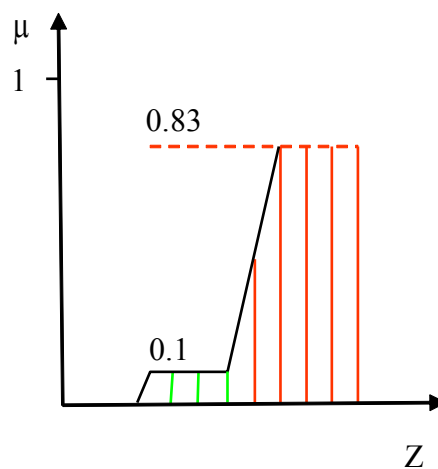


Figure 4.15 The combination of two conclusion membership functions

4.3.4.4 Defuzzification

For a system whose final output needs to be a crisp (nonfuzzy) form, it is necessary to convert the final combined fuzzy conclusion into a crisp one. There are two major defuzzification techniques:

1. The Mean Of Maximum (MOM) method
2. The Center Of Area (COA) or the centroid method.

4.3.4.4.1 The mean of maximum method

The mean of maximum defuzzification calculates the average of all variables with maximum membership degree. Suppose z is a fuzzy conclusion to be defuzzified. The mean of maximum method can be expressed using the following formula:

$$\text{MOM}(A) = \sum_{j=1}^m \frac{z_j}{m} \quad (4.18)$$

where z_j is the support value at which the membership function reaches the maximum value and m is the number of such support number. Figure 4.16 (a) shows the defuzzification using MOM method.

4.3.4.4.2 The center of area

The Center of Area method (COA also referred to as the center-of-gravity, or centroid method in the literature) is the most popular defuzzification techniques. Unlike MOM, the COA method takes into account the entire possibility distribution in calculating its representative point. The defuzzification method is similar to the formula for calculating the center of gravity in physics, if the membership function $\mu_A(z)$ is viewed as the density of mass at z . alternatively, we can view the COA method as calculating a weighted average. The defuzzification formula can be expressed with the continuous form as:

$$\text{COA}(A) = \frac{\int \mu_A(z) z dz}{\int \mu_A(z) dz} \quad (4.19)$$

The main disadvantage of the COA method is its high computational cost. The output using the COA method is shown in Figure 4.16 (b).

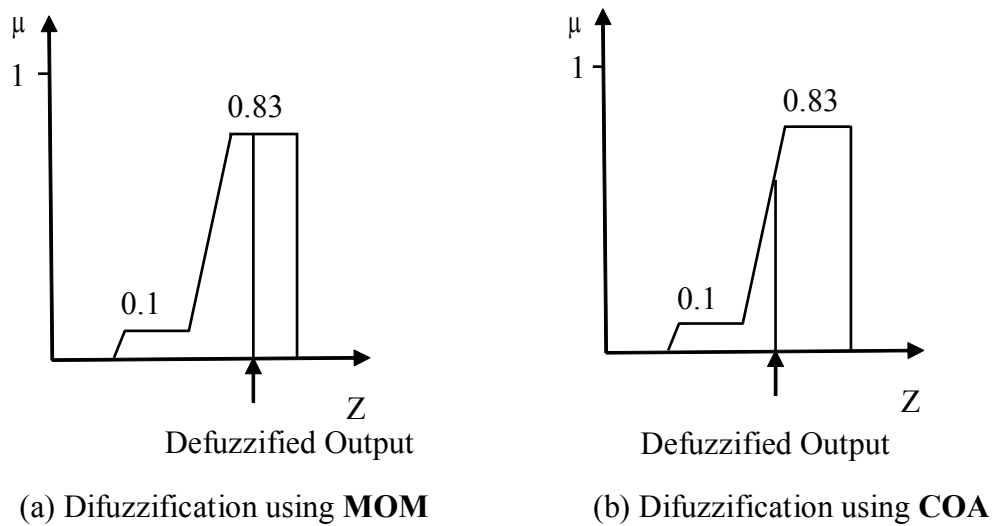


Figure 4.16 Two different defuzzification methods

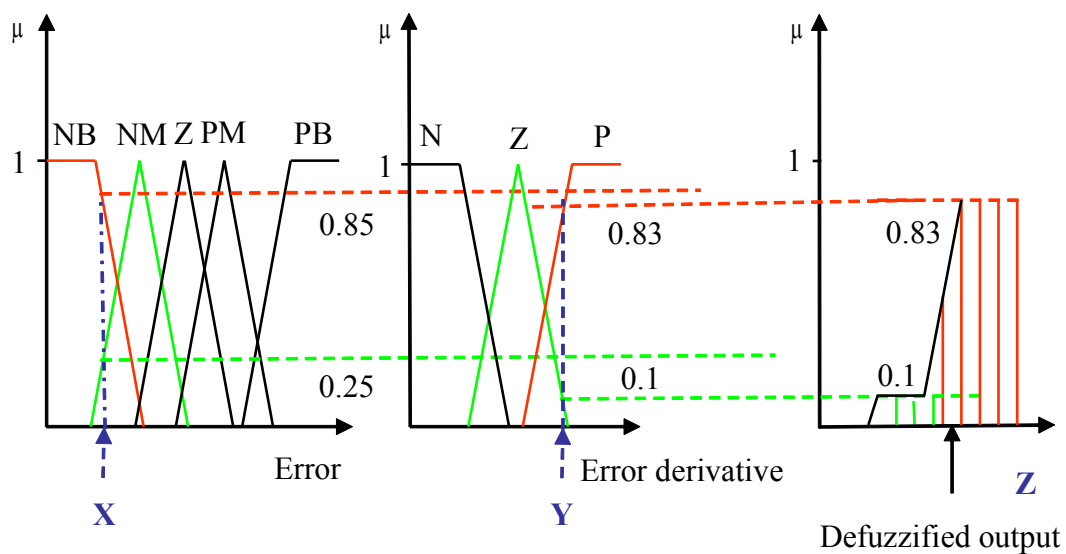


Figure 4.17 Fuzzy rule-based inference for a terminal voltage control

Figure 4.17 shows the result of combining all four steps of the fuzzy control system for terminal voltage control system. The centroid defuzzification technique is used in this example. Here X and Y are two input signals to fuzzy sets.

4.4 Neural network

The neural network, which had its beginning at the Dartmouth Research Conference in 1956, is capable of making machines to perform human-like or intelligent tasks. The first perceptron, a generalization of the McCulloch-Pitt concept of the function of the brain by adding learning, was proposed by Frank Rosenblatt to identify both abstract and geometrical patterns[62].

An artificial neuron is a model whose components have direct analogs to components of an actual neuron. Figure 4.18 shows the schematic representation of an artificial neuron. Input signals are represented by p_0, p_1, \dots, p_R , which are continuous signals. Each input is modified by a weighted value w_i . This processing element consists of two parts. The first part simply aggregates (sums) the weighted inputs; the second part is effectively a nonlinear filter, usually called the activation function. The activation function can be a threshold function, sigmoid function, linear function, etc..

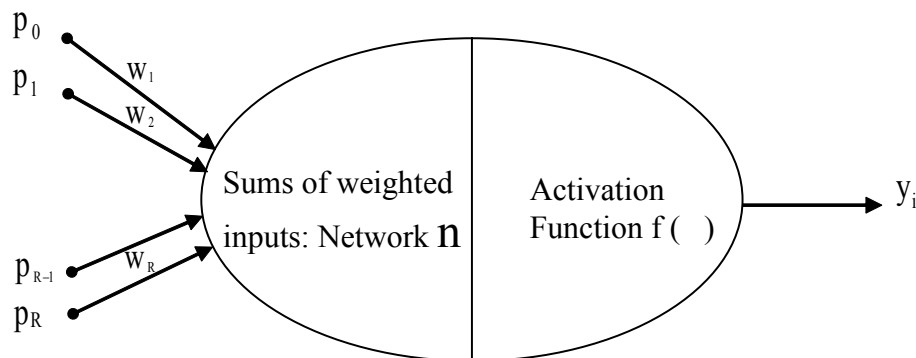


Figure 4.18 Schematic representation of an artificial neuron

4.4.1 The structure of neural network

There are two major neural network (NN) structures. The first structure is a feed forward multilayer networks, as shown in Figure 4.19. It has been proved that the multiple layer networks are quite powerful. A network of two layers, where the first layer is sigmoid and the second layer is linear, can be trained to approximate any arbitrary function of interest, provided sufficiently many hidden units are available [52].

The second neural network structure is a recurrent neural network. This is a network with feedback; some of its outputs are connected to its inputs. Recurrent networks are potentially more powerful than feedforward networks, since they are able to recognize and recall temporal, as well as spatial, patterns. But the behavior of recurrent networks is much more complex than that of feedforward networks. Figure 4.20 shows one type of discrete-time recurrent network. D in Figure 4.20 represents a sampled delay time, P is the input signal, W and b are weighting value and bias respectively. The purpose of this network is used to store one or more stable vectors. These stable vectors can be viewed as memories that the network recalls [63].

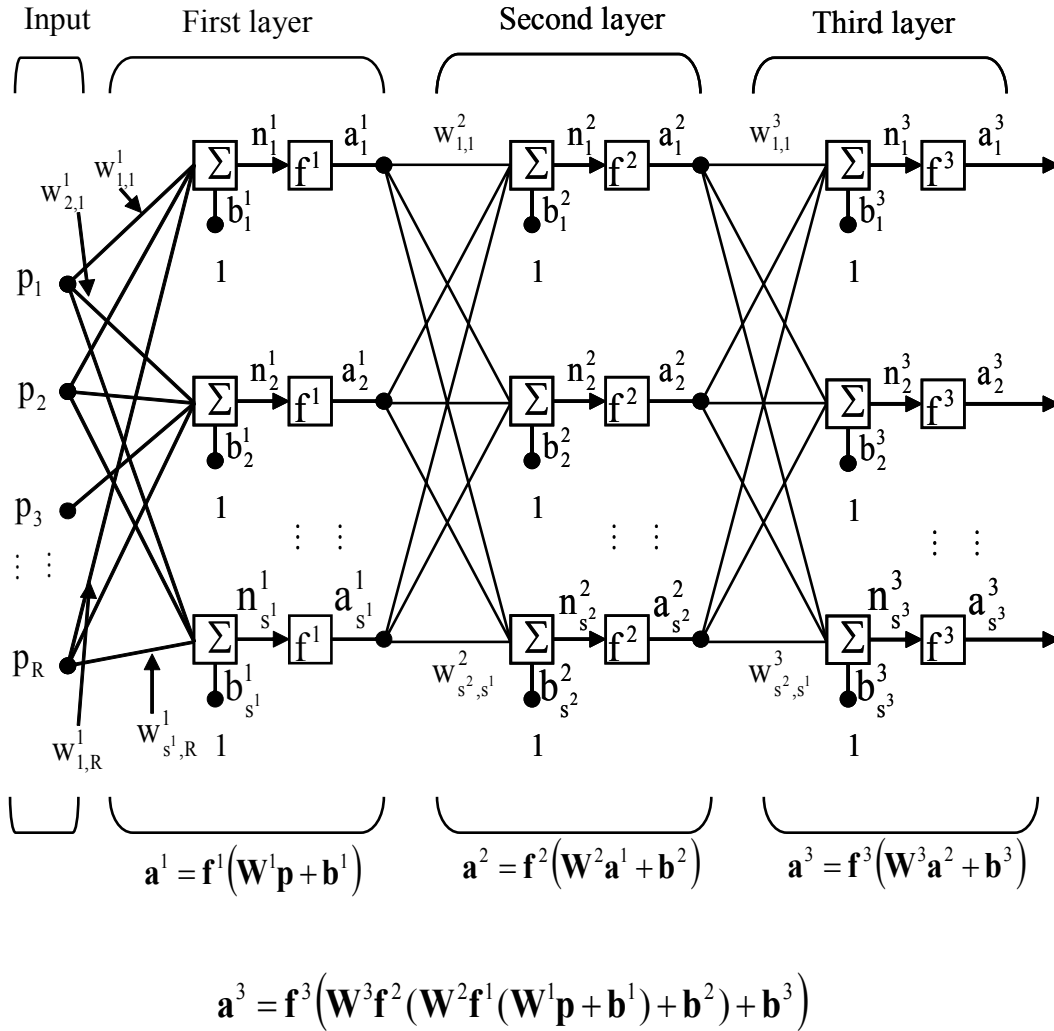


Figure 4.19 The multilayer feedforward network

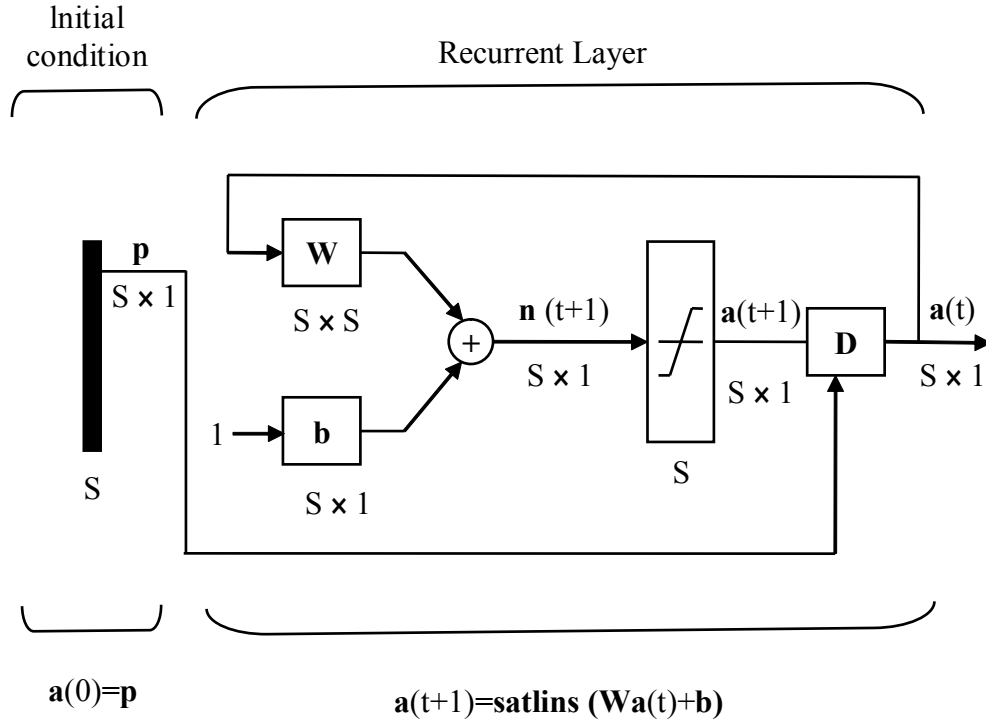


Figure 4.20 Discrete-time recurrent network

4.4.2 The steepest descent method

To train the neural network there are several different classes of network learning rules. Performance learning is an important class of learning law, in which the network parameters are adjusted to optimize the performance of the network. There are two steps involved in this optimization process. At first we must find a quantitative measure of network performance, i.e. a performance index $F(\mathbf{x})$. The second step of the optimization process is to search the parameter space in order to reduce the performance index.

Given a performance index $F(\mathbf{x})$, where \mathbf{x} are parameters we are adjusting:

$$F(\mathbf{x}) = F(x_1, x_2, \dots, x_n) \quad (4.20)$$

The Taylor series expansion for this function $F(\mathbf{x})$ about the point \mathbf{x}^* will be:

$$\begin{aligned}
F(\mathbf{x}) = & F(\mathbf{x}^*) + \frac{\partial}{\partial x_1} F(\mathbf{x}) \Big|_{\mathbf{x}=\mathbf{x}^*} (x_1 - x_1^*) + \frac{\partial}{\partial x_2} F(\mathbf{x}) \Big|_{\mathbf{x}=\mathbf{x}^*} (x_2 - x_2^*) \\
& + \dots + \frac{\partial}{\partial x_n} F(\mathbf{x}) \Big|_{\mathbf{x}=\mathbf{x}^*} (x_n - x_n^*) + \frac{1}{2} \frac{\partial^2}{\partial x_1^2} F(\mathbf{x}) \Big|_{\mathbf{x}=\mathbf{x}^*} (x_1 - x_1^*)^2 \\
& + \frac{1}{2} \frac{\partial^2}{\partial x_1 \partial x_2} F(\mathbf{x}) \Big|_{\mathbf{x}=\mathbf{x}^*} (x_1 - x_1^*) (x_2 - x_2^*) + \dots
\end{aligned} \tag{4.21}$$

This can be written in matrix form as following:

$$F(\mathbf{x}) = F(\mathbf{x}^*) + \nabla F(\mathbf{x})^T \Big|_{\mathbf{x}=\mathbf{x}^*} (\mathbf{x} - \mathbf{x}^*) + \frac{1}{2} (\mathbf{x} - \mathbf{x}^*)^T \nabla^2 F(\mathbf{x}) \Big|_{\mathbf{x}=\mathbf{x}^*} (\mathbf{x} - \mathbf{x}^*) + \dots \tag{4.22}$$

where the gradient $\nabla F(\mathbf{x})$ is defined as:

$$\nabla F(\mathbf{x}) = \left[\frac{\partial}{\partial x_1} F(\mathbf{x}) \quad \frac{\partial}{\partial x_2} F(\mathbf{x}) \quad \dots \quad \frac{\partial}{\partial x_n} F(\mathbf{x}) \right]^T \tag{4.23}$$

and $\nabla^2 F(\mathbf{x})$ is called a Hessian matrix.

$$\nabla^2 F(\mathbf{x}) = \begin{bmatrix} \frac{\partial^2}{\partial x_1^2} F(\mathbf{x}) & \frac{\partial^2}{\partial x_1 \partial x_2} F(\mathbf{x}) & \dots & \frac{\partial^2}{\partial x_1 \partial x_n} F(\mathbf{x}) \\ \frac{\partial^2}{\partial x_2 \partial x_1} F(\mathbf{x}) & \frac{\partial^2}{\partial x_2^2} F(\mathbf{x}) & \dots & \frac{\partial^2}{\partial x_2 \partial x_n} F(\mathbf{x}) \\ \vdots & \vdots & \dots & \vdots \\ \frac{\partial^2}{\partial x_n \partial x_1} F(\mathbf{x}) & \frac{\partial^2}{\partial x_n \partial x_2} F(\mathbf{x}) & \dots & \frac{\partial^2}{\partial x_n^2} F(\mathbf{x}) \end{bmatrix} \tag{4.24}$$

Now in order to minimize $F(\mathbf{x})$ the value \mathbf{x} must be found. The optimization algorithm is assumed to be iterative. Some initial guess, \mathbf{x}_0 are given and then update our guess in stages according to an equation of the form:

$$\mathbf{x}_{k+1} = \mathbf{x}_k + \eta \mathbf{u}_k \tag{4.25}$$

or

$$\Delta \mathbf{x}_k = (\mathbf{x}_{k+1} - \mathbf{x}_k) = \eta \mathbf{u}_k \tag{4.26}$$

For finding the proper \mathbf{x} , we would like the performance index $F(\mathbf{x})$ to decrease at each iteration, as following:

$$F(\mathbf{x}_{k+1}) < F(\mathbf{x}_k) \quad (4.27)$$

Consider a first-order Taylor series expansion as shown in equation (4.22).

$$F(\mathbf{x}_{k+1}) = F(\mathbf{x}_k + \Delta\mathbf{x}_k) \cong F(\mathbf{x}_k) + \mathbf{g}_k^T \Delta\mathbf{x}_k \quad (4.28)$$

where \mathbf{g}_k is the gradient evaluated at our old guess \mathbf{x}_k .

$$\mathbf{g}_k^T \equiv \nabla F(\mathbf{x})|_{\mathbf{x}=\mathbf{x}_k}$$

For $F(\mathbf{x}_{k+1})$ to be less than $F(\mathbf{x}_k)$, then the second term on the right hand side of equation (4.28) must be negative, i.e.

$$\mathbf{g}_k^T \Delta\mathbf{x}_k = \eta \mathbf{g}_k^T \mathbf{u}_k < 0 \quad (4.29)$$

η is the learning rate and is selected as a small but greater than zero. This implies:

$$\mathbf{g}_k^T \mathbf{u}_k < 0 \quad (4.30)$$

The \mathbf{u}_k is the unit direction vector and it satisfies the condition of the equation (4.30). Equation (4.30) is an inner product between the gradient and the unit direction vector. It will be the most negative when the direct of the unit direction vector is the negative of the gradient. Therefore a vector that points in the steepest decent direction is:

$$\mathbf{u}_k = -\mathbf{g}_k \quad (4.31)$$

Using this in the iteration of equation (4.25) produces the method of the steepest descent:

$$\mathbf{x}_{k+1} = \mathbf{x}_k - \eta \mathbf{g}_k \quad (4.32)$$

4.4.3 The backpropagation algorithm

The first description of an algorithm to train multilayer networks was contained in the thesis of Paul Werbos in 1974 [64]. It was not until the mid 1980s that the backpropagation algorithm was rediscovered and widely publicized [65]. The multilayer perceptrons, trained by the backpropagation algorithm, is currently the most widely used neural network.

Figure 4.19 is a diagram of a three-layer perceptron. The output of the first layer is the input to the second network, and the output of the second layer is the input to the third network. Each layer may have different number of neurons, and even different functions.

As shown in Figure 4.19 the output signal of first layer can be expressed as:

$$\mathbf{a}^1 = f^1(\mathbf{W}^1 \mathbf{p} + \mathbf{b}^1) \quad (4.33)$$

The superscript 1 is used to identify the layer number.

\mathbf{p} is the input variables with dimension $R \times 1$.

\mathbf{W}^1 is the weight matrix of the first layer with dimension $S^1 \times R$.

\mathbf{b}^1 is the bias of layer one with dimension $S^1 \times 1$.

The detailed matrix expression can be described as:

$$\begin{bmatrix} a_1^1 \\ a_2^1 \\ \vdots \\ a_{S^1}^1 \end{bmatrix} = f^1 \left(\begin{bmatrix} w_{1,1}^1 & w_{1,2}^1 & \cdots & w_{1,R}^1 \\ w_{2,1}^1 & w_{2,2}^1 & \cdots & w_{2,R}^1 \\ \vdots & \vdots & \cdots & \vdots \\ w_{S^1,1}^1 & w_{S^1,2}^1 & \cdots & w_{S^1,R}^1 \end{bmatrix} \begin{bmatrix} p_1 \\ p_2 \\ \vdots \\ p_R \end{bmatrix} + \begin{bmatrix} b_1^1 \\ b_2^1 \\ \vdots \\ b_{S^1}^1 \end{bmatrix} \right) \quad (4.34)$$

For multilayer networks the output of one layer becomes the input to the following layer, the equations that describe this operation are:

$$\mathbf{a}^{m+1} = f^{m+1}(\mathbf{W}^{m+1} \mathbf{a}^m + \mathbf{b}^{m+1}) \quad \text{for } m = 0, 1, \dots, M-1 \quad (4.35)$$

M is the number of layers in the network. The neurons in the first layer receive external inputs:

$$\mathbf{a}^0 = \mathbf{p} \quad (4.36)$$

The output of the neurons in the last layer is considered the networks outputs as:

$$\mathbf{a} = \mathbf{a}^M \quad (4.37)$$

A feed forward three-layer network shown in Figure 4.19 is represented with abbreviated notation shown in Figure 4.21.

A reference model using to train the neural network at sampled time of kT is written as:

$$\{ p(k), y(k) \} \quad (4.38)$$

where $p(k)$ is an input to the network, and $y(k)$ is corresponding to the output of the reference model at sampled time of kT .

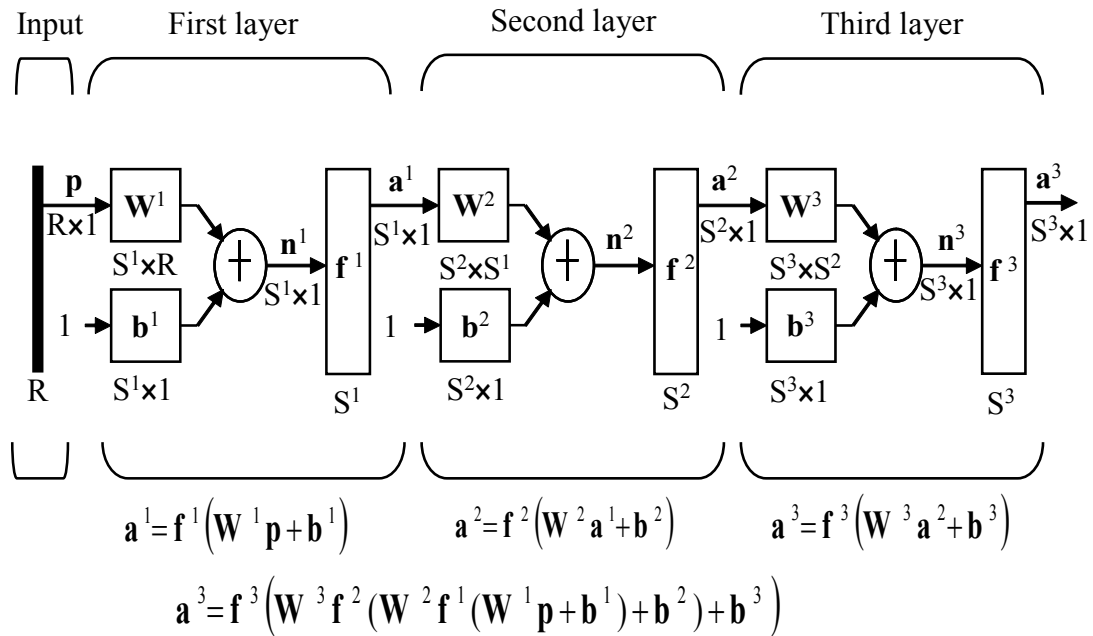


Figure 4.21 Three-layer network, Abbreviated Notation

The performance index $F(\mathbf{x})$ is defined as mean square error as:

$$F(\mathbf{x}) = \mathbf{e}^T(k) \mathbf{e}(k) = (\mathbf{y}(k) - \mathbf{a}(k))^T (\mathbf{y}(k) - \mathbf{a}(k)) \quad (4.39)$$

where

- \mathbf{x} is the vector of network weights and biases.
- $\mathbf{e}(k)$ is the error between the outputs of reference model and neural network.
- $\mathbf{y}(k)$ is the output of reference model at sampled time of kT .
- $\mathbf{a}(k)$ is the output of neural network of final stage at sampled time of kT .

The algorithm should adjust the network parameters in order to minimize the mean square error. The steepest descent algorithm is used for this.

According the steepest descent method the weights and biases can be updated by following equation:

$$\begin{aligned} \mathbf{w}_{i,j}^m(k+1) &= \mathbf{w}_{i,j}^m(k) - \eta \frac{\partial F}{\partial \mathbf{w}_{i,j}^m} \\ \mathbf{b}_i^m(k+1) &= \mathbf{b}_i^m(k) - \eta \frac{\partial F}{\partial \mathbf{b}_i^m} \end{aligned} \quad (4.40)$$

where η is the learning rate.

The derivative term in equation (4.40) can be treated more detail by the chain rule.

Figure 4.21 is supported as m layers network. According to the chain rule the derivative term in equation (4.40) can be expressed as:

$$\frac{\partial F}{\partial \mathbf{w}_{i,j}^m} = \frac{\partial F}{\partial \mathbf{n}_i^m} \frac{\partial \mathbf{n}_i^m}{\partial \mathbf{w}_{i,j}^m} \quad (4.41)$$

$$\frac{\partial F}{\partial \mathbf{b}_i^m} = \frac{\partial F}{\partial \mathbf{n}_i^m} \frac{\partial \mathbf{n}_i^m}{\partial \mathbf{b}_i^m} \quad (4.42)$$

where

$$\mathbf{n}_i^m = \sum_{j=1}^{S^{m-1}} (\mathbf{w}_{i,j}^m \mathbf{a}_j^{m-1} + \mathbf{b}_i^m)$$

therefore

$$\frac{\partial \mathbf{n}_i^m}{\partial \mathbf{w}_{i,j}^m} = \mathbf{a}_j^{m-1} \quad , \quad \frac{\partial \mathbf{n}_i^m}{\partial \mathbf{b}_i^m} = 1 \quad (4.43)$$

s_i^m is defined as:

$$s_i^m = \frac{\partial F}{\partial \mathbf{n}_i^m} \quad (4.44)$$

where s_i^m is in behalf of the sensitivity of F to change in the i th element of network input at layer m . The equation (4.40) can be modified as following expression:

$$\mathbf{w}_{i,j}^m(k+1) = \mathbf{w}_{i,j}^m(k) - \eta s_i^m \mathbf{a}_j^{m-1} \quad (4.45)$$

$$\mathbf{b}_i^m(k+1) = \mathbf{b}_i^m(k) - \eta s_i^m$$

In matrix form this becomes:

$$\mathbf{W}^m(k+1) = \mathbf{W}^m(k) - \eta \mathbf{s}^m (\mathbf{a}^{m-1})^T \quad (4.46)$$

$$\mathbf{b}^m(k+1) = \mathbf{b}^m(k) - \eta \mathbf{s}^m$$

$$\mathbf{s}^m = \frac{\partial F}{\partial \mathbf{n}^m} = \begin{bmatrix} \frac{\partial F}{\partial \mathbf{n}_1^m} \\ \frac{\partial F}{\partial \mathbf{n}_2^m} \\ \vdots \\ \frac{\partial F}{\partial \mathbf{n}_{s^m}^m} \end{bmatrix} \quad (4.47)$$

Now only the sensitivity s_i^m needs to be calculated. The meaning of backpropagation is that it describes a recurrence relationship in which the sensitivity at layer m is computed from the sensitivities at layer $m+1$.

To drive the recurrence relationship for the sensitivities we consider the i, j element of

the matrix according Figure 4.19.

$$\begin{aligned}
\frac{\partial \mathbf{n}_i^{m+1}}{\partial \mathbf{n}_j^m} &= \frac{\partial \left(\sum_{l=1}^{S^m} w_{i,l}^{m+1} \mathbf{a}_l^m + \mathbf{b}_i^{m+1} \right)}{\partial \mathbf{n}_j^m} = w_{i,j}^{m+1} \frac{\partial \mathbf{a}_j^m}{\partial \mathbf{n}_j^m} \\
&= w_{i,j}^{m+1} \frac{\partial f^m(\mathbf{n}_j^m)}{\partial \mathbf{n}_j^m} = w_{i,j}^{m+1} f^m(\mathbf{n}_j^m)
\end{aligned} \tag{4.48}$$

where

$$f^m(\mathbf{n}_j^m) = \frac{\partial f^m(\mathbf{n}_j^m)}{\partial \mathbf{n}_j^m}$$

Equation (4.48) can be expressed as matrix form:

$$\frac{\partial \mathbf{n}^{m+1}}{\partial \mathbf{n}^m} = \mathbf{W}^{m+1} \mathbf{F}^m(\mathbf{n}^m) \tag{4.49}$$

where

$$\frac{\partial \mathbf{n}^{m+1}}{\partial \mathbf{n}^m} = \begin{bmatrix} \frac{\partial \mathbf{n}_1^{m+1}}{\partial \mathbf{n}_1^m} & \frac{\partial \mathbf{n}_1^{m+1}}{\partial \mathbf{n}_2^m} & \dots & \frac{\partial \mathbf{n}_1^{m+1}}{\partial \mathbf{n}_{S^m}^m} \\ \frac{\partial \mathbf{n}_2^{m+1}}{\partial \mathbf{n}_1^m} & \frac{\partial \mathbf{n}_2^{m+1}}{\partial \mathbf{n}_2^m} & \dots & \frac{\partial \mathbf{n}_2^{m+1}}{\partial \mathbf{n}_{S^m}^m} \\ \vdots & \vdots & \dots & \vdots \\ \frac{\partial \mathbf{n}_{S^{m+1}}^{m+1}}{\partial \mathbf{n}_1^m} & \frac{\partial \mathbf{n}_{S^{m+1}}^{m+1}}{\partial \mathbf{n}_2^m} & \dots & \frac{\partial \mathbf{n}_{S^{m+1}}^{m+1}}{\partial \mathbf{n}_{S^m}^m} \end{bmatrix} \tag{4.50}$$

Equation (4.50) is called as the Jacobian matrix.

and

$$\mathbf{F}^m(\mathbf{n}^m) = \begin{bmatrix} f^m(\mathbf{n}_1^m) & 0 & \dots & 0 \\ 0 & f^m(\mathbf{n}_2^m) & \dots & 0 \\ \vdots & \vdots & \dots & \vdots \\ 0 & 0 & \dots & f^m(\mathbf{n}_{S^m}^m) \end{bmatrix} \tag{4.51}$$

The recurrence relationship of the sensitivity can be written out by using the chain rule in matrix form.

$$\begin{aligned}\mathbf{s}^m &= \frac{\partial F}{\partial \mathbf{n}^m} = \left(\frac{\partial \mathbf{n}^{m+1}}{\partial \mathbf{n}^m} \right)^T \frac{\partial F}{\partial \mathbf{n}^{m+1}} \\ &= \mathbf{F}^m(\mathbf{n}^m) (\mathbf{W}^{m+1})^T \mathbf{s}^{m+1}\end{aligned}\quad (4.52)$$

According to equation (4.52), the sensitivities can be propagated backward through the network from the last layer to the first layer. The final step required to complete the back propagation algorithm for the recurrence relationship in equation (4.52) is that we need to find the start point \mathbf{s}^M . This is obtained at the final layer:

$$s_i^M = \frac{\partial F}{\partial n_i^M} = \frac{\partial (y - \mathbf{a})^T (y - \mathbf{a})}{\partial n_i^M} = \frac{\partial \sum_{j=1}^{S^M} (y_j - a_j)^2}{\partial n_i^M} = -2(y_i - a_i) \frac{\partial a_i}{\partial n_i^M} \quad (4.53)$$

since

$$\frac{\partial a_i}{\partial n_i^M} = f^M(n_i^M)$$

We can write the equation (4.53) as follows:

$$s_i^M = -2(y_i - a_i) f^M(n_i^M) \quad (4.54)$$

This can be expressed in matrix form as:

$$\mathbf{s}^M = -2\mathbf{F}^M(\mathbf{n}^M)(\mathbf{y} - \mathbf{a}) \quad (4.55)$$

Equation (4.55), (4.52) and (4.46) are used to describe the backpropagation algorithm completely.

4.5 The description of fuzzy neural network

Recently much research has been accomplished by applying fuzzy neural network (FNN) systems, which combine the capability of fuzzy reasoning in handling uncertain information [53-54] and the capability of neural networks in learning from processes [20-22], in control fields to deal with nonlinearities and uncertainties of control systems [55-59]. In this section the FNN structure is constructed with four layers at first, and then the learning algorithm will be developed in detail.

4.5.1 Fuzzy neural network

A fuzzy logic rule with constant consequent part is adopted in the FNN as follows:

$$R_j : \text{IF } x_1 \text{ is } A_1^j \text{ and } \dots \text{ and } x_n \text{ is } A_n^j \text{ THEN } y = d_j \quad (4.56)$$

where x_i and y are the input and output variables, respectively; A_i^j is the linguistic term of the antecedent part with membership function $\mu_{A_i^j}$; d_j is the constant consequent part; subscript n is the number of input variables. The structure of the FNN is shown in Figure 4.22 where the functions of the node in each layer are described as follows:

Layer 1:

Each node in this layer is an input node, which corresponds to one input variable. These nodes only pass input signal to the next layer. In this study, the input variables are:

$$\begin{aligned} x_1 &= e_m \\ &\vdots \\ x_2 &= e_m \end{aligned}$$

where e_m is the error between the output signal of reference model V_m and the

terminal voltage V_t , \dot{e}_m is the derivative of e_m .

Layer 2:

Each node in this layer acts as a linguistic label of one of the input variables in layer 1, i.e., the membership value specifying the degree to which an input value belongs to a fuzzy set, is determined in this layer. The Gaussian function, as follows, is adopted as the membership function:

$$\mu_{A_i^j} = \exp\left(-\frac{(x_i - m_{ji})^2}{\sigma_{ji}^2}\right) \quad (4.57)$$

where m_{ji} and σ_{ji} are, respectively, the mean and standard deviation of the Gaussian functions in the j th term associated with i th input variable x_i .

Layer 3:

Each node in this layer represents one of fuzzy logic rules. Therefore, each node of this layer is denoted by Π , which multiplies the incoming signals and outputs the result of product. For the j th rule node can be expressed as:

$$\begin{aligned} u_j &= \mu_{A_1^j}(x_1) \mu_{A_2^j}(x_2) \dots \mu_{A_n^j}(x_n) \\ &= \Pi \mu_{A_i^j}(x_i) \end{aligned} \quad (4.58)$$

where u_j is the output of the j th rule node.

Layer 4:

This layer acts as a defuzzifier. This node in this layer is labeled as Σ , and it sums all incoming signals to obtain the final inferred result:

$$y = \sum_{j=1}^K \omega_j u_j \quad (4.59)$$

where the link weight ω_j is the output action strength associated with the j th rule; y

is the output of the FNN.

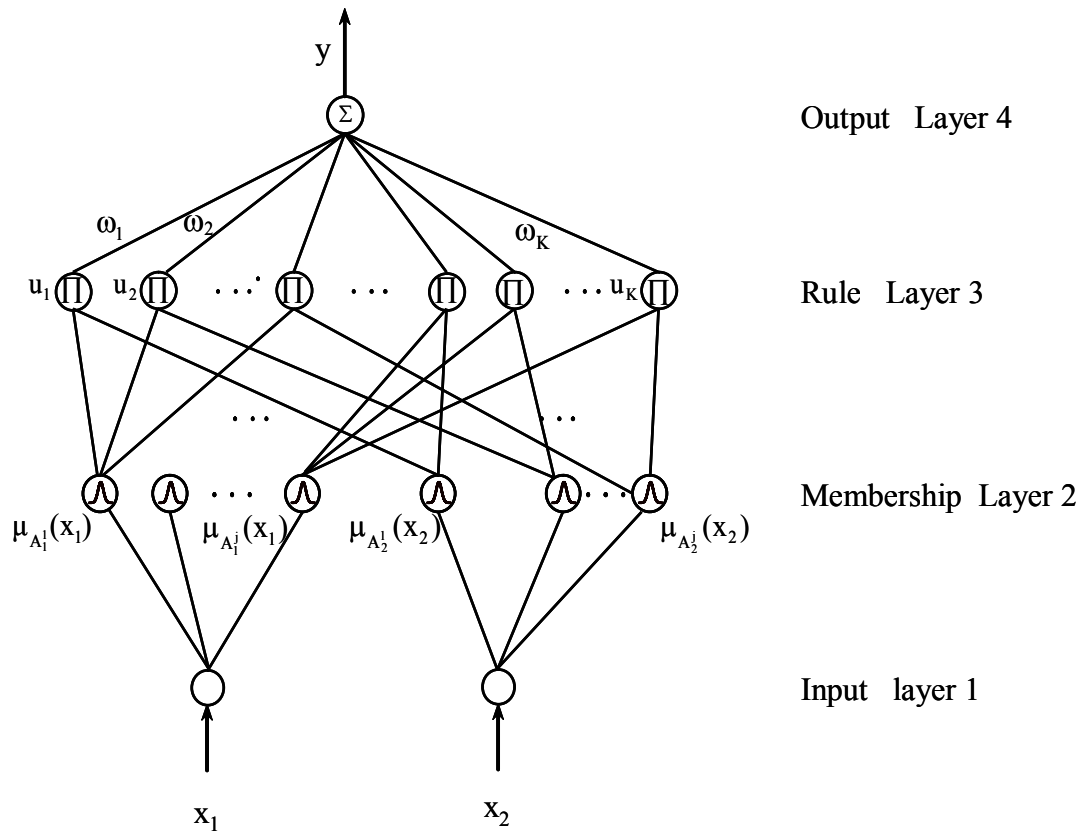


Figure 4.22 The structure of the FNN

4.5.2 Parameter Learning

The central part of the parameter learning algorithm for the FNN concerns how to recursively obtain a gradient vector in which each element in the learning algorithm is defined as the derivative of a performance index with respect to a parameter of the network. The most common used method is called backpropagation learning law. To describe the on-line parameter learning algorithm of the FNN using the gradient descent method and backpropagation learning law the performance index F is defined as:

$$F = \frac{1}{2} (V_m - V_t)^2 = \frac{1}{2} e_m^2 \quad (4.60)$$

The parameter learning algorithm based on backpropagation can be described as follows:

Layer 4:

The error term to be propagated is computed as:

$$\delta^4 = -\frac{\partial F}{\partial y} = \left[-\frac{\partial F}{\partial e_m} \frac{\partial e_m}{\partial y} \right] = \left[-\frac{\partial F}{\partial e_m} \frac{\partial e_m}{\partial V_t} \frac{\partial V_t}{\partial y} \right] \quad (4.61)$$

and the link weight is updated by the amount:

$$\begin{aligned} \Delta \omega_j &= -\eta_w \frac{\partial F}{\partial w_j} = -\left[\eta_w \frac{\partial F}{\partial y} \right] \left[\frac{\partial y}{\partial w_j} \right] \\ &= \eta_w \delta^4 u_j \end{aligned} \quad (4.62)$$

where factor η_w is the learning-rate parameter of the link weight. The link weights in layer 4 are updated according to the following equation:

$$\omega_j(k+1) = \omega_j(k) + \Delta \omega_j \quad (4.63)$$

where k denotes the sampled time of kT .

Layer 3:

In this layer only the error term needs to be calculated and propagated:

$$\begin{aligned} \delta_j^3 &= -\frac{\partial F}{\partial u_j} = \left[-\frac{\partial F}{\partial y} \right] \left[\frac{\partial y}{\partial u_j} \right] \\ &= \delta^4 \omega_j \end{aligned} \quad (4.64)$$

Layer 2:

The error term is computed as follows:

$$\delta_{ji}^2 = -\frac{\partial F}{\partial \mu_{A_i^j}} = \left[\frac{\partial F}{\partial y} \frac{\partial y}{\partial u_j} \right] \left[\frac{\partial u_j}{\partial \mu_{A_i^j}} \right] = \delta_j^3 \quad (4.65)$$

The update law of m_{ji} is:

$$\begin{aligned} \Delta m_{ji} &= -\eta_m \frac{\partial F}{\partial m_{ji}} = \left[-\eta_m \frac{\partial F}{\partial \mu_{A_i^j}} \frac{\partial \mu_{A_i^j}}{\partial m_{ji}} \right] \\ &= \eta_m \delta_{ji}^2 \frac{2(x_i^2 - m_{ji})}{(\sigma_{ji})^2} \end{aligned} \quad (4.66)$$

The update law of σ_{ji} is:

$$\begin{aligned} \Delta \sigma_{ji} &= -\eta_\sigma \frac{\partial F}{\partial \sigma_{ji}} = \left[-\eta_\sigma \frac{\partial F}{\partial \mu_{A_i^j}} \frac{\partial \mu_{A_i^j}}{\partial \sigma_{ji}} \right] \\ &= \eta_\sigma \delta_{ji}^2 \frac{2(x_i^2 - m_{ji})^2}{(\sigma_{ji})^3} \end{aligned} \quad (4.67)$$

where η_m and η_σ are the learning-rate of the mean and the standard deviation of the Gaussian function, respectively. The mean and standard deviations of the membership functions in this layer are updated as follows:

$$m_{ji}(k+1) = m_{ji}(k) + \Delta m_{ji} \quad (4.68)$$

$$\sigma_{ji}(k+1) = \sigma_{ji}(k) + \Delta \sigma_{ji} \quad (4.69)$$

The exact calculation of $\partial V_t / \partial y$, which is contained in $\partial F / \partial y$, can't be determined due to the uncertainties of the plant dynamic, such as parameter variations and external disturbance. To overcome this problem and to increase the on-line learning rate of the network parameters, the delta adaptation law proposed in [60] is adopted:

$$\delta^4 = N e_m + \dot{e}_m \quad (4.70)$$

where N is a positive constant.

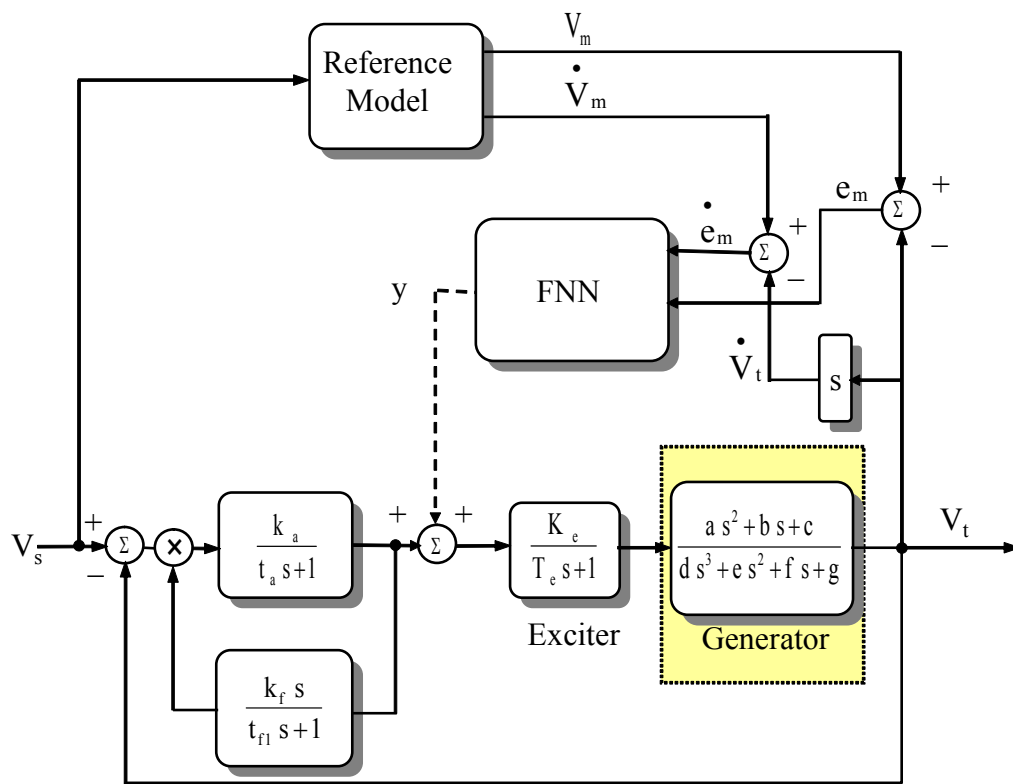


Figure 4.23 The flow chart of generator system with FNN

The complete structure of terminal voltage control system of a synchronous generator with FNN is represented as Figure 4.23. In Figure 4.23 the signal e_m and its derivative are fed to FNN as input signals. The sum for the output signal between FNN and conventional controller is used for controlling the field current of main exciter.

Chapter 5 Simulation of a voltage control system

In this chapter, the simulation will be divided into two parts. The first part is the simulation of the terminal voltage response of generator system using the conventional controller, in which the different test conditions are applied. In the second part, an FNN signal will be added to the conventional controller as an extra control signal. The same test condition as in the first part will be simulated again.

5.1 Simulation of a conventional controller for a 412 MVA generator

A 412 MVA generator connected to an infinite bus system will be used to test the controller performance. In this system the equivalent transmission impedance is $0.02+0.4j$ and the voltage in the infinite bus is set as 1 p.u.. The linear mathematic model of the generator, which is developed in chapter 3, is expressed as equation (5.1), where the input and output signals are exciter voltage and terminal voltage, respectively.

The main exciter model is shown as equation (5.2). The transfer function block of this generator system is shown in Figure 5.1

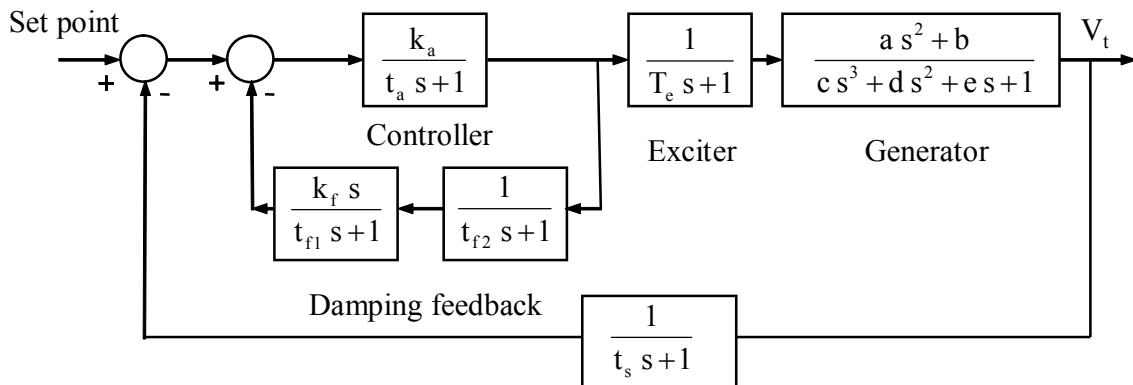


Figure 5.1 The linear generator transfer function block

The generator transfer function in Figure 5.1 is:

$$G_s(s) = \frac{a s_2 + b}{c s_3 + d s_2 + e s + f} \quad (5.1)$$

The coefficient of equation 5.1 is shown as follows:

$a=0.0463$	$b=4.6002$	$c=1.0$
$d=0.6745$	$e=52.608$	$f=4.663$

$$G_E(s) = \frac{K_e}{T_e s + 1} \quad (5.2)$$

where

$K_e=1.0$	$T_e=0.98$
-----------	------------

The root locus of the main exciter and generator together are plotted in Figure 5.2.

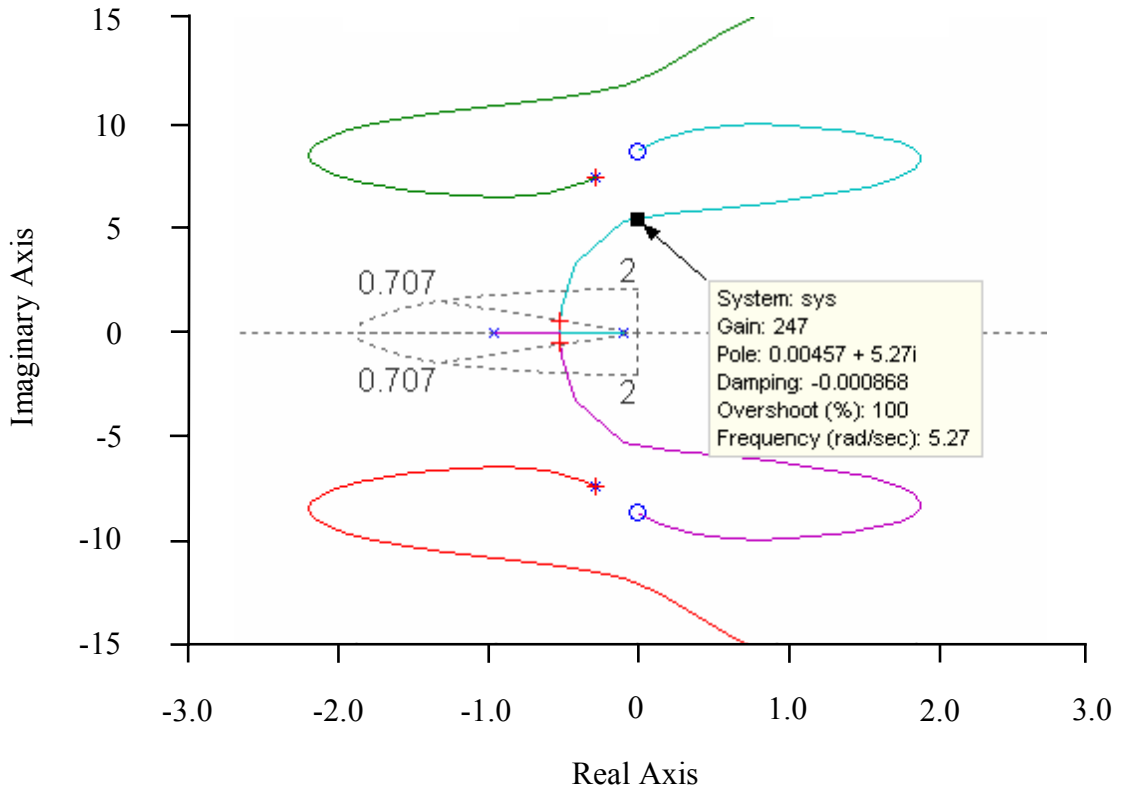


Figure 5.2 Root trajectories of main exciter and generator

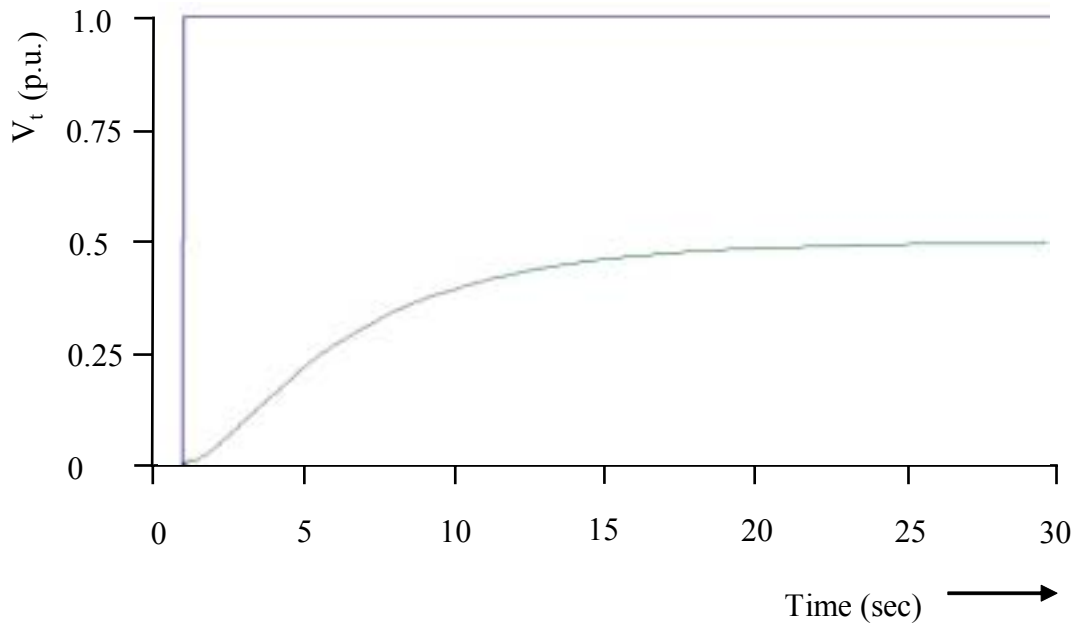


Figure 5.3 The time response for an uncompensated generator system

The Figure 5.3 shows the time response for an uncompensated generator system with an unity feedback. It is obvious that the system has a steady state error of 50 %. If the roots in Figure 5.2 are located on an imaginary axis, then the system will have a gain k_a of 247 and sustains oscillation under the step input response.

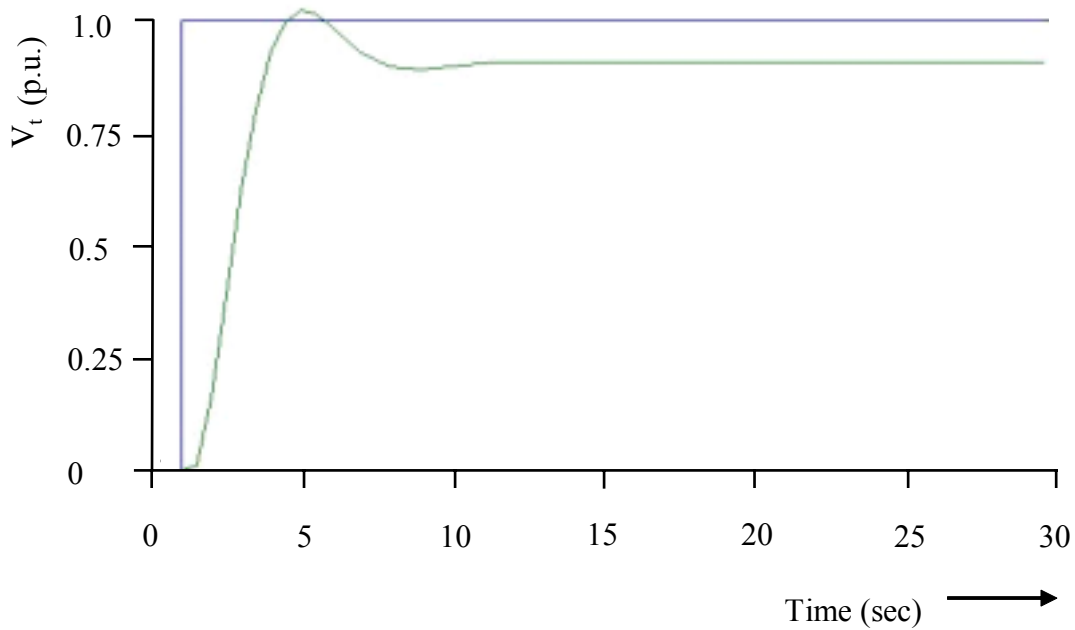


Figure 5.4 The step time response with system gain k_a of 10

On the other hand, if we choose the damping ratio in Figure 5.2 as 0.53, the system will have a gain k_a of 10. The dominant complex roots are $-0.55 \pm 0.88j$. The values of maximum overshoot, rise time and settling time are 12.8 %, 1.7 and 7.8 s under step input response, respectively. It will result in the system steady state error of 9.2 %. The simulation result of the terminal voltage response for giving a step input is also shown on Figure 5.4. A compensation for this system must be made to satisfy system specification.

5.1.1 The tuning of AVR parameters

As noted above, the AVR has four parameters, which need to be tuned; these are k_a , k_f , t_{f1} and t_{f2} .

The transfer function of the controller loop in Figure 5.1 can be expressed as:

$$tf = \frac{k_a (t_{f1} s + 1)(t_{f2} s + 1)}{(t_{f1} s + 1)(t_{f2} s + 1) + k_a k_f s} \quad (5.3)$$

Usually the k_a is quite large so that the system has quickly response at steady state for the occurring of error. If we assume that:

$$t_{f1} t_{f2} \ll t_{f1} + t_{f2} + k_a k_f \quad (5.4)$$

Then equation (5.3) can be modified as a lag-lead compensator with the form as:

$$tf = \frac{k_a (t_{f1} s + 1)(t_{f2} s + 1)}{(k t_{f1} s + 1)(t_{f2} s / k + 1)} \quad (5.5)$$

where

$$k = 1 + \frac{t_{f2} + k_a k_f}{t_{f1}} \quad (5.6)$$

The time domain performance indexes of a control system are rise time t_r , maximum overshoot M_p and settling time t_s . The specifications of this system are:

- Maximum overshoot: 15 %.
- Settling time: 7 s.
- Rise time: 2 s

As we have seen in Figure 5.4, the transient response of the system meets the system specification except the steady state error. A lag compensator is applied to correct the steady state error without appreciably reducing the system stability. Therefore equation 5.5 can be reduced to a lag compensator as t_{f2} is set to zero. The new controller form for lag compensator is:

$$tf = \frac{t_{f1}s + 1}{k_f s} \quad (5.7)$$

where k_a is very larger than 1.0.

A large k_a is selected so that it can correct the voltage error quickly and reduces the system steady state error. For the purpose of designing the controller, a set consisting of k_f and t_{f1} is used first so that the system specification can be met. The position of roots on the root locus plot decides the system dynamic characteristics. In this example k_f is selected as 1.0 and t_{f1} is 10.0, then the root locus plot of this generator system for variable k_a is shown on Figure 5.5. Some of roots in Figure 5.5 are $-0.495 \pm 0.792j$ at $k_a = 600$ and $-0.496 \pm 0.783j$ at $k_a = 300$. The damping ratio ξ and natural frequency ω_n are 0.529 and 0.936 at $k_a = 600$, 0.535 and 0.927 at $k_a = 300$; respectively. This shows that the root location of characteristics equation is affected to some extent by the gain k_a between 300 and 600. Therefore the controller gain of 600 is selected so that the system steady state error will be minimized. After the value of k_a has been set, the values of k_f and t_{f1} will be fine-tuned.

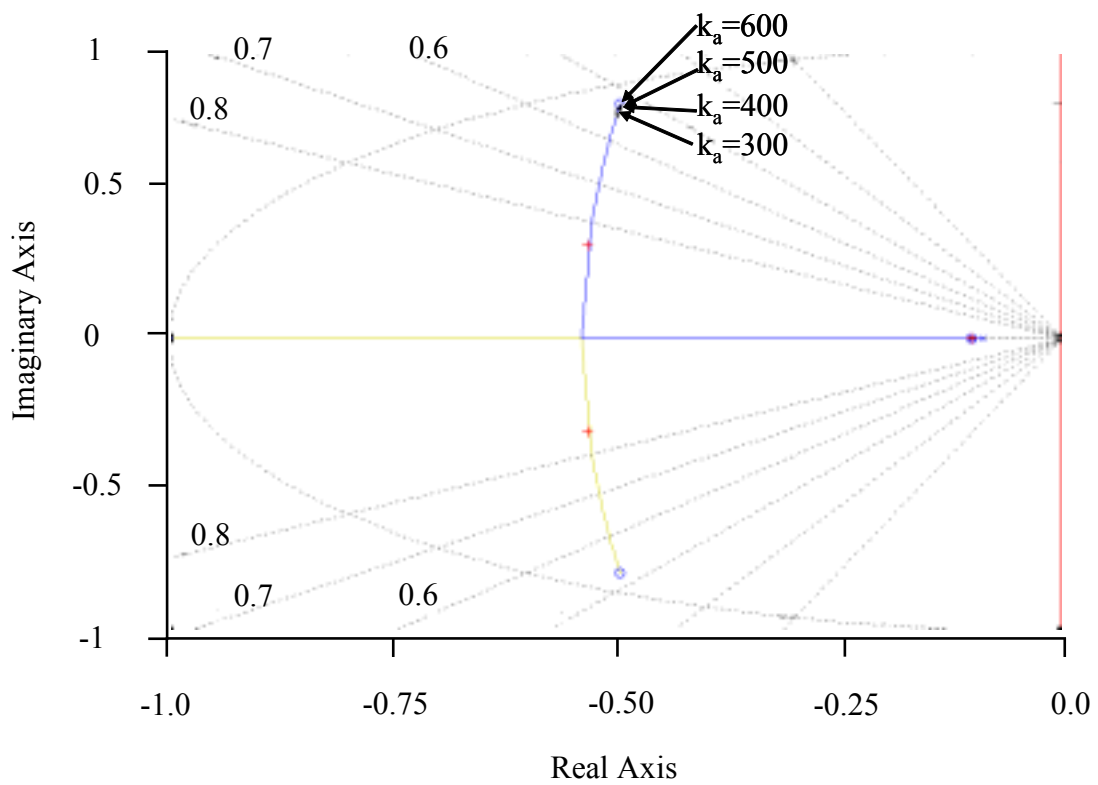


Figure 5.5 The root locus of generator system with $k_f=1.0$; $t_{f1}=10.0$

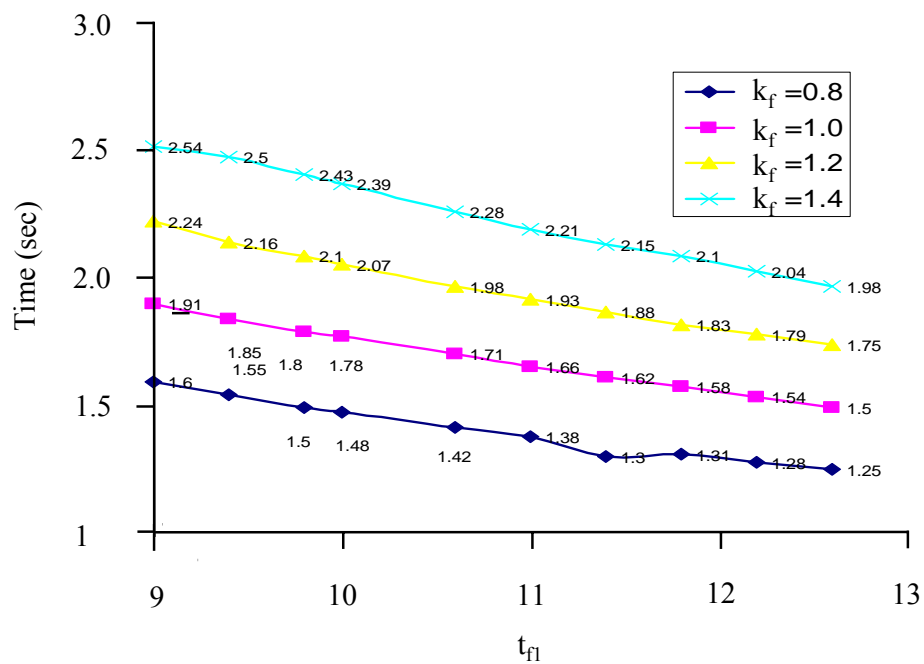


Figure 5.6 Comparison of rise time for different combination of k_f and t_{f1}

First, the rise time will be compared using different combinations of k_f and t_{fl} . The value k_f ranges from 0.8 to 1.4; t_{fl} varies from 9 s to 12.6 s. The various combinations of k_f and t_{fl} are set on the AVR. The simulation on the linear generator system indicates that the maximum rise time of 2.5 s occurs at $k_f = 1.4$ and $t_{fl} = 9$ s; the minimum rise time of 1.25 s occurs with the combination of $k_f = 0.8$ and $t_{fl} = 12.6$ s. The rise times for different combinations of k_f and t_{fl} are shown in Figure 5.6.

The same combinations of k_f and t_{fl} are also set on AVR to find the maximum overshoot (M_p).

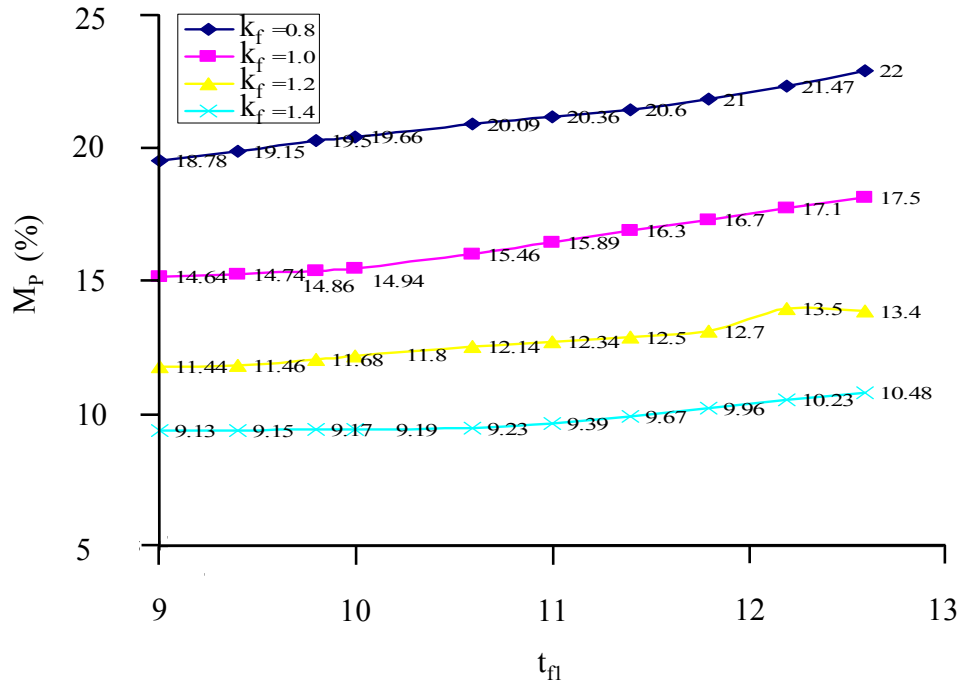


Figure 5.7 Comparison of M_p for different combination of k_f and t_{fl}

Figure 5.7 shows the result of simulation. The greatest M_p is found with a combination of $k_f = 0.8$ and $t_{fl} = 12.6$ s; the lowest value of M_p occurs at $k_f = 1.4$ and $t_{fl} = 9$ s respectively. It is impossible to obtain the minimum rise time and M_p for the same combination of k_f and t_{fl} because the smallest rise time has greatest M_p and, on the contrary, the greatest rise time has the lowest M_p .

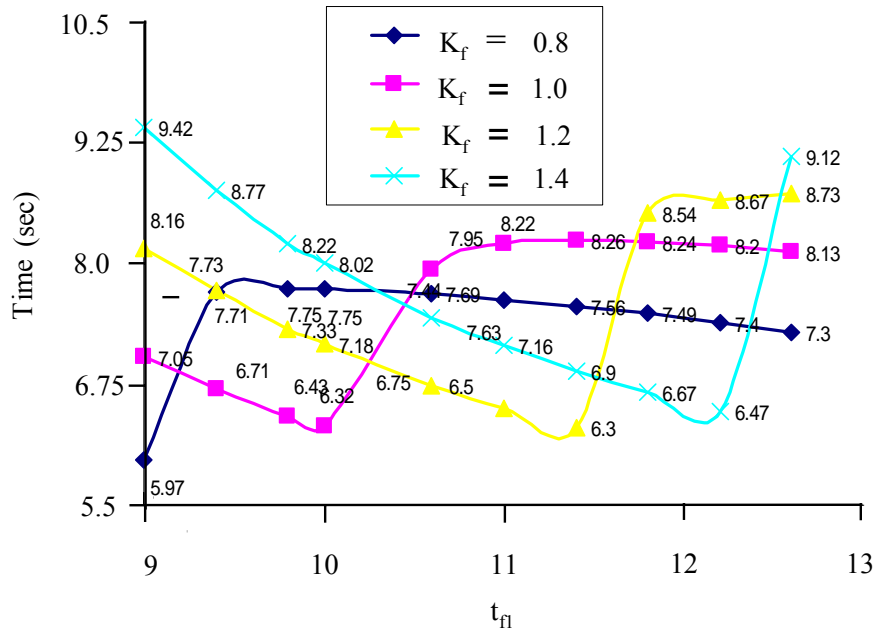


Figure 5.8 Comparison of settling time for different combination of k_f and t_{f1}

Finally, the settling time t_s for various combinations of k_f and t_{f1} are also shown in Figure 5.8. In this Figure, the minimum settling time occurs at four different settings of k_f and t_{f1} . A good generator system requires small overshoot and short settling time. Therefore, a compromise must be made and the shortest settling time will be considered especially.

A step input response for the generator is shown in Figure 5.9. The values of $k_f = 1$ and $t_{f1} = 10$ are set on AVR in this simulation. As shown in Figure 5.9, the maximum overshoot happens at time 4.0 s and its value is 15 %. The settling time is only 6.4 s and the rise time is under 2 s.. Therefore the parameters set on the controller meet the system requirement.

Four different combinations of k_f and t_{f1} are set on the controller; the simulations of step input responses are also shown in Figure 5.10. This plot indicates that the system time responses are very similar. Therefore, these combinations of k_f and t_{f1} are suitable for using in the controller.

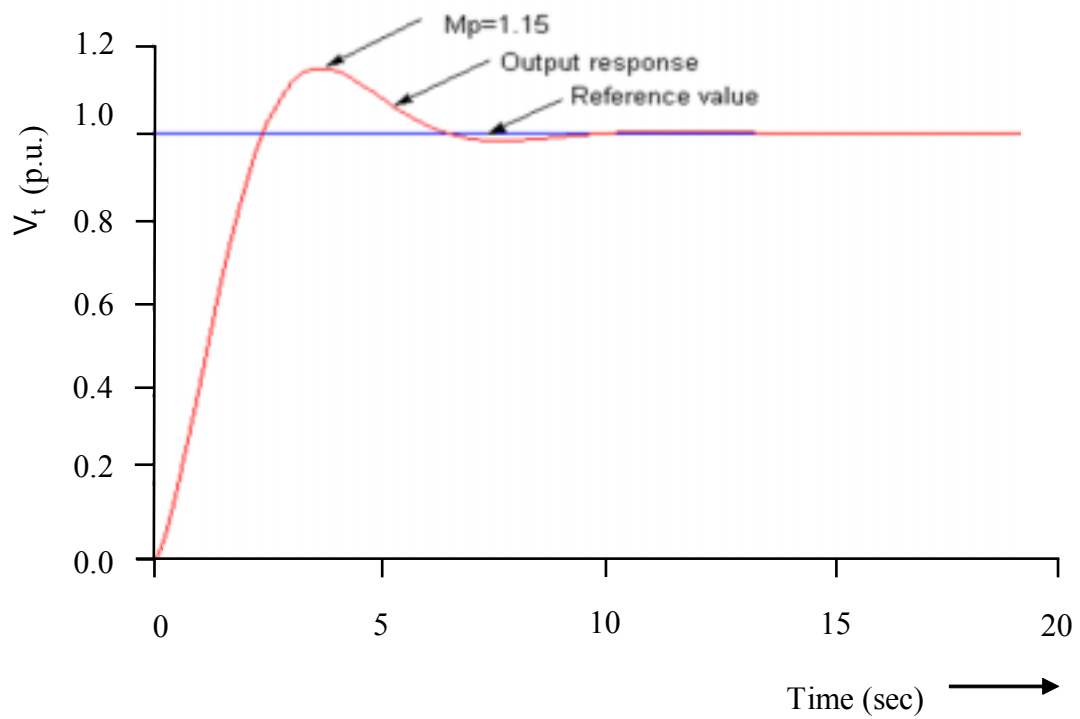


Figure 5.9 The step response of the system with $k_a=600$; $k_f=1.0$ and $t_{fl}=10$.

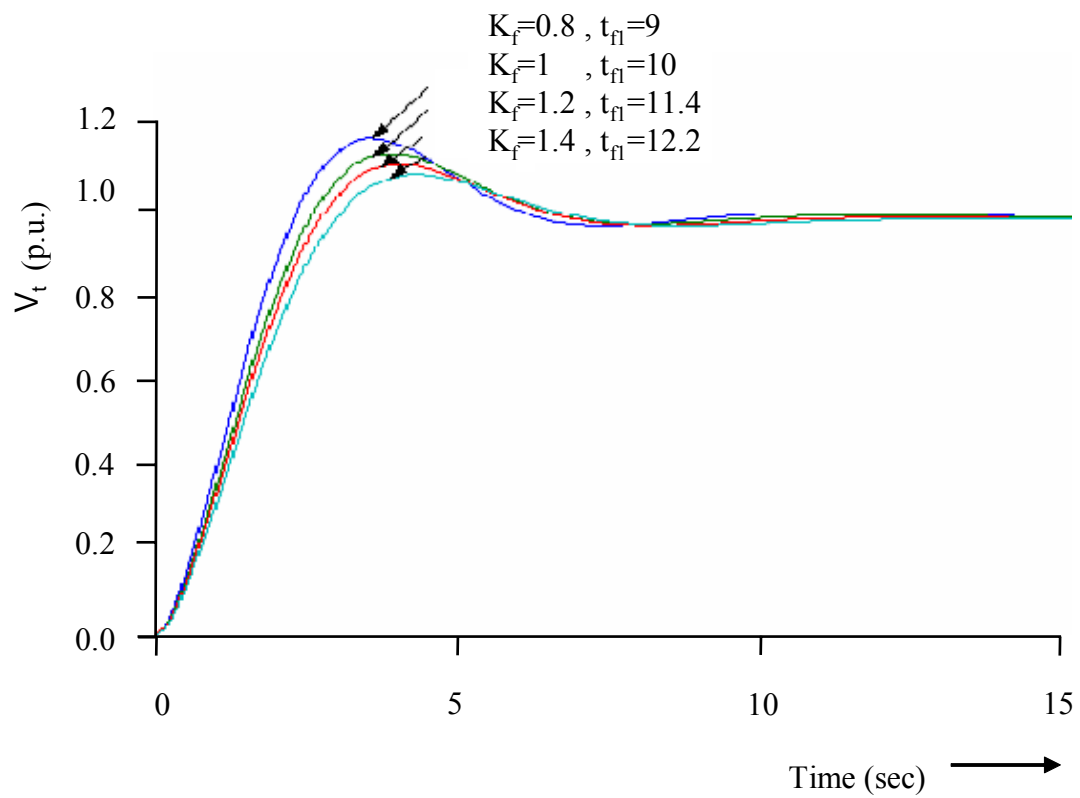


Figure 5.10 The step response of the system with different combination of k_f and t_{fl}

5.1.2 Training of FNN with the AVR for 412 MVA generator

Figure 5.11 represents a system in which a fuzzy neural network (FNN) works in conjunction with an AVR. The input signal, which is the combination of the output signal of FNN and AVR, is fed to main exciter. In order to train the parameters of the FNN, a reference model, constructed in accordance with the modified system specifications of the complete generator system, is given.

The purpose of the FNN compensator is to maintain the terminal voltage of generator system, which response is, in any cases, identical to the output of the reference model. In this system, a square wave signal is fed to the reference model and the generator

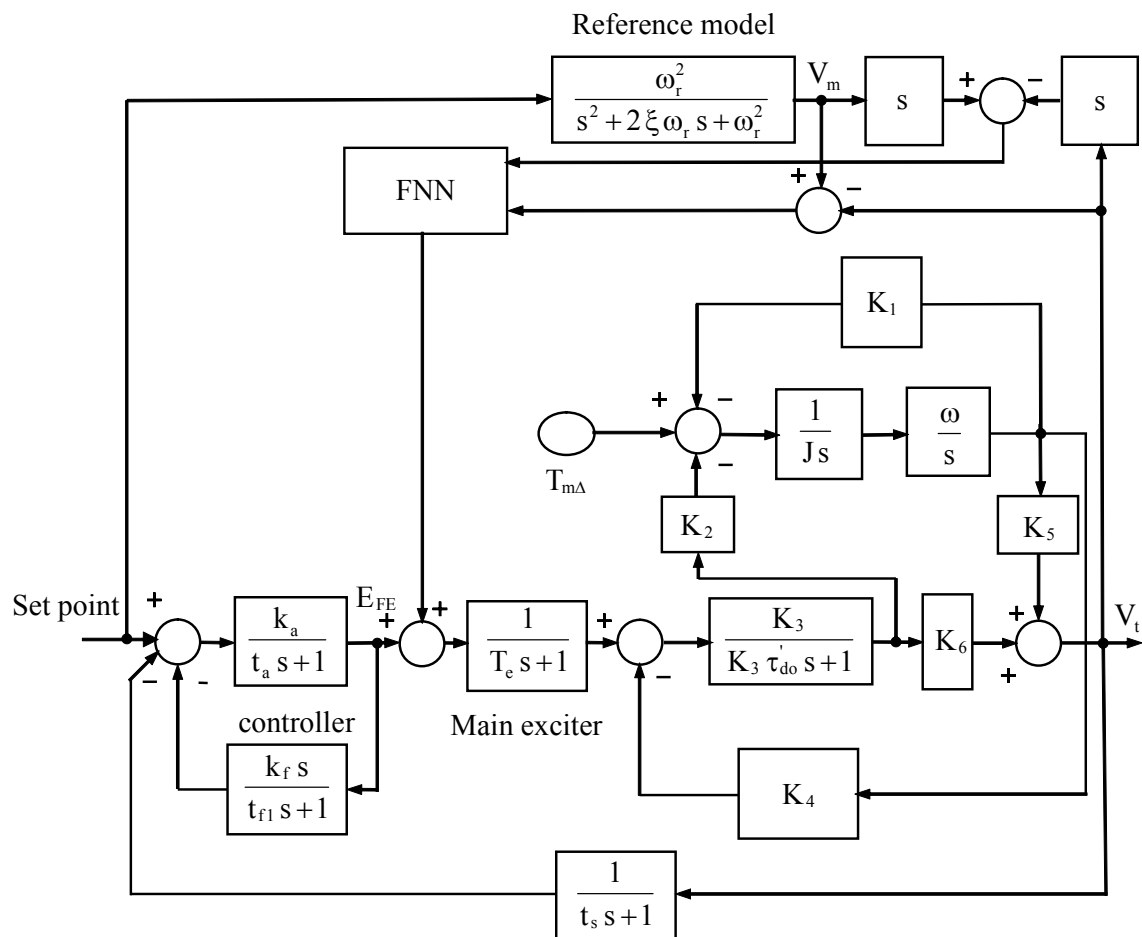


Figure 5.11 A simulation plot for a rate feedback controller with FNN

system simultaneously so that the parameters of the FNN can be trained.

Figure 5.12 shows that the conventional controller with FNN compensator works very well. The terminal voltage follows, almost flawlessly, the output signal of the

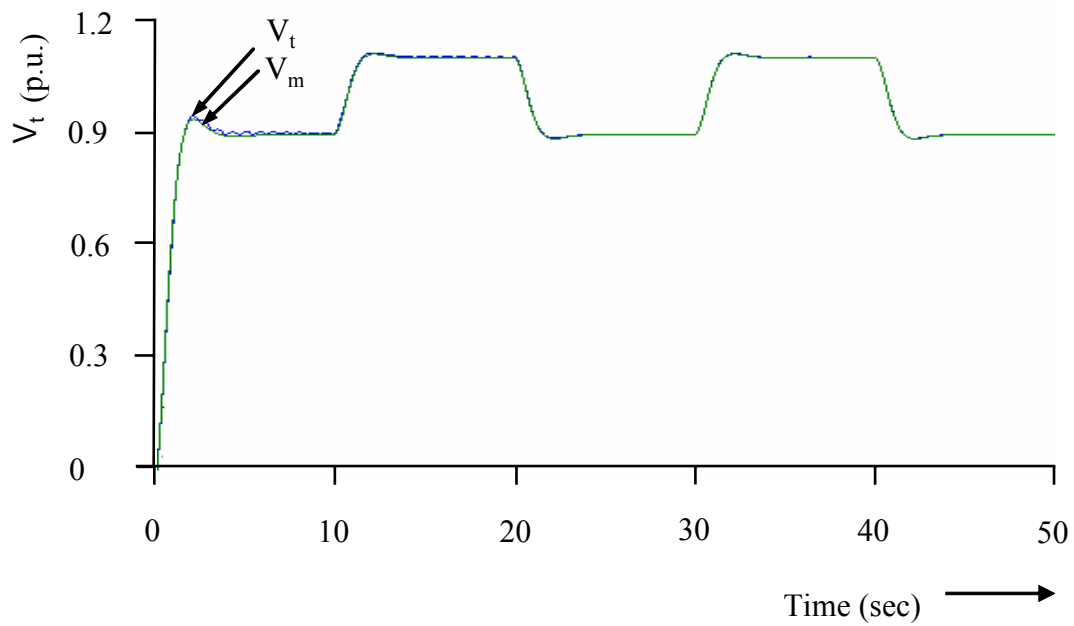


Figure 5.12 The output signal of FNN compensator

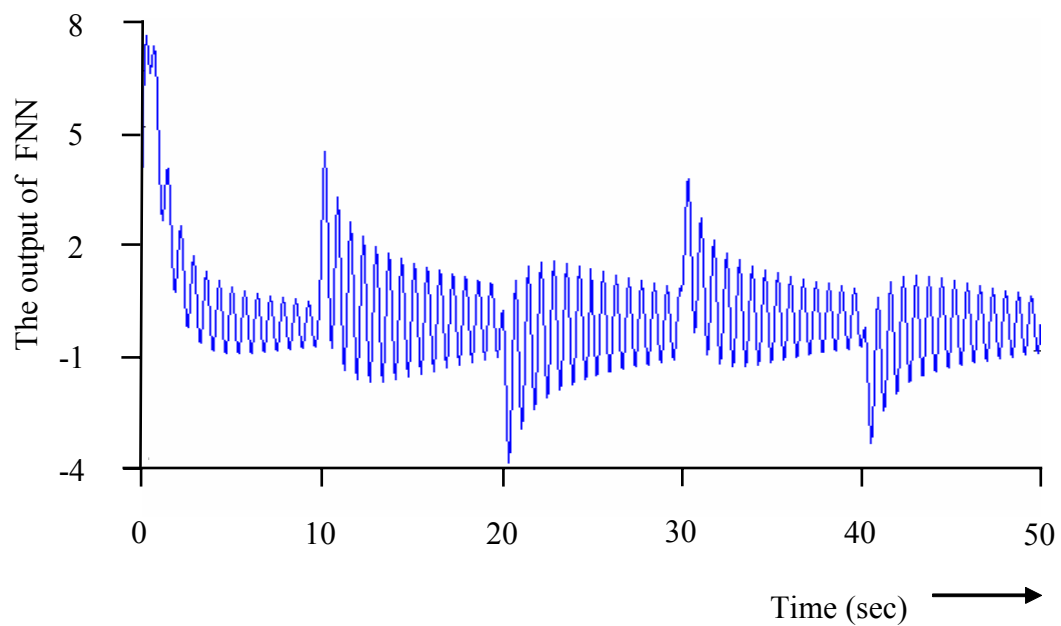


Figure 5.13 The output signal of the FNN

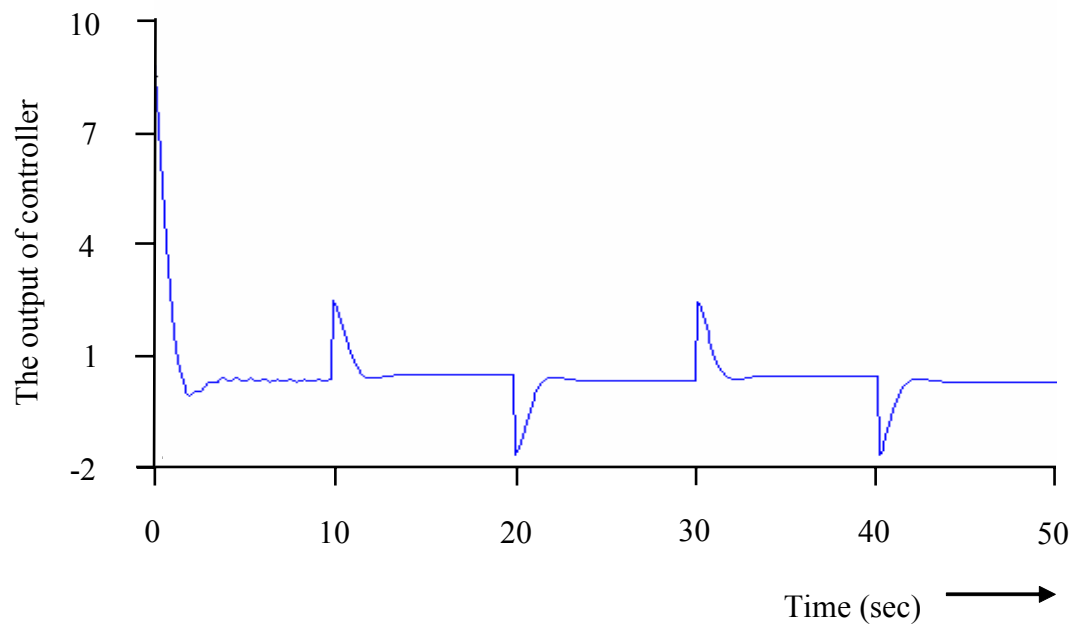


Figure 5.14 The output signal of controller

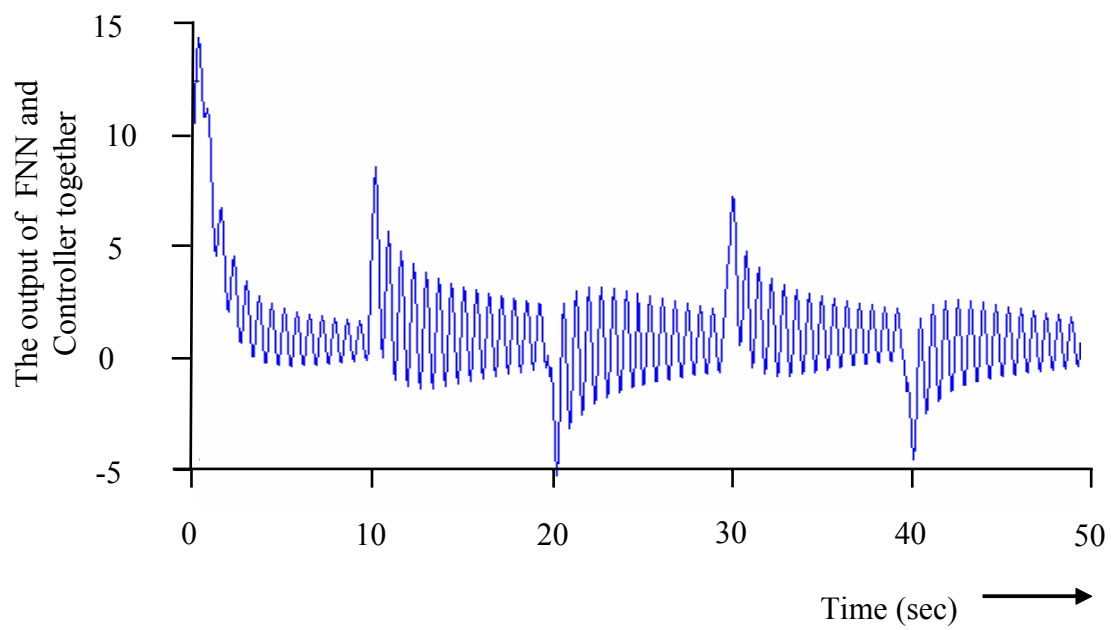


Figure 5.15 The output signal of FNN and controller together

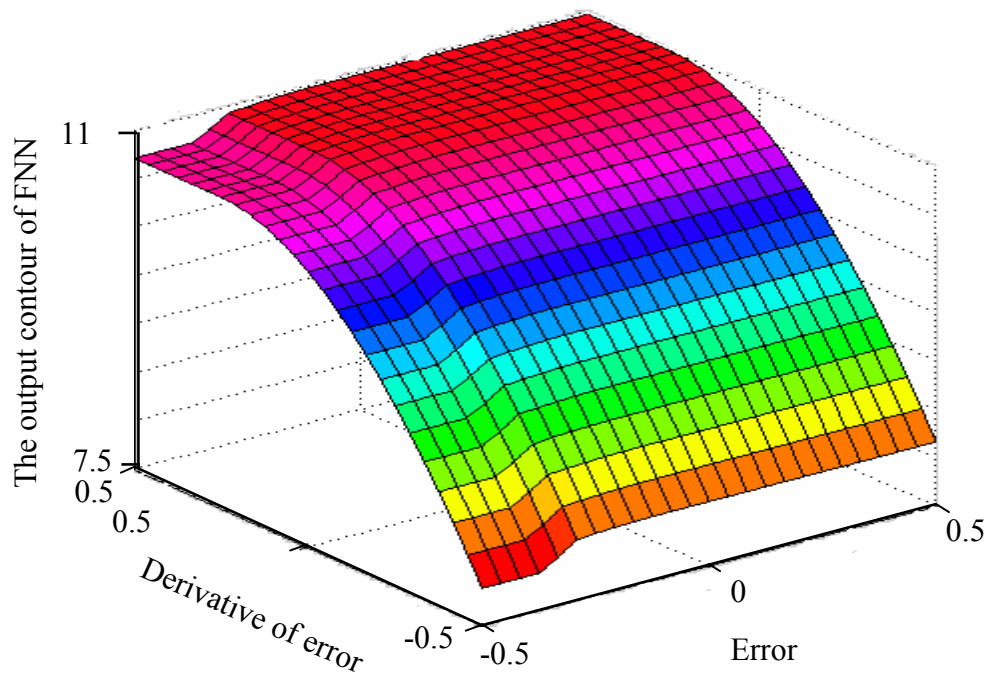


Figure 5.16 The output contour of FNN

reference model. This indicates that the parameters of the FNN have been trained properly and the dynamic characteristics of the complete generator system are identical to the reference model.

The output signal of the FNN during the training phase is also shown in Figure 5.13. Figure 5.14 is the output signal of controller and Figure 5.15 is the combination of the output signal of the AVR and FNN. The output contour of FNN varies with the time because the FNN in this system is on-line training. Figure 5.16 represents the output contour of FNN at time of 5 second.

During the training of FNN, some important views must be paid attention.

1. The learning rate in FNN is important. It affects the learning speed of FNN and system stability. A large learning rate provides FNN a large correction signal and the effect of a large learning rate is that the FNN system is easily diverging. A small learning rate provides FNN a small correction signal and it cannot supply

an enough correction signal to follow the reference model. Therefore a suitable learning rate must be tested on the learning stage.

2. The selection of initial values for the parameters in FNN is very important. The initial values in the FNN depend on the characteristics of the system. An unsuitable initial value will cause system unstable.
3. The small error accumulation on FNN will lead FNN system to diverge. Therefore the learning rate must be reduced, as the error is very small.

5.2 Time response under the impact of a mechanical disturbance

For the purpose of understanding the system response when it suffers a disturbance, two disturbance test cases are simulated for AVR controller with and without FNN.

1. A disturbance signal with 10 % mechanical torque, which occurs at time 1.0 s, is applied to the point $T_{m\Delta}$ shown in Figure 5.11. This disturbance signal last for a period of 100 ms.

The terminal voltage response caused by the variation of mechanical torque is shown in Figure 5.17. It is clearly seen in Figure 5.17 that the terminal voltage variation is very small when a 10 % mechanical torque is applied. The maximum deviation of terminal voltage is less than the value of 0.015 p.u. for using AVR controller. It is also evident that the FNN reinforces the generator system robustness. The terminal voltage response, which is caused by the variation of mechanical torque, is almost canceled by FNN. Therefore FNN can reject the disturbance of mechanical torque and maintain the terminal voltage constant. The output signal of the FNN in this simulation is also shown in Figure 5.18.

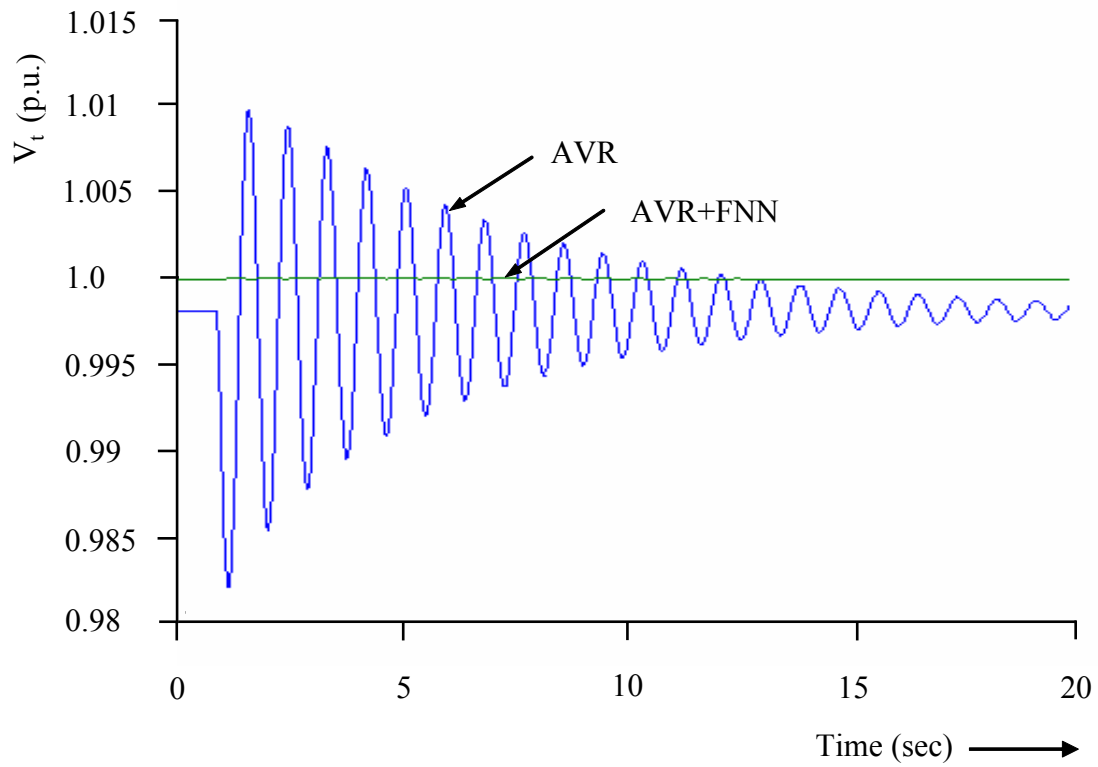


Figure 5.17 Terminal voltage response suffering a 10% variation in mechanical torque for controller with and without FNN.

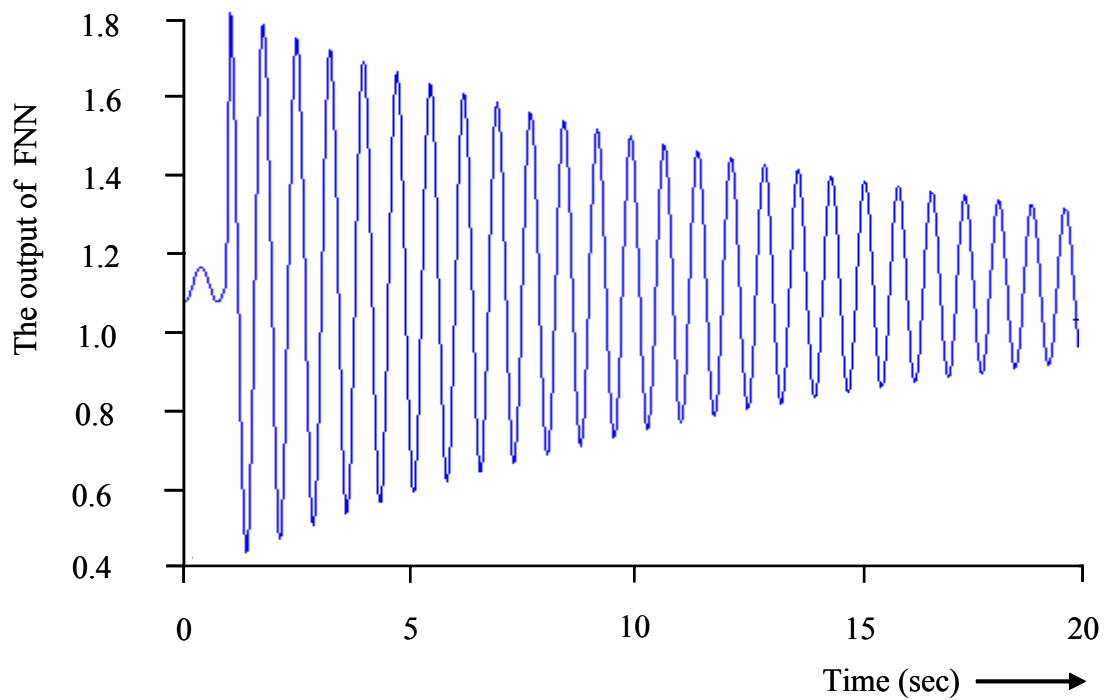


Figure 5.18 The output signal of an FNN compensator after 10% variation in mechanical torque for 100 ms happening at time 1.0 second.

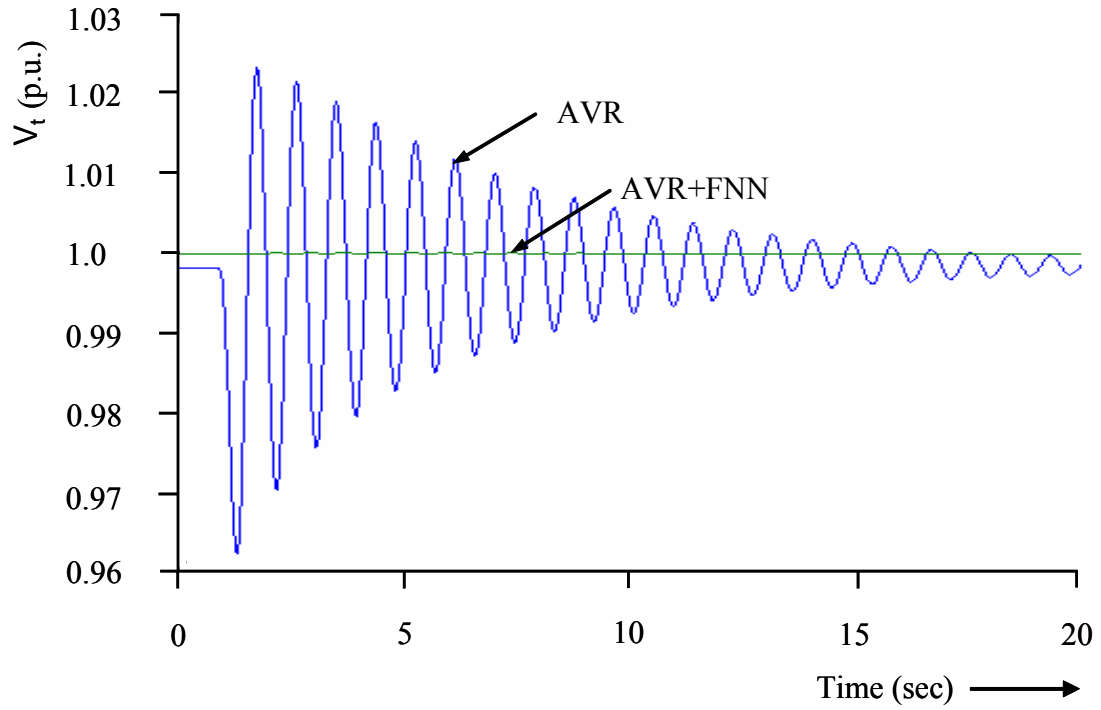


Figure 5.19 Terminal voltage response using an FNN compensator suffering a 20% variation in mechanical torque for 300 ms

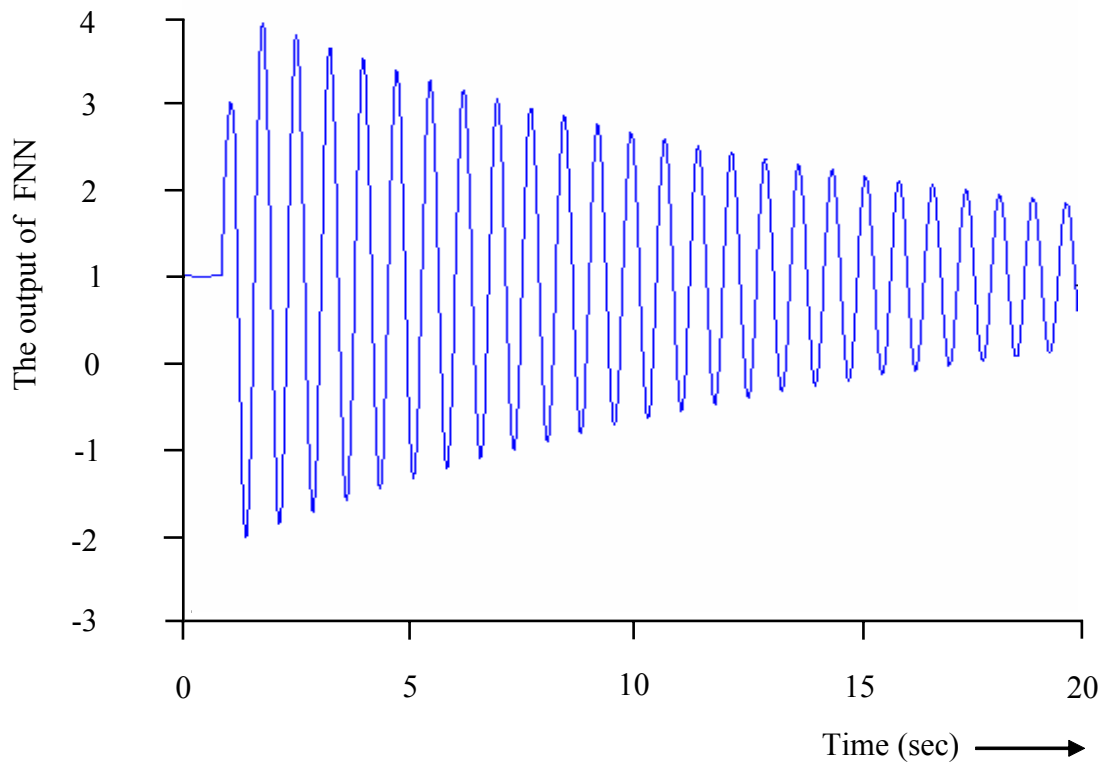


Figure 5.20 The output signal of an FNN compensator after application of a 20% variation in mechanical torque for 300 ms, at time 1.0 second.

2. A disturbance of 20 % variation of the mechanical torque for a period of 300 ms is simulated.

The maximum deviation of terminal voltage in this simulation shown in Figure 5.19 is less than the value of 0.037 p.u. for AVR controller only. It is also shown in Figure 5.19 that the deviation of terminal voltage is very small for AVR+FNN. It is evident that FNN can increase the system robustness. The output signal of the FNN in this simulation is also shown in Figure 5.20.

The above simulations indicate that FNN compensator provides a suitable compensation for the generator system caused by the external disturbance signal.

5.3 The fault condition simulated on the NETOMAC software

In previous section, an AVR and FNN compensator are simulated in a simplified linear generator system model. The FNN proves itself to work properly in such a simplified linear generator system. But another question is whether the effect of FNN in a complete generator system is same as in simplified linear generator or not. In order to obtain more detailed information about the behavior of the generator system, an AVR and FNN compensator will be simulated by using NETOMAC software. NETOMAC software was developed by Siemen Company, it is used to simulate magnetic and electrical mechanical phenomenon for the transmission network. Another interesting topic regarding the FNN compensator is whether or not the critical fault clearing time of synchronous generator (SG) can be prolonged under fault conditions.

Figure 5.21 shows the test circuit in which a generator is connected to the transmission line. There are three switches that are used to isolate the generator and transmission line in case of fault conditions.

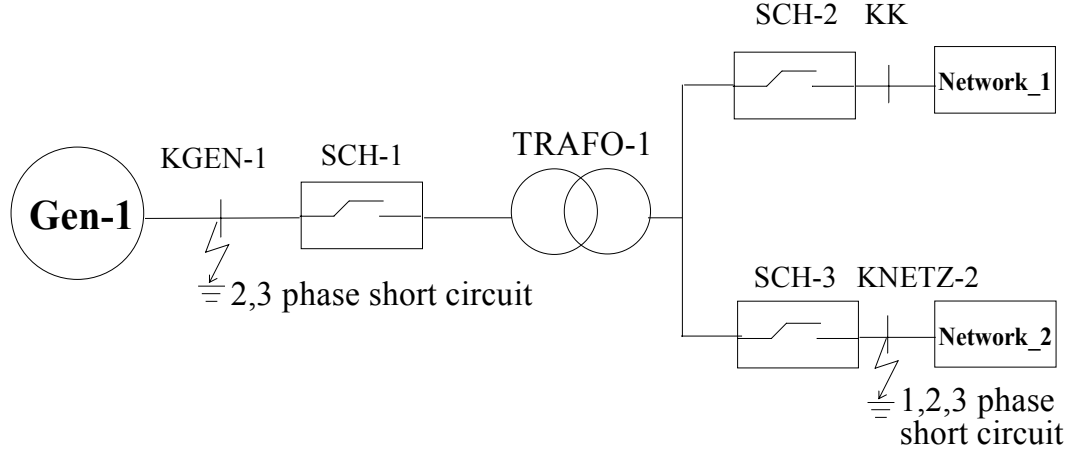


Figure 5.21 Test Networks for different fault conditions

This network is tested on a three-phase, double line-to-ground fault at node KGEN-1. It can also be tested on single-phase, two-phase and three-phase fault at node KNETZ-2. If the fault is found at node KGEN-1, the current switch SCH-1 will open after a short of time (80 ~100 ms) to protect power transmission system. If the fault happens at KNETZ-2, the current switch SCH-3 will shut off after a period of 100 - 150 ms.

5.3.1 Training of FNN parameters on NETOMAC software

The training procedure for the FNN described in the previous section will also be utilized in NETOMAC software. A reference model is taken and then we train parameters of FNN so that the response of terminal voltage of the generator system is same as that of the reference model.

The generator system with the controller AVR is simulated on NETOMAC software first. Some of the output signals of the generator system are displayed in Figure 5.22. The output signal of the reference model in this test is not the same as the response of the terminal voltage. Other signals, such as controller output, input signal to main exciter and the output of main exciter, are also displayed in Figure 5.22.

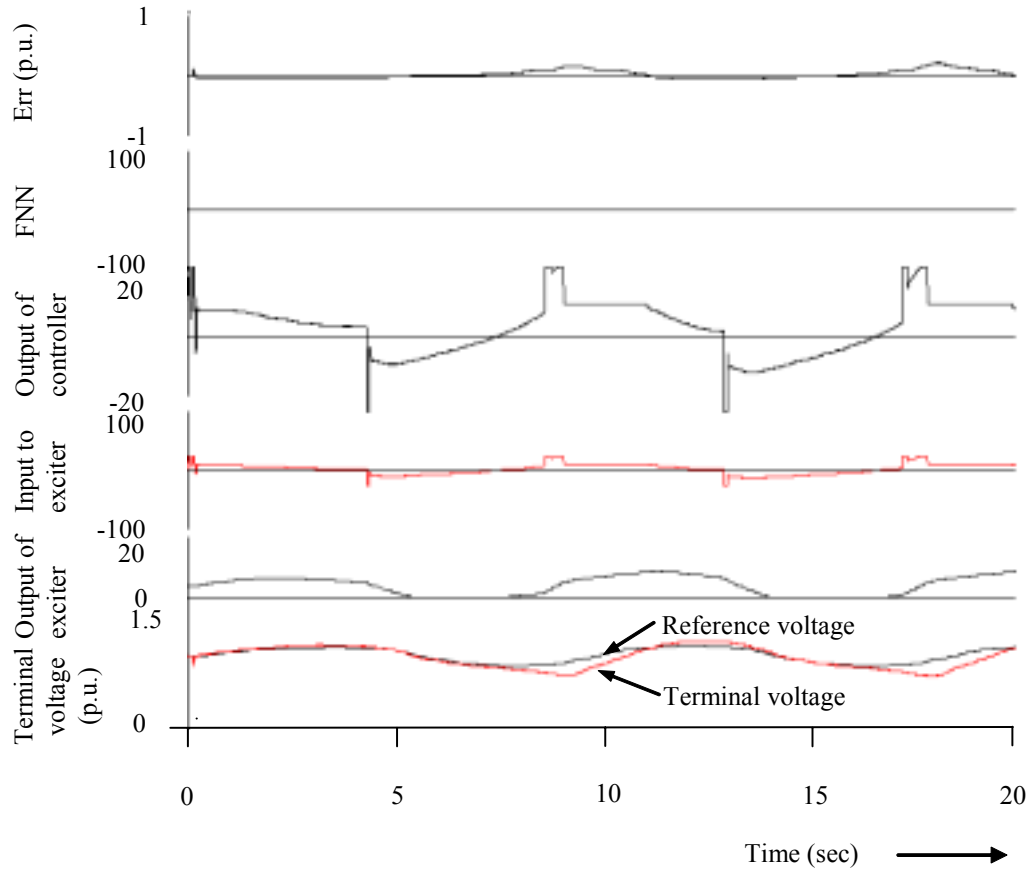


Figure 5.22 Terminal voltage response following reference voltage without FNN

In order to train the parameters of FNN, the generator system for a controller with FNN compensator is simulated in NETOMAC software again. The output signals of the terminal voltage, reference model, FNN and main exciter in this simulation are shown in Figure 5.23. The purpose of the FNN compensator working in conjunction with the controller is to maintain the characteristics of generator system same as the characteristics of reference model whenever the change of dynamic characteristics of generator system is. Figure 5.23 also shows that the terminal voltage follows the output of reference model accurately. It means that the parameters in FNN are already trained properly. Other generator datas, such as terminal voltage, current, mechanical torque, power, reactive power and so on are included in Figure 5.24. Park's variables of the generator system are displayed in Figure 5.25.

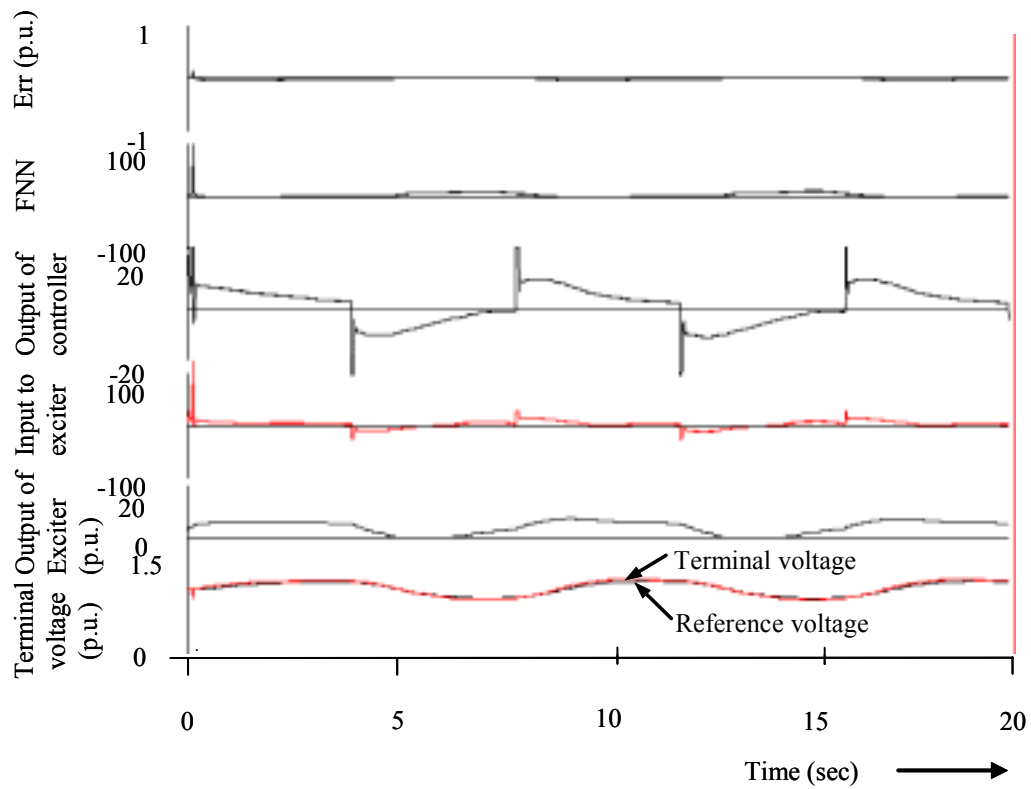


Figure 5.23 Terminal voltage response following reference voltage with FNN

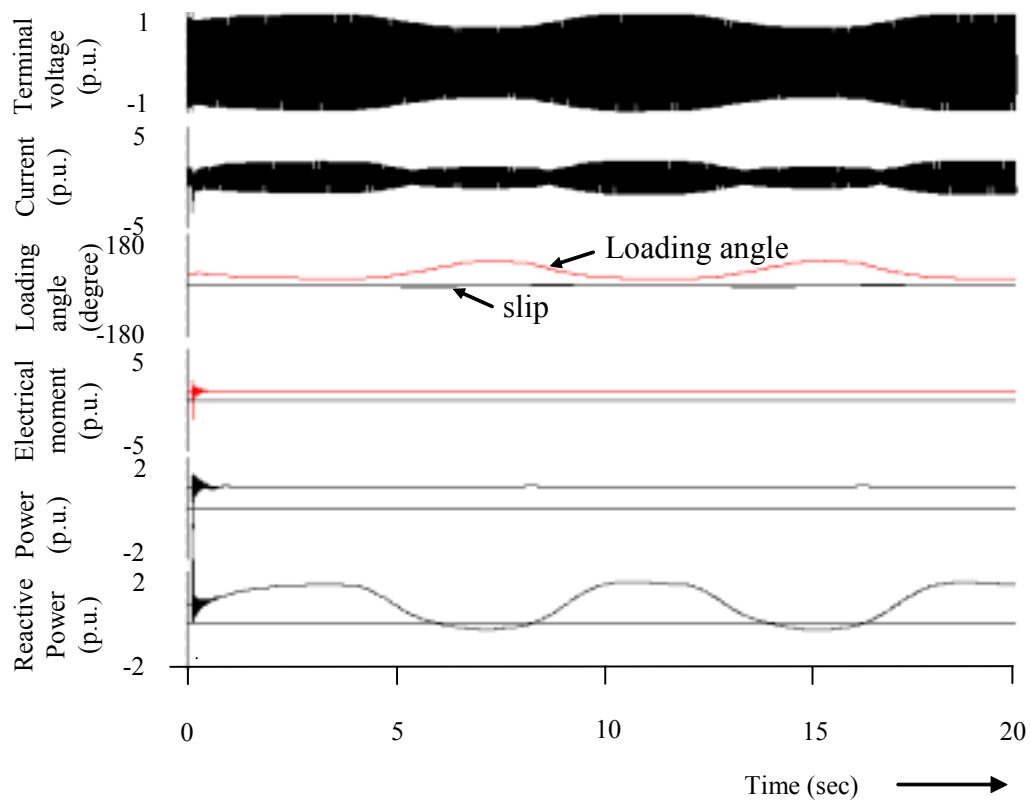


Figure 5.24 Generator output variables, including reactive power

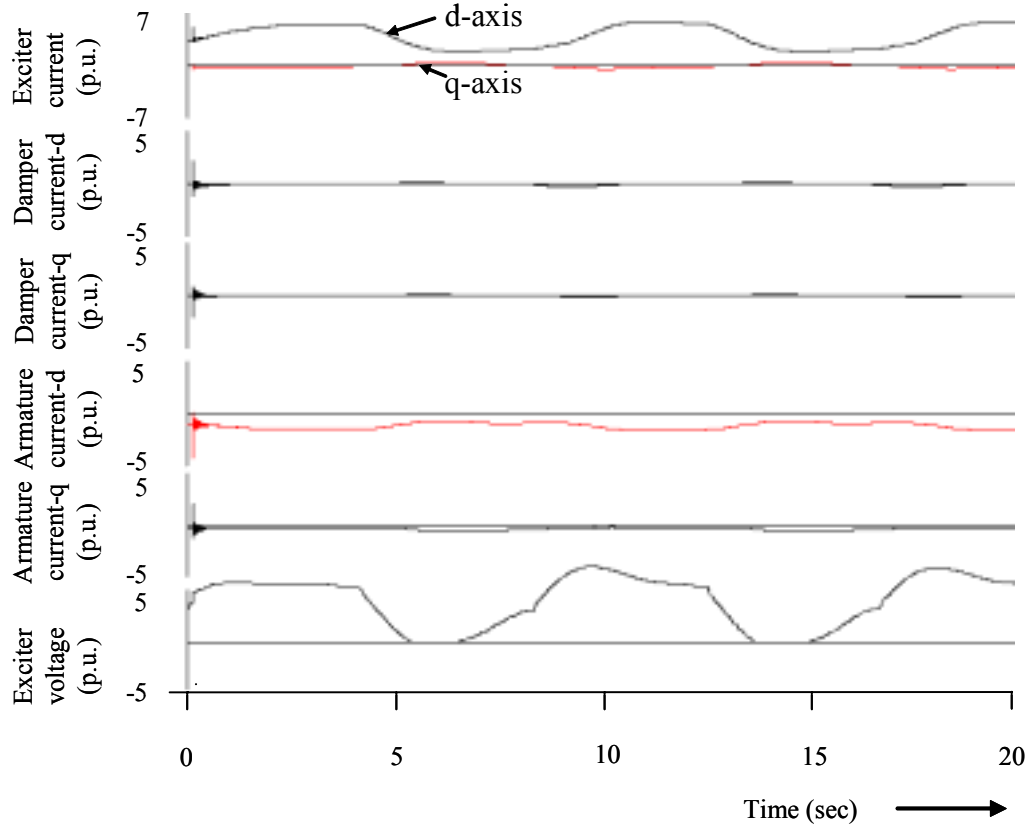


Figure 5.25 Generator output variables such as field current etc.

5.3.2 Simulation of different fault conditions

In this research, one of the topics of interest is on whether the critical fault clearing time of the synchronous generator can be prolonged under fault conditions by using FNN or not. The critical fault clearing time is defined as a period of time between the occurrence of the fault and the synchronous generator losing its synchronization.

When a generator system is shut down due to an unpredictable condition, it may lead to serious consequence. Therefore it is of the utmost importance to keep generator system stable as long as possible. In order to understand the critical fault clearing time of the generator system under different fault conditions, some simulations are made.

The simulation is divided into two parts, representing two different situations:

1. The fault occurs on the transmission line.

This fault happens at node KNETZ-2 in Figure 5.21. An AVR and AVR with FNN will be tested for single-phase, two-phase and three-phase faults.

2. The fault happens on the generator terminal.

Node KGEN-1 in Figure 5.21 is the place where the fault happens. An AVR and AVR with FNN are simulated for three-phase and two-phase faults.

5.3.2.1 Single-phase fault occurring on the transmission line

The single-phase fault at node KNETZ-2 in Figure 5.21 is simulated first. AVR controller with and without an FNN will be simulated separately.

A a-phase fault begins at time 0.1 s and the fault condition last until time 6.8 second. The comparison of the terminal voltage response on phase a for AVR controller with and without FNN is presented in Figure 5.26. As shown in figure 5.26, it indicates that the generator system is stable under single-phase fault condition. It does not lose synchronizing for AVR controller either with or without FNN. It also shows that the settling time and maximum overshoot of terminal voltage response for AVR controller with FNN are better than that for the AVR controller without FNN.

For the reason to understand the transient response of the generator under single-phase fault, a one second fault condition is simulated again. Figure 5.27 presents some of the simulation results of the parameters of the generator. The blue line is in behalf of the generator system controlled by an AVR only and the red line represents system controlled by an AVR + FNN. It is evident that the terminal voltage response at transient time for controller AVR + FNN displays a stronger reaction than that of the controller without FNN. The reason for this is that the FNN wants to

maintain the same dynamic characteristics in the generator at fault condition as in the reference model. The exciter voltage therefore increases rapidly. The exciter voltage in Figure 27 (d) for an AVR + FNN increases to the maximum limit of the exciter quickly. This effect is devoted by the compensator FNN. For the same reason, the current, electrical torque, reactive power and exciter current in the d-axis (Figure 5.27 (b,c,e,f)) show a stronger response of the generator system for the AVR controller with FNN. The disadvantage of an FNN under fault condition is the causation of high oscillation in the generator at transient time.

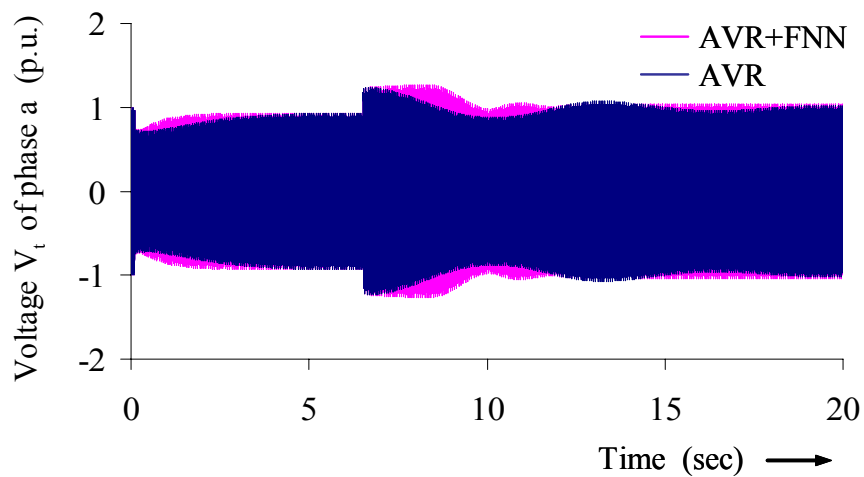


Figure 5.26 Terminal voltage response for a single-phase fault condition

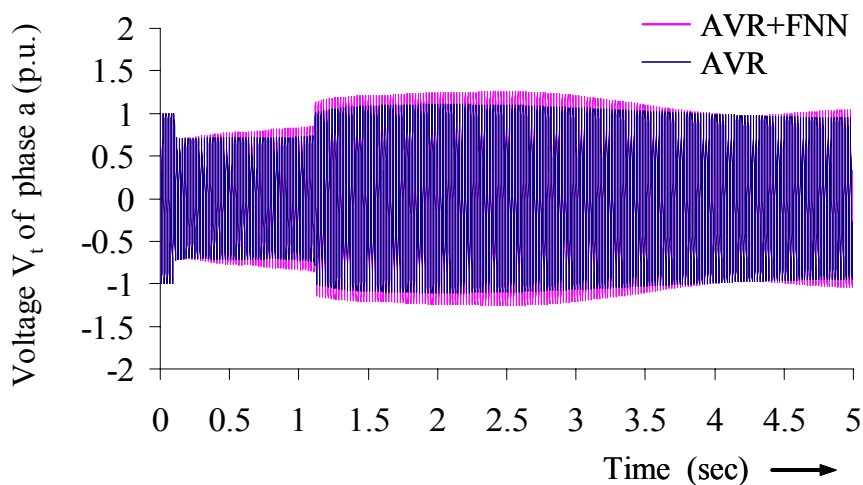


Figure 5.27 (a) Comparison of terminal voltage for a single-phase fault

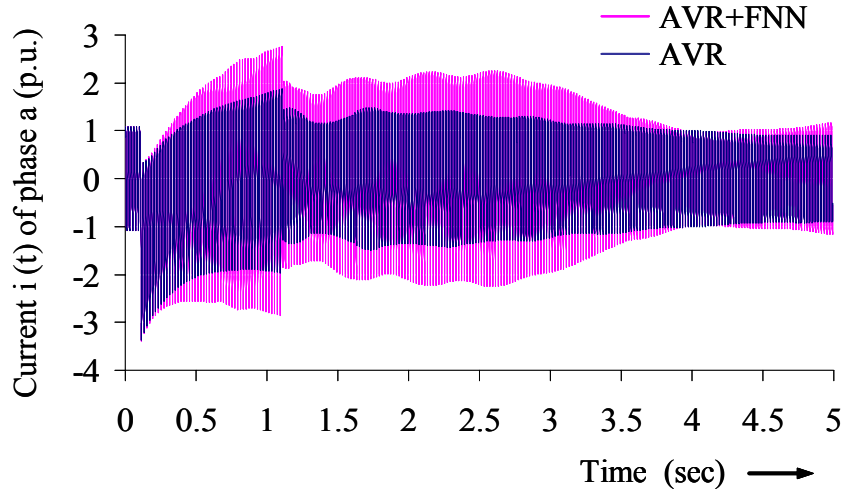


Figure 5.27 (b) Current comparison for a single-phase fault

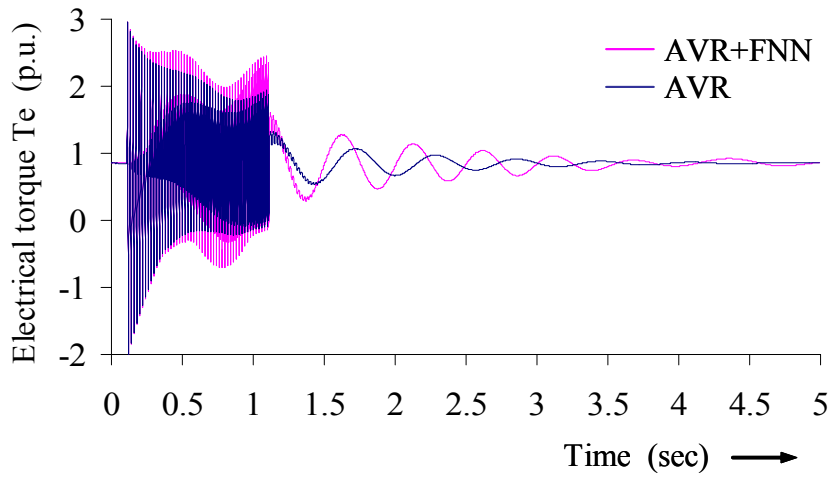


Figure 5.27 (c) Electrical torque comparison for a single-phase fault

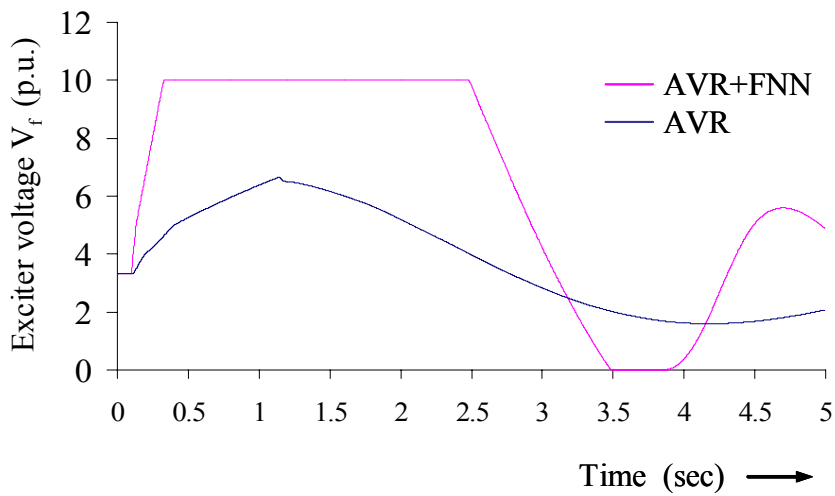


Figure 5.27 (d) Exciter voltage comparison for a single-phase fault

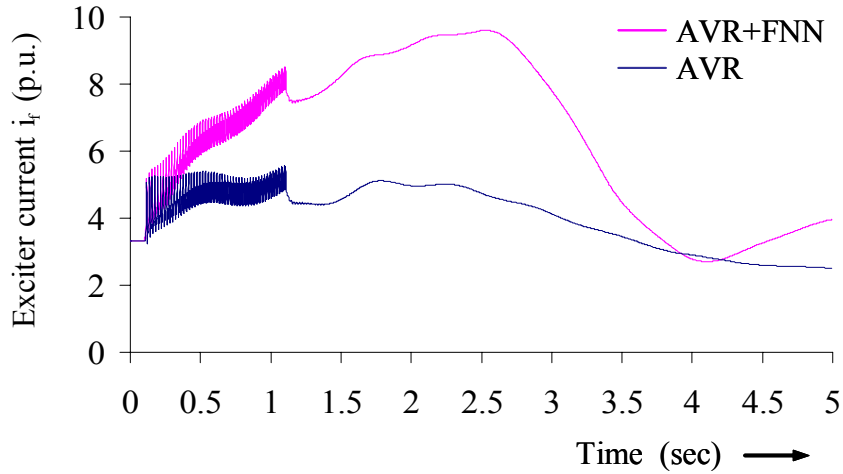


Figure 5.27 (e) Comparison of exciter current on the d-axis for a single-phase fault

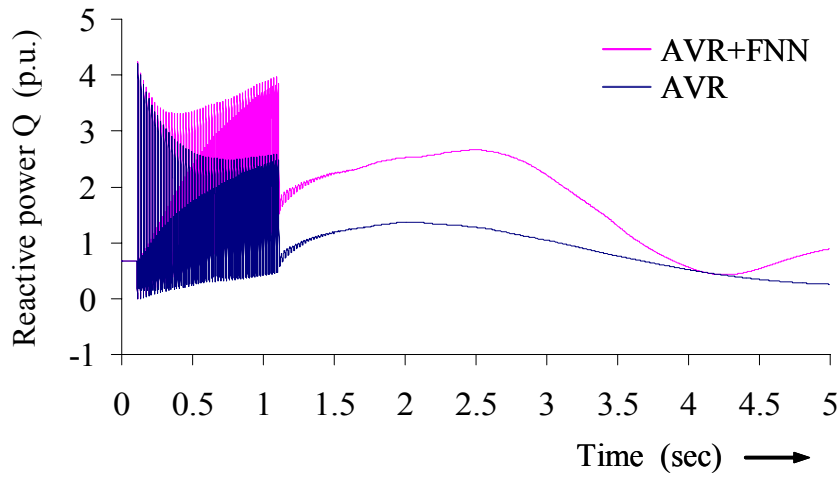


Figure 5.27 (f) Reactive power comparison for a single-phase fault

5.3.2.2 Two-phase fault occurring on the transmission line

A two-phase fault happening at node KNETZ-2 lasts 450 ms. The terminal voltage at a two-phase fault (Figure .5.28 (a)) is lower than that at a single-phase fault. Hence, the output of the exciter should increase so that the terminal voltage can be corrected to the set point as soon as possible. The output of exciter for AVR controller with FNN, shown in Figure 5.28 (d), increases to maximum limit of the exciter immediately. A comparison of electrical torque between single-phase fault in Figure 5.27 (c) and two-phase fault in Figure 5.28 (c) shows that the maximum value of 3.8 p.u. in two-phase fault is greater than that of the single-phase fault, a value of 3 p.u..

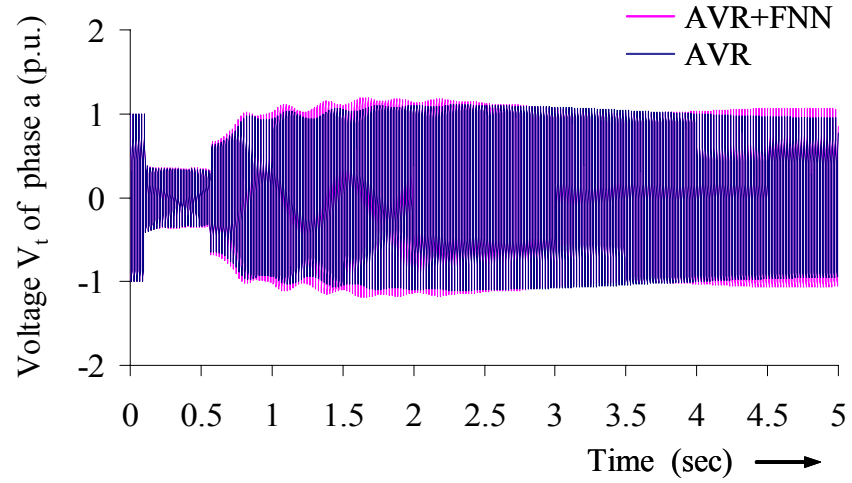


Figure 5.28 (a) Comparison of terminal voltage for a two-phase fault

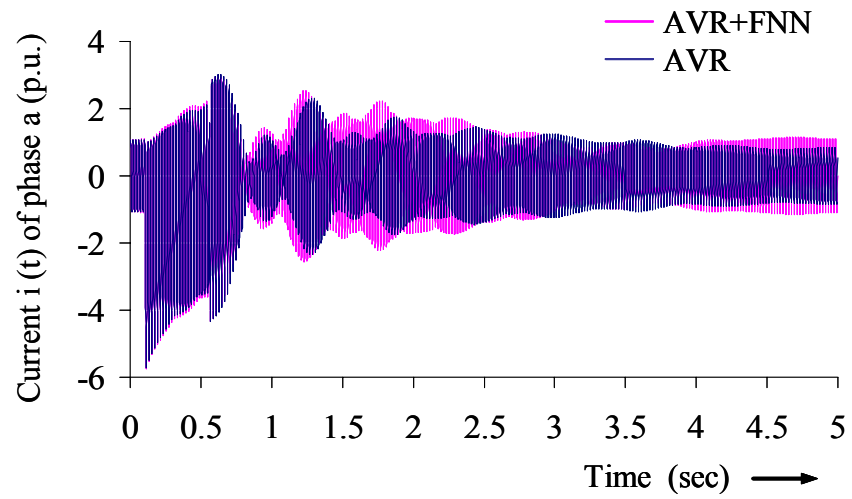


Figure 5.28 (b) Comparison of current for a two-phase fault

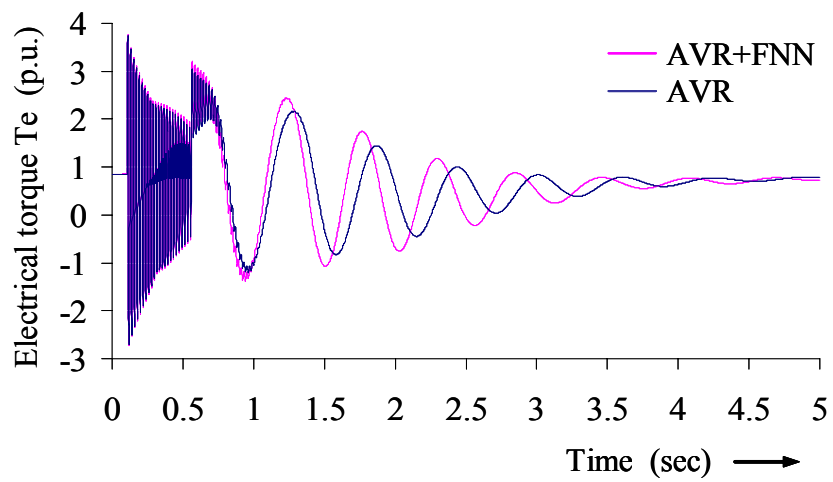


Figure 5.28 (c) Comparison of electrical torque for a two-phase fault

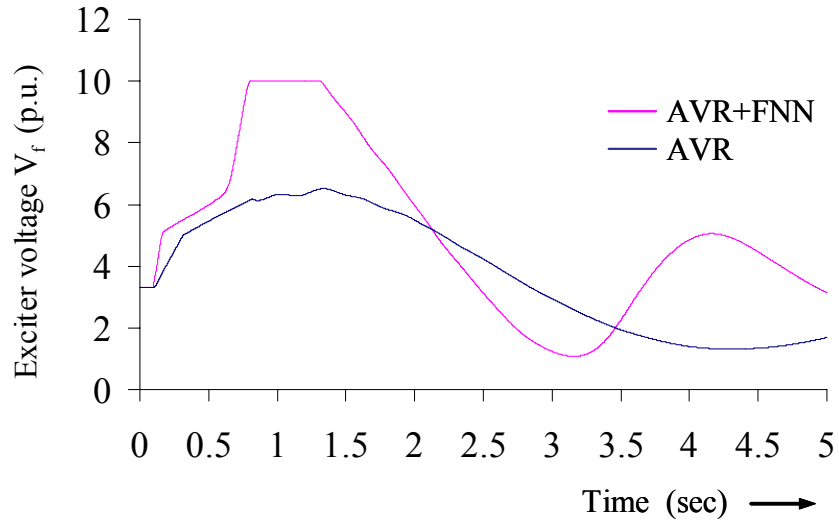


Figure 5.28 (d) Comparison of exciter voltage for a two-phase fault

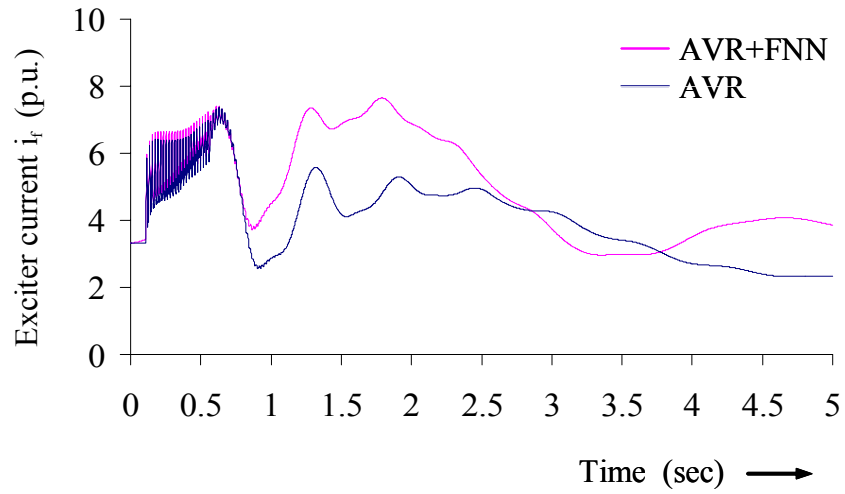


Figure 5.28 (e) Comparison of exciter current on d-axis for a two-phase fault

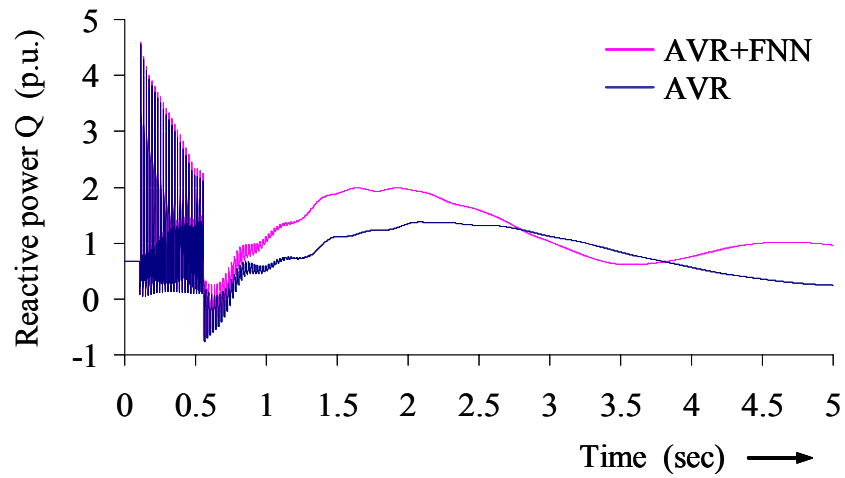


Figure 5.28 (f) Comparison of virtual power for a two-phase fault

The reason is that the terminal voltage drop is greater at a two-phase fault as stated above; the controller must be able to impose a strong corrective signal upon the main exciter. Other parameters for two-phase fault are included in Figure 5.28 (a-f).

5.3.2.3 Three-phase fault occurring on the transmission line

Power conservation theorem states that the input power should be the same as the output power for a balance system. Upon the occurrence of three-phase fault, the generator cannot transmit power to the network, therefore the mechanical power will accelerate the rotor speed and the generator rapidly loses its synchronization. The critical fault clearing time is the shortest under conditions of a three-phase fault.

This simulation of a three-phase fault lasts 240 ms.. The terminal voltage declines to a very small value at the fault time. The output of exciter is increased to its limit rapidly. As shown in Figure 5.29 (d), the response of exciter voltage for a controller with FNN is quite rapid. Its response to the occurrence of a three-phase fault is almost identical to that of two-phase fault. Other parameters, including terminal voltage, current, electrical torque, exciter voltage, and reactive power for controller with and without FNN are also shown in Figure 5.29 (a-f).

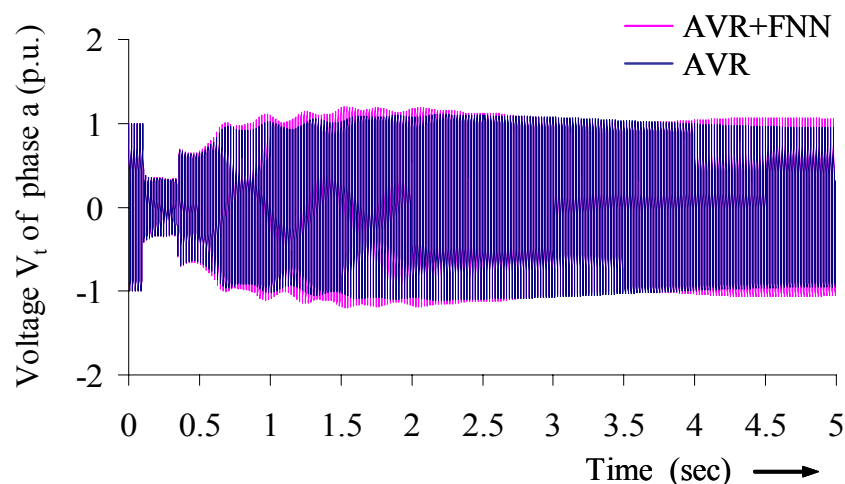


Figure 5.29 (a) Comparison of terminal voltage for a three-phase fault

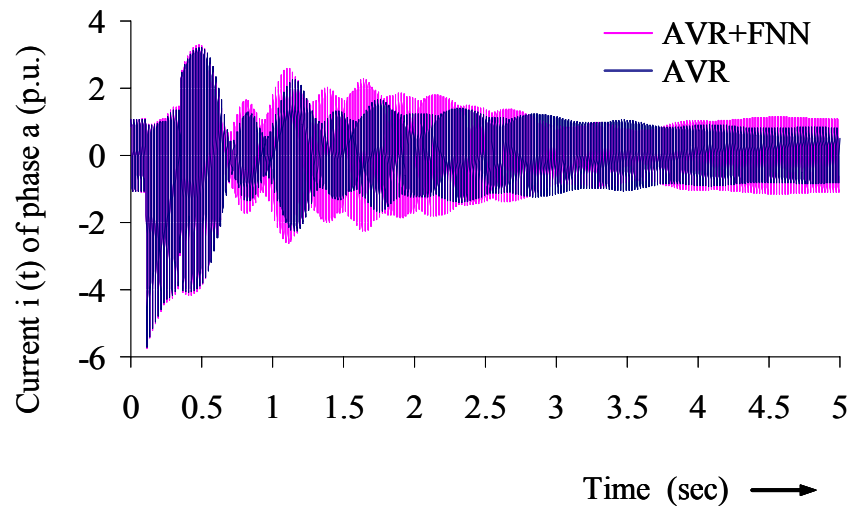


Figure 5.29 (b) Comparison of current for a three-phase fault

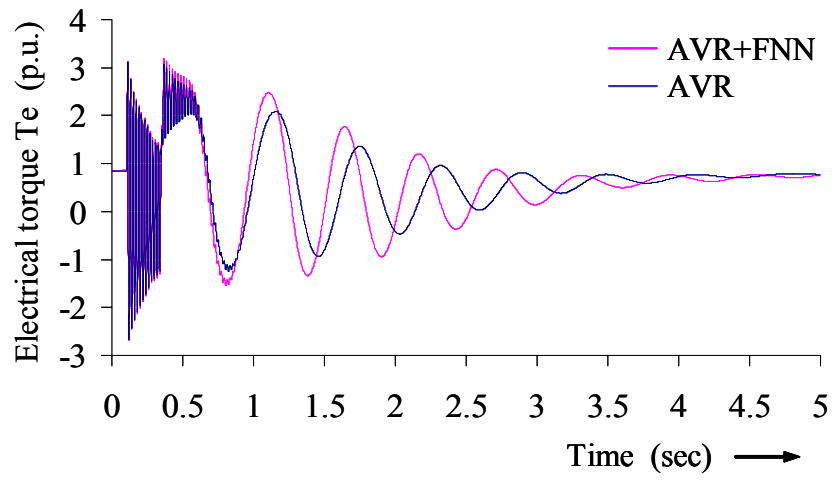


Figure 5.29 (c) Comparison of electrical torque for a three-phase fault

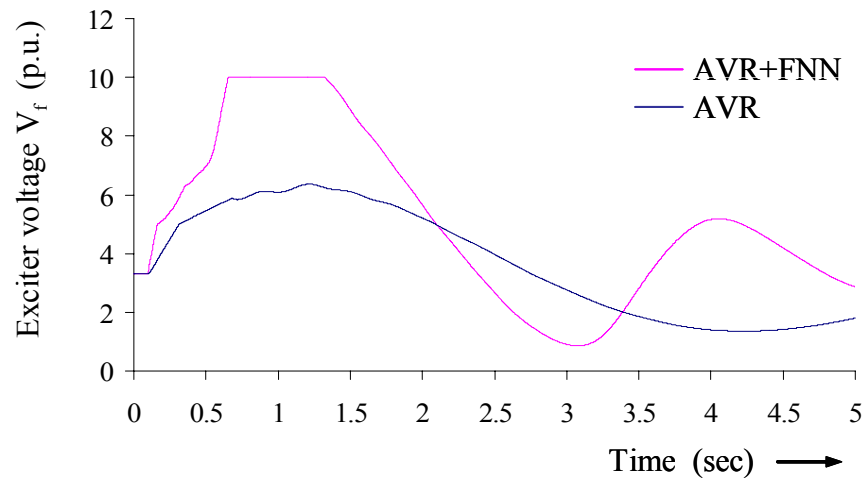


Figure 5.29 (d) Comparison of exciter voltage for a three-phase fault

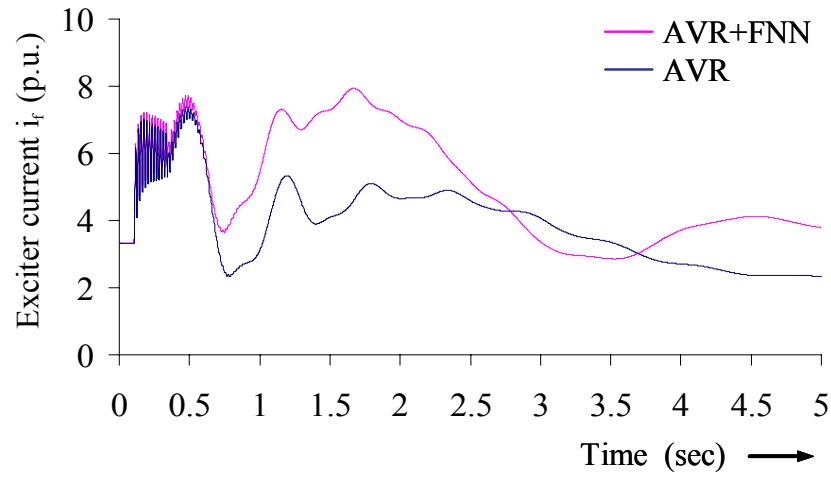


Figure 5.29 (e) Comparison of exciter current for a three-phase fault

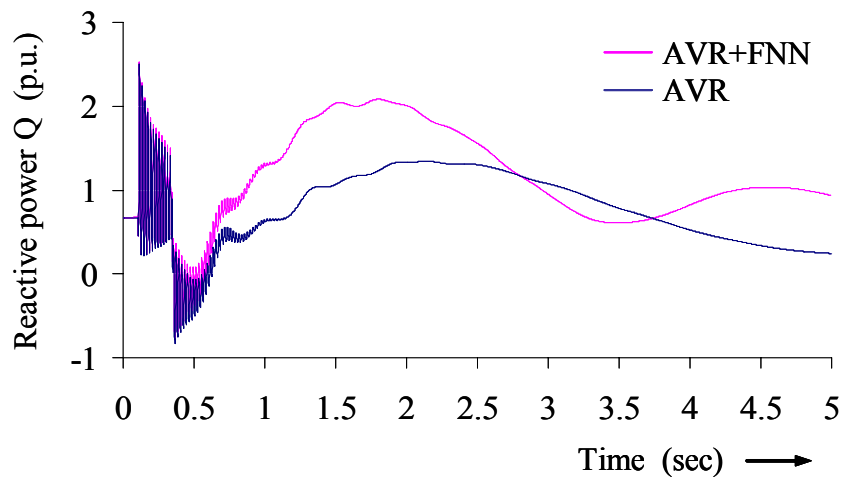


Figure 5.29 (f) Comparison of reactive power for a three-phase fault

Upon the occurrence of a single-, two-, or three-phase fault, a conventional controller with FNN will increase the output of exciter to the limit of the exciter immediately (see Figures 5.27 (d), 5.28 (d) and 5.29 (d)); the critical fault clearing time of a generator, which is affected by FNN signal, reaches its limit.

5.3.2.4 Fault condition happening on generator terminal

If a two- or three-fault condition occurs on the generator terminal, the terminal voltage of the generator will reduce to zero. Conservation of power theorem cannot be maintained. Under these conditions, the generator system loses its synchronization immediately, whether the controller AVR is equipped with FNN or not.

5.3.2.5 Critical fault clearing time for fault happening on transmission line

The simulation results of the critical fault clearing time (CFCT) for all faults happening at node KNETZ-2 are summarized in table 5.1. The first column represents different faults situations, the second column shows the CFCT of generator with an AVR alone and the third shows the CFCT of a generator with an AVR + FNN.

As can be seen from an examination of table 5.1, the CFCT of a generator with FNN under two-phase fault is longer than that of a controller without FNN by 25 ms. For three-phase fault, the CFCT of a generator with an AVR+FNN is 5 ms longer than that of a controller without FNN. The results show us that FNN working as a compensator can enhance, slightly, the CFCT performance of a generator under both two- and three-phase fault conditions.

Under single-phase fault condition, however, the generator system always remains stable, with both simple AVR and AVR+ FNN controllers.

The CFCT of a generator system is affected by many factors. In this research, an AVR controller with FNN compensator is used to try to extend the CFCT of the generator. It is evident, however, that the improvement in controller structure by the addition of an FNN cannot prolong the CFCT of a generator effectively.

Type of fault at node KNETZ-2	Critical fault clearing time (CFCT)		
	AVR	AVR+FNN	
Single-phase ground	stable	stable	Testing until 6.8 s
Two-phase ground	570 ms	595 ms	
Three-phase ground	265 ms	270 ms	

Table 5.1 Testing for different fault conditions

Chapter 6 Discussion and conclusion

The research of AVR is widely investigated using different control methods. In recent years, fuzzy system and neural network are widely applied to several industrial applications. The study of a fuzzy neural network combined with conventional controller is used to control the terminal voltage. One of the main objectives of this FNN compensator is used to reinforce generator system robust. Another objective of this research is to understand the effect of FNN on critical fault clearing time of a generator. The simulation result appeared that FNN worked properly.

In this simulation some of results can be discussed.

1. The simulation shows that the loading variation of the system does not affect the terminal voltage seriously when FNN compensator is used. The robust of this system with FNN compensator is better than that of the system only with the conventional controller alone.
2. The learning rate in FNN is important. It affects learning speed of FNN and system stability. A large learning rate provides FNN a large correction signal such that the FNN system is easily diverging. A small learning rate provides FNN a small correction signal such that it cannot supply an enough correction signal to follow the reference model. Therefore a suitable learning rate must be tested on the learning stage.
3. FNN compensator prolongs the critical fault clearing time of a synchronous generator, 25 ms for two-phase fault and 5 ms for three-phase fault. It shows that the FNN can't make an obvious improvement on the critical fault clearing time of a generator. The reason is that the output of the main exciter affected by AVR+FNN under fault conditions reaches to its limit, therefore, the effect of AVR+FNN on the critical fault clearing time is also limited.
4. If fault condition happens on the transmission line, the generator system has a

shorter settling time for the controller with FNN. It means that AVR+FNN reduces the settling time of the system.

Future works corresponding to this dissertation are listed as follows:

1. FNN compensator combined with voltage controller presents the robustness of the system when it suffered from an impact disturbance. But if the system is on fault condition, it can't obviously last the critical fault clearing time of a generator. One of possible reasons is that the turbine does not react simultaneously. The possible solution to last the critical fault clearing time of a generator on fault conditions is that the voltage controller of generator and speed controller of turbine work together.
2. The initial values of parameters of FNN decide whether the FNN system can be well trained or not. A systematic method to find the initial values for the parameters in FNN can reduce the time to train FNN.
3. To increase the system robust, the integration of FNN with other control laws, such as variable structure system, H_∞ algorithm ..., is another research topic in the future.

List of symbols

<u>Symbol</u>	<u>unit</u>	<u>meaning</u>
A_i^j		The linguistic term of the precondition part with membership function $\mu_{A_i^j}$
\mathbf{b}		Bias vector on FNN
d_j		The constant consequent part
E	V	The induced voltage in stator winding due to the field current
E_{FD}	V	The main exciter voltage
E_q	V	The stator induced voltage proportional to main winding flux linkage on d-axis.
e_m	V	The error between V_m and V_t used in FNN
F		Energy function
$G(s)$		The transfer function of a process
$H(s)$		The feedback transfer function
i	A	Current
i_a, i_b, i_c	A	Three phase current on stator
i_d, i_q, i_o	A	Stator current on odq-axis
i_F, i_D, i_Q	A	Winding current on rotor

<u>Symbol</u>	<u>unit</u>	<u>meaning</u>
i_{Dd} , i_{Dq}	A	Damping current on odq-axis
J	kg.m ²	The moment inertial of generator
K		A variable positive constant
K ₁		Deviation in electrical torque for a change in rotor angle with constant flux linkages in the d axis
K ₂		Deviation in electrical torque for a change in d-axis flux linkages with constant rotor angle
K ₃		Impedance factor
K ₄		Demagnetizing effect of a change in rotor angle
K ₅		Change in terminal voltage with change in rotor for a constant E _q
K ₆		Change in terminal voltage with change in E' _q for constant rotor angel
L	H	Inductance
L _{ασ}	H	Leakage inductance
L _e	H	The equivalent inductance of transmission line
L _d , L _q	H	Stator winding inductance on d-axis and q-axis
L _{Dd} , L _{Dq}	H	Damping winding inductance on d-axis and q-axis
L _f	H	Field winding inductance

<u>Symbol</u>	<u>unit</u>	<u>meaning</u>
L_{hd}, L_{hq}	H	Main mutual inductance on odq-axis
m_{ji}		The mean value of Gaussian functions of jth term
P	W	The output power of generator
p_1, p_2, \dots, p_n		The poles of $G(s)$ $H(s)$
R_a		Winding resistance at stator
R_{Dd}		Damping winding resistance on d-axis
R_{Dq}		Damping winding resistance on q-axis
R_{inf}		The equivalent resistance of transmission line
R_f		Winding resistance at rotor winding
T		Transformation matrix from fixed axis to rotary axis
T_e	N m	Electrical torque
T_m	N m	Mechanical torque
v_a, v_b, v_c	V	Stator voltage of the generator
v_F, v_D, v_Q	V	Winding voltage on the rotor of the generator
V_m	V	The reference voltage signal of FNN
V_t	V	The terminal voltage of generator
x_1	V	The input signal of FNN

<u>Symbol</u>	<u>unit</u>	<u>meaning</u>
\dot{x}_2	V/sec	The derivative of input signal x_1 of FNN
x_i		The i th input variables of FNN
X_d		Unsaturated d-axis synchronous impedance
X_q		Unsaturated q-axis synchronous impedance
X_e		The equivalent inductance impedance of transmission line
X'_d		Unsaturated d-axis transient impedance
y		The output variable of FNN
z_1, z_2, \dots, z_n		The zeros of $G(s) H(s)$
$\Delta\delta$	rad	The deviation of rotor angle
θ	rad	The rotor angle
ω	rad/sec	The rotor velocity
ω_d	rad/sec	Oscillation frequency of system
ω_n	rad/sec	Natural frequency
ω_R	rad/sec	The rated angular velocity of rotor
$\Delta\omega$	rad/sec	The deviation of rotor speed
Ψ_d, Ψ_q, Ψ_o	Wb	Magnetic flux linkage on odq-axis
Ψ_{Dd}, Ψ_{Dq}	Wb	Magnetic flux linkage of damping winding on odq-axis

<u>Symbol</u>	<u>unit</u>	<u>meaning</u>
Ψ_f	Wb	Magnetic flux linkage of rotor winding on odq-axis
δ	rad	Angle between induced voltage and reference voltage
α	rad	Angle between reference axis and infinite bus voltage
	rad	Angle between induced voltage and terminal voltage.
$\mu_{A_i^j}$		The membership function of A_i^j .
σ_{ji}		The standard deviation of Gaussian functions of jth term associated with ith input variable x_i
ξ		Damping ratio
η_ω		The learning-rate parameter of the link weight
η_m		The learning-rate parameter of the mean deviation of the Gaussian function
η_σ		The learning-rate parameter of the standard deviation of the Gaussian function
τ'_{do}	s	The d axis transient open circuit time constant

Notation:

Scalars : letters
 Matrices : BOLD nonitalic letters
 Vector : BOLD nonitalic letters

Appendix

Appendix A: Data of an AC synchronous generator

Parameters of equivalent circuit of the generator and exciter are listed in appendix A.

The machine data of main AC generator offered by the manufactory is shown as table A.1 and A.2.

	Stator	Rotor	Damping	Main-inductance
Resistance d-axis (p.u.)	$R_a=0.0011$	$R_{fd}=0.00125$	$R_{Dd}=0.01042$	
Resistance q-axis (p.u.)	$R_a=0.0011$	$R_{fq}=0.00441$	$R_{Dq}=0.00842$	
Inductance d-axis (p.u.)	$X_a=0.1959$	$X_{fd}=0.1121$	$X_{Dd}=0.03363$	$X_{hd}=1.953$
Inductance q-axis (p.u.)	$X_a=0.1959$	$X_{fq}=0.8887$	$X_{Dq}=0.06935$	$X_{hq}=1.846$
Rated MVA $S_r=412$ MVA, Rated voltage $V_r=21$ kV, Frequency $f_r=50$ Hz, $T_a=7.0$ sec				

Table A.1 Parameters of the equivalent circuit of the AC main generator

	Subtransient impedance (p.u.)	Transient impedance (p.u.)	Main impedance (p.u.)	Subtransient time constant (sec)	Transient time constant (sec)
d-axis	$X_d''=0.23459$	$X_d'=0.314$	$X_d=2.1489$	$T_d''=0.03188$	$T_d'=0.77658$
q-axis	$X_q''=0.25807$	$X_q'=0.7958$	$X_q=2.0419$	$T_q''=0.08205$	$T_q'=0.7693$

Table A.2 The parameter of short circuit of the AC main generator

The machine data of the main exciter used in the simulation is listed on table A.3 and A.4.

	Stator	Rotor	Damping	Main-inductance
Resistance d-axis (p.u.)	$R_a=0.0057$	$R_{fd}=0.00112$	$R_{Dd}=0.043$	
Resistance q-axis (p.u.)	$R_a=0.0057$	$R_{fq}=*****$	$R_{Dq}=0.0191$	
Inductance d-axis (p.u.)	$X_a=0.1779$	$X_{fd}=0.5491$	$X_{Dd}=0.6227$	$X_{hd}=2.1775$
Inductance d-axis (p.u.)	$X_a=0.1779$	$X_{fq}=*****$	$X_{Dq}=0.0629$	$X_{hq}=1.2336$
Rated MVA $S_r=2.67$ MVA, Rated voltage $V_r=0.387$ kV, Frequency $f_r=150$ Hz				

Table A.3 The parameter of equivalent circuit of the main exciter

	Subtransient impedance (p.u.)	Transient impedance (p.u.)	Main impedance (p.u.)	Subtransient time constant (sec)	Transient time constant (sec)
d-axis	$X_d''=0.31279$	$X_d'=0.51661$	$X_d=2.3554$	$T_d''=0.04728$	$T_d'=1.60736$
q-axis	$X_q''=0.23776$	$X_q'=1.41148$	$X_q=1.41145$	$T_q''=0.0364$	$T_q'=*****$

Table A.4 The parameter of short circuit of the main exciter

Appendix B: P.u. base of the generator system

The base of AC main generator and main exciter are listed in table B.1 and B.2, which is supplied by the manufacturer.

Stator voltage V_B (kV)	Stator current I_B (A)	Stator impedance Z_B ()	Rotor voltage V_{fB} (kV)	Rotor current I_{fB} (A)	Rotor impedance Z_{fB} ()
21	11327	1.070388	179.643	2293.393	78.33488

Table B.1 The base value of the AC main generator

Stator voltage V_B (V)	Stator current I_B (A)	Stator impedance Z_B ()	Rotor voltage V_{fB} (V)	Rotor current I_{fB} (A)	Rotor impedance Z_{fB} ()
286.5659	5355.98176	0.0535	17829.68	86.083548	207.121

Table B.2 The base value of the main exciter

Appendix C: Data of the main exciter

The manufacturer supplies test data of the main exciter. Appendix C.1 is the open circuit test data for the main exciter. Appendix C.2 is the test data of the main exciter which is connected with a resistor with a value of 0.0976 .

C.1 Test data of the main exciter under open circuit

I_{fo} The current in rotor (A)	U_g The terminal voltage of exciter (V)
21.93	193.5
26.31	232.2
30.7	270.9
35.08	309.6
39.47	348.3
43.86	387.0
48.24	425.7
52.63	464.4
57.02	503.1
61.46	541.8
65.91	580.5
70.36	619.2
90.0	774.0

C.2 Test data of the main exciter connected with a load.

I_n The current in rotor (A)	I_G The current through the load (A)
57.73	1983.0
69.27	2379.6
80.82	2776.2
92.36	3172.8
103.91	3569.4
115.45	3966.0
127.00	4362.6
138.55	4759.2
150.15	5155.8
161.74	5552.4
173.34	5949.0
185.02	6345.6
236.00	7932.0

C.3 The base of the main exciter on stator and rotor

The base of the main exciter on stator and rotor are:

$$U_{GN}=387 \text{ V} \quad ; \quad I_{GN}=3966.0 \text{ A} \quad \text{in stator}$$

$$U_{FN}=26.63 \text{ V} \quad ; \quad I_{FN}=115.45 \text{ A} \quad \text{in rotor}$$

The maximum value of the main exciter in stator and rotor are:

$$U_{GS}=774 \text{ V} \quad ; \quad I_{GS}=7932.0 \text{ A} \quad \text{in stator}$$

$$U_{FS}=54.44 \text{ V} \quad ; \quad I_{FS}=236.00 \text{ A} \quad \text{in rotor}$$

Appendix D: NETOMAC Software

D.1 Introduction of the NETOMAC software

NETOMAC program, which is developed by Siemens Company, is used to simulate the magnetic and electrical mechanical phenomenon for the transmission network. This software has been simulated on thousands of cases for the different power systems in the world. It has many different functions that can be applied on power system simulation analysis. Those functions of this software can be stated as following:

- The system analysis can be executed in time domain and frequency domain.
- Parameters of transmission system or controller can be optimized by optimal function which is supplied by NETOMAC software.
- Plenty of linear and nonlinear elements of power system can be available.
- Plenty of synchronous and asynchronous machine models can be available. User himself can construct a special generator structure.
- The eigenvalue of the transmission system can be found.
- Order reduction of dynamic loading model.
- Identification of the parameters of the asynchronous machine with the effect of saturation can be executed.
- User can define himself program to work with NETOMAC software together.

D.2 Integration of FORTRAN program with NETOMAC

The user program, which is written in FORTRAN language, can be called as subroutine from the controller section in the NETOMAC program.

The standard procedure to call a FORTRAN program from the controller section in NETOMAC software will be described as following.

D.2.1 The NETOMAC format for calling an external program

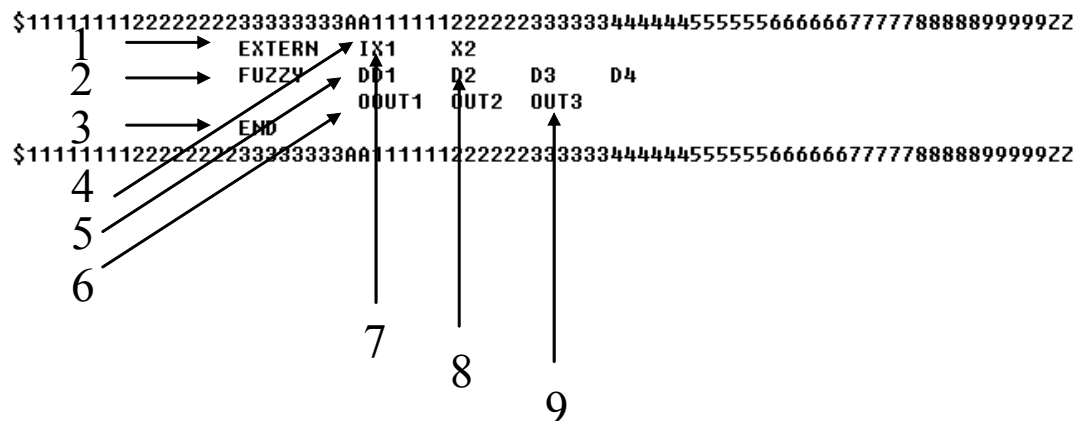


Table D.1 The format to call FORTRAN program

Table D.1 is the format that is used in controller section of NETOMAC program to call the FORTRAN program. The parameter in this section is declared as following in detailed.

1. “EXTERN”: Declaration to call an external program in control section. (i.e. the extra program, which is not included in NETOMAC database, will be used).
2. “FUZZY”: The external program filename written with FORTRAN language. The filename must be declared in NETOMAC controller section (here FUZZY is the filename of FORTRAN subroutine).
3. “END”: The end of this format.
4. “I”: It represents variables in NETOMAC which will be transmitted to FORTRAN program during the running of program. Here x1 and x2 two variables, that are defined in NETOMAC program before.

5. “D”: It is in behalf of data transmission from NETOMAC to FORTRAN if this program is simulated at the first time. Here D1, D2, D3 and D4 are four different data that are delivery to FORTRAN program.
6. “O”: It is in behalf of the output symbol. The selected output variables in FORTRAN program will be transmitted to parameter out1, out2 and out3.
7. x1, x2 are two parameters which will be transmitted to the subroutine.
8. D1, D2, D3 and D4 will be passed to the subroutine when the program runs at first time.
9. out1, out2 and out3 are three variables got the data from FORTRAN subroutine.

D.2.2 The format of FORTRAN subroutine

The standard format to call an external subroutine in the NETOMAC program is explained above. The subroutine program written with FORTRAN has also a fixed format. This fixed format is listed as following:

```

1      SUBROUTINE EXTERN (NENTRY,EINMAX,X0,X1,CX,      &
                                AUSMAX,Y0,Y1,CY,      &
                                &                    DATMAX,DATA,      &
                                &                    T0,T1,STEUER,*)
!
2      IMPLICIT  REAL*8(A-I,O-U,W-Z,M), integer  (K,N),REAL*8(V)
!
3      INTEGER  , PARAMETER :: NEXMAX = 1

4      CHARACTER  NENTRY*8  !NAME DES FORTRAN UP (2.zeile , name3
!                           der netomac-eingabe

```

! einmax,ausmax und datmax werden durch den netomac-Interpreter aus

! der Notation in den Regler-Datensaetzen ermittelt:

!

```

5      INTEGER      EINMAX      !ZAHL DER EINGANGS-GROESSEN
6      INTEGER      AUSMAX      !ZAHL DER AUSGANGS-GROESSEN
7      INTEGER      DATMAX      !ZAHL DER DATEN (vielfaches von 9 )
!
! jeder Eingangs- und Ausgangsname umfasst 4 real*8-Zahlen
! X0 : vor dem Integrationsschritt
! X1 : nach dem Integrationsschritt
! CX1: Realteil und
! CX2: Imaginaerteil fuer die komplexe Start-Rechnung
!
8      REAL*8        X0(EINMAX)   !EINGANGS-GROESSEN T-DT
9      REAL*8        X1(EINMAX)   !EINGANGS-GROESSEN T
10     COMPLEX*16 CX(EINMAX)
!
! die Return-Werte sind wie die Input-Werte aufgebaut:
!
11     REAL*8        Y0(AUSMAX)   !AUSGANGS-GROESSEN T-DT
12     REAL*4        Y1(AUSMAX)   !AUSGANGS-GROESSEN T
13     COMPLEX*16 CY(AUSMAX)
!
! im Unterschied zu den X- und Y-Werten bestehen die Daten-Werte nicht
! aus einem Quartett, sondern aus nur einem Real*8-Wert:
!
14     REAL*8        DATA(DATMAX) !DATEN
!
15     REAL*8        T0            !INTEGRATION: Zeit am Intervallanfang
16     REAL*8        T1            !INTEGRATION: Zeit am Intervallende
!
!ZEITSCHRITT BEI ANFANGSBED.
! steuer wird durch den Zustand des Hauptprogrammes bestimmt.
! damit kann Anfangsbedingung von normaler Integration unterschieden
! werden
17     INTEGER      STEUER        !STEUERT DATENEINLESEN,ANFGBD,INTEGR
!
18     REAL*8 AUS(2)
!-----
! >>hier die Anzahl der gueltigen externen UP's eintragen:
! typmax1:   Anzahl der EXTERN-Gruppen (tab,exfu,imfu,hsim,...)

```



```

34      SELECT CASE(KENTRY)
35      CASE(1)
36      CALL FUZZY_INITIAL_VALUE(*2222)
37      END SELECT
38      ELSEIF(STEUER.EQ.3)THEN      ! 3   die eigentliche Integration
39      SELECT CASE(KENTRY)
40      CASE(1)
41      CALL FUZZY_INTEGRATION(X1,Y1)
42      END SELECT
43      ENDIF
!
44      RETURN
45 2222 RETURN 1                      !FEHLER BEIM EINLESEN
!-----
46      END

!-----
!-----
47      SUBROUTINE FUZZY_READ_myDATA(*)
48      CHARACTER(LEN=80) :: PUFF
!
49 REAL*8 :: ERR_TOR,ERRD_TOR
50      ERR_TOR=D1
51      ERRD_TOR=D2
!
52      RETURN

53 2222 RETURN 1                      !FEHLER BEIM EINLESEN
54      END

!-----
55      SUBROUTINE FUZZY_INITIAL_VALUE(*)
56      CHARACTER(LEN=80) :: PUFF
!
57 REAL*8 :: ERR_TOR,ERRD_TOR
58      ERR_TOR=.001
59      ERRD_TOR=.005

```

```

!
60      RETURN

61  2222 RETURN 1                                !FEHLER BEIM EINLESEN
62      END
!-----
63      SUBROUTINE FUZZY_INTEGRATION (X1,Y1)
64      REAL*8 :: X1(2),Y1(2)
!-----
65      Y1(1)=X1(1)
66      Y1(2)=X1(2)
67      Y1(3)=5.
67      RETURN
!
68      END
!-----
!-----

```

where

STEUER: An index, which is used in this subroutine, decides which subroutine must be run. It is controlled by program itself.

STEUER=1; Executing the data reading program. Here the subroutine name is

FUZZY_READ_myDATA

STEUER=2; Executing the data initialization. The subroutine name is

SUBROUTINE FUZZY_INITIAL_VALUE(*)

STEUER=3; Executing the main program. The filename is called as
FUZZY_INTEGRATION.

The main FORTRAN program is coded in this part.

X1: It is an array. The parameters such as x1, x2 variables declared in controller section in NETOMAC program are passed to X1 array during the running of program.

Y1: It is also an array. The output variables of FORTRAN subroutine are stored in Y1. The values in Y1 are passed to the out1, out2, and out3 in the NETOMAC controller section.

Filename: the filename of FORTRAN program is declared in line number 20. The format is declared as

DATA CENTRY / filename/.

The filename in this demo is “fuzzy”. It is the same file name which is declared in controller section of NETOMAC program.

D.2.3 How to produce an extern.dll file

The FORTRAN program described in section D.2.2 must be translated as an executive filename. The executive filename needs to be named as extern.dll. In order to produce the extern.dll file, the following steps can be executed.

- 1 Using FORTRAN compiler (Salford compiler) to compile this FORTRAN subroutine, then a filename.obj file can be available.
- 2 Executing the slink.exe program included in Salford FORTRAN 95 software and then key in the following command under the slink window.


```
.dll  
.load filename.obj  
.exportall  
.file
```

- 3 A filename.dll will be produced after step 2. Rename this filename.dll file as extern.dll
- 4 Copy this extern.dll file and paste it under the main directory of NETOMAC.

After above-mentioned steps, the NETOMAC program can work together with FORTRAN program.

References

- [1] O. Faucon, L. Dousset, “Coordinated defense plan protects against transient instabilities”, IEEE Computer Applications in Power, Vol. 10, pp. 20-26, 1997.
- [2] R. Parsi-Feraidoonian, Xiang-Lin Sun and M.D. Wvong, “Catastrophe theory model of multimachine power systems for transient stability studies” IEEE TENCON 93’, Beijing, 1993.
- [3] E. Orduna, F. Garces, and E. Handschin, “Algorithmic-knowledge-based adaptive coordination in transmission protection”, IEEE Tran. on Power Delivery, Vol. 18, No. 1, pp. 61-65, January 2003.
- [4] Youyi Wang, D.J. Hill, R.H. Middleton, “Transient stability enhancement and voltage regulation in power systems”, IEEE Tran. on Power Systems, Vol. 8, No. 2, May 1993.
- [5] F. Paulo Toledo, “Power flow control in city center infeed”, IEEE Bologna Power Tech. Conference, June 2003.
- [6] E. Handschin, N. Schnurr, W.H. Wellssow, “Damping potential of FACTS devices in the european power system”, Power Engineering Society General Meeting, IEEE, Vol. 4, 13-17 July 2003.
- [7] R. Adapa,” FACTS system studies”, IEEE Power Engineering Review, Volume 22, pp. 17 – 22, Dec. 2002.
- [8] X.P. Zhang, E. Handschin, “Optimal power flow control by converter based FACTS controller”, IEEE AC-DC Power Transmission 2001, Seventh International Conference, pp. 250-255, 2001.
- [9] A. Edris, “FACTS technology development: an update”, IEEE Power Engineering Review, pp. 4-9, March 2000.
- [10] IEEE Committee Report, “Excitation system models for power system stability studies”, PAS-100, No.2, February 1981.

- [11] IEEE Committee Report, "Computer representation of excitation systems", PAS-87, No. 6, June 1968.
- [12] P.M. Anderson and A.A. Fouad, "Power system and stability", Iowa State University Press, Ames IA, 1977.
- [13] O.P. Malik, G.S. Hope, M.A.L. Badr, "A computer study of a PID automatic voltage regular, part ii: digital PID voltage regulator with dynamically varying weighting parameters", 1982 IEEE PES Summer Meeting, San Francisco, California, 1982.
- [14] V.H. Quitana and M.A. Zohdy and J.H. Anderson, "On the design of output feedback excitations controllers of synchronous machines", IEEE Tran. Power Appar. Syst., PAS-95, pp. 954-961, 1976.
- [15] D. Xia and G.T. Heydt, "Self_tunning controller for generator", IEEE Tran. Power Appar. Syst., PAS-102, pp.1877-1885, 1983.
- [16] A. Mietek and G.J. Kulawsski, "Dynamic neural controllers for induction motor", IEEE Trans. On Neural Network, Vol. 10, No. 2, 1999.
- [17] I. Hassanzadeh, M.B.B. Sharifian, S. Khanmohammadi, R. Kenarangui, "A FLN artificial neural network based fuzzy controller for generator excitation control", Electrical and Computer Engineering, 2000 Canadian Conference on Volume 2, pp. 702 – 706, March 2000.
- [18] Takashi Hiyama, Koushi Miyazaki and Hironori Satoh, "A fuzzy logic excitation system for stability enhancement of power systems with Multi-Mode oscillations", IEEE Tran. on Energy Conversion, pp. 449-454, 1996.
- [19] L.X. Wang, "Adaptive fuzzy systems and control: design and stability analysis", Prentice-Hall, NJ, 1994.
- [20] T. Fukuda and T. Shibata, "Theory and applications of neural networks for industrial control systems", IEEE Trans. Ind. Electron., Vol. 39, No. 6, pp. 472-491, 1992.

- [21] P.S. Sastry, G. Santharam and K.P. Unnikrishnan, "Memory neuron networks for identification and control of dynamical systems", IEEE Trans. Neural Networks, Vol. 5, No. 2, pp. 306-319, 1994.
- [22] C.C. Ku and K.Y. Lee, "Diagonal recurrent networks for dynamic systems control," IEEE Trans. Neural Networks, Vol. 6, No. 1, pp. 144-156, 1995.
- [23] F.P. Demello and C. Concordia, "Concepts of synchronous machine stability as affected by excitation control", IEEE Tran. Power Appar. Syst., PAS-38, pp. 316-329, 1969.
- [24] M.S. ghazizadeh and F.M. Hughes, "A generator transfer function regulator for improved excitation control", IEEE Tran. on Power Systems, Vol. 13, No. 2, May 1998.
- [25] G.K.I. Mann, B.G. Hu, R.G. Gosine, "Time-domain based design and analysis of new PID tuning rules", Control Theory and Applications, IEE Proceedings, Vol. 148, pp. 251 – 261, May 2001.
- [26] R. Aguilar, A. Poznyak, R. Martinez-Guerra, R. Maya-Yescas, "Temperature control in catalytic cracking reactors via a robust PID controller", Journal Process Control 12, pp. 695-705, 2002.
- [27] J.G. Ziegler and N.B. Nichols, "Optimal setting for automatic controllers", Trans. ASME, Vol. 64, pp. 759-768, 1942.
- [28] M. Zhung, and D.P. Atherton, "Automatic tuning of optimum PID controllers", IEE Proc., Control Theory Appl., pp. 67-69, 1993.
- [29] K.J. Astrom and T. Hagglund, "Automatic tuning of simple regulators with specifications on phase and amplitude ratios", Automatica, Vol. 20, pp. 645-651, 1988.
- [30] Y.Y. Hsu and C.J. Wu, "Adaptive control of asynchronous machine using the auto_searching method", IEEE Tran. Power Appar. Syst., PWRS_3, pp. 1434-1440, 1988.

- [31] Y.Y. Hsu and C.H. Cheng, "Variable structure and adaptive controller of a synchronous generator", IEEE Trans. Aerosp. Electro, Syst., AES-24, pp. 337-345, 1989.
- [32] A.S. Abraham, B.W. Hogg, M.M. Sharaf, "Self-tuning automatic voltage regulators for a synchronous generator", IEE Proceedings, Vol. 136, No. 5, Sep. 1989.
- [33] C.L. Brasca, M.A. Johnson, "On automatic voltage regulator design for synchronous generators", Control Application Proceedings of the Third IEEE Conference on 24-26 Aug., 1994.
- [34] Ching-Tzong Su, Hong-Rong Hwung and Guor-Rung Li, "Fuzzy logic based voltage control for a synchronous generator", Electric Power Systems Research 41, pp. 225-231, 1997.
- [35] E. Handschin, W. Hoffmann, F. Reyer, Th. Stephanblome, U. Schlueking, D. Westermann and S.S. Ahmed, "A new method of excitation control based on fuzzy set theory", IEEE Tran. On Power System, Vol. 9. No. 1, 1994.
- [36] Faa_Jeng Lin and Chin Chong Lin, "Online gain-tuning IP Controller using RFNN", IEEE Tran. On Aeros. and Elec. Syst. Vol. 37, No. 2, April 2001.
- [37] A. Haririr and O.P. Malik, "A fuzzy logic based power system stabilizer with learning ability", IEEE Tran. on Energy Conversion, pp. 722-727, 1996.
- [38] H. Bissig, K. Reichert, and S. Kulig, "Modeling and identification of synchronous machines, a new approach with an extended frequency range", IEEE Tran. on Energy Conversion, 270, 1993.
- [39] R.H. Park, "Two reaction theory of synchronous machine", Pt. 1 AIEE Tran. 48, pp. 716-730, 1929.
- [40] R.H. Park, "Two reaction theory of synchronous machine". Pt. 2 AIEE Tran. 52, pp. 352-355, 1933.
- [41] IEEE trial use standard procedures for obtaining synchronous machine parameters by standstill frequency response testing. IEEE Std. 115A, 1984.

- [42] N. Ataei, "Simulation of brushless exciter model for a three-machine-system", Proceeding of the IASTED International Conference, Power and Energy Systems, February 2003.
- [43] R.W. Ferguson, H. Herbst, and R.W. Miller, "Analytical studies of brushless excitation system", AIEE Tran. of Power Apparatus and Systems (part III), Vol. 79, pp. 1815-1821, Feb. 1960.
- [44] R.L. Witzke, J.V. Kressner, and J.K. Dillard, "Influence of AC reactance on voltage regulation of six-phase rectifiers", AIEE Transactions, Vol. 27, pp. 244-253, July 1953.
- [45] A. Kandel, "Fuzzy expert systems", Reading, MA: Addison-Wesley, 1988.
- [46] T. Takagi and M. Sugeno, "Fuzzy identification of system and its application to modeling and control", IEEE Trans. Syst., Man, Cybern, Vol. 15, pp. 116-132, 1985.
- [47] M. Sugeno, "Industrial applications of fuzzy control", New York: Elsevier, 1985.
- [48] B. Widrow and R. Winter, "Neural nets for adaptive filtering and adaptive pattern recognition", IEEE Computer, pp. 25-39, Mar. 1988.
- [49] Y.Y. Hsu, C.R. Chen, "Tuning of power system stabilizing using an artificial neural network", IEEE Trans. on Energy Conversion, Vol. 6, No. 4, pp. 612-619, Dec. 1991.
- [50] Q.I. Wu, B.W. Hogg, G.W. Irwin, "A neural network regular for turbogenerators", IEEE Trans. on Neural Networks", Vol. 3 No. 1, pp. 95-100, Jan. 1992.
- [51] Y. Zhang, O.P. Malik, G.P. Chen, "Artificial neural network power system stabilizer in multi-machine power system environment", IEEE Trans. on Energy Conversion, Vol. 10, No. 1, pp. 147-155, March. 1995.

- [52] K. M. Hornik, M. Stinchcombe and H. White, "Multilayer feedforward networks are universal approximators", *Neural Networks*, Vol. 2, no. 5, pp. 359-366, 1989.
- [53] C.C. Lee, "Fuzzy logic in control systems: fuzzy logic controller-part I and part II," *IEEE Trans. Sys. Man Cybern.*, Vol. 20, No. 2, pp. 404-436, 1990.
- [54] R.R. Yager and D.P. Filev, "Essentials of fuzzy modeling and control", John Willy & Sons, NY, 1994.
- [55] S. Horikawa, T. Furuhashi and Y. Uchikawa, "On fuzzy modeling using fuzzy neural networks with the backpropagation algorithm," *IEEE Trans. Neural Networks*, Vol. 3, No. 5, pp. 801-806, 1992.
- [56] Y.C. Chen and C.C. Teng, "A model reference control structure using a fuzzy neural network," *Fuzzy Sets and Syst.*, Vol. 73, pp. 291-312, 1995.
- [57] T.S.R. Jang and C.T. Sun, "Neural-fuzzy modeling and control," *Proc. IEEE*, Vol. 83, No. 3, pp. 378-405, 1995.
- [58] F.J. Lin, R.F. Fung, and R.J. Wai, "Comparison of sliding mode and fuzzy neural network control for motor-toggle servomechanism," *IEEE/ASME Tran. Mechatronics*, Vol. 3, No. 4, pp. 302-318, 1998.
- [59] F.J. Lin, W.J. Huang, and R.J. Wai, "A supervisory FNN control system for tracking periodic inputs.", *IEEE Tran. Fuzzy Syst.*, Vol. 7, No. 1, pp. 41-52, 1999.
- [60] F.J. Lin, R.J. Wai and C.C. Lee, "Fuzzy neural network position controller for ultrasonic motor drive using push-pull DC-DC converter," *IEE Proc. Control Theory Appl.*, Vol. 146, No. 1, pp. 99-107, 1999.
- [61] R.B. Chedid, S.H. Karaki and El-Chamali, "Adaptive fuzzy control for wind-diesel weak power systems", *IEEE Tran. on Energy Conversion*, Vol. 15, No. 1, March 2000.
- [62] F. Rosenblatt, "The perceptron: A probabilistic model for information storage and organization in the brain", *Psychological Review*, Vol. 65, pp. 386-408,

1958.

- [63] J. Li, A. N. Michel, and W. Porod, "Analysis and synthesis of a class of neural networks: linear systems operating on a closed hypercube", IEEE Tran. On Circuits and Systems, Vol. 36, no. 11, pp. 1405-1422, 1989.
- [64] P. J. Werbos, "Beyond regression: New tools for prediction and analysis in the behavioral sciences", PH. D. Thesis, Harvard University, Cambridge, MA, 1974.
- [65] D. E. Rumelhart and J. L. McClelland , eds., "Parallel distributed processing: Explorations in the microstructure of cognitions", Vol. 1, Cambridge, MA: MIT Press, 1986.
- [66] K. Hirota, Michio Sugeno, "Industrial applications of fuzzy technology in the world", published by world scientific in 1995.

AUTHOR:

NAME : MING-KUAN LIN
DATE OF BIRTH : 10,10,1957
PLACE OF BIRTH : TAIWAN

EDUCATION:

DATE	DEGREE	SUBJECT
1984-1987	MASTER OF SCIENCE IN FENG-CHIA UNIVERSITY	AUTOMATIC CONTROL ENGINEERING
1976-1980	BACHELOR OF SCIENCE IN FENG-CHIA UNIVERSITY	AUTOMATIC CONTROL ENGINEERING

OCCUPATION:

DATE	DUTY	COOPERATION
1987-1999	INSTRUCTOR IN ELECTRIC ENGINEERING	NATIONAL LIEN-HO COLLEGE OF TECHNOLOGY AND COMMERCE
2004-2005	INSTRUCTOR IN ELECTRIC ENGINEERING	NATIONAL UNITED UNIVERSITY

PROFESSIONAL TRAINING AND EXPERIENCE

1998	GRANT:CO-INVESTIGATOR FOR STUDIES OF HARDWARE SIMULATION : PROCESS CONTROL ON THE BASIS OF DSP
1993	INDUSTRIAL INSTRUMENT TRAINING COURSE: SPONSORED BY LIEN-HO COLLEGE OF TECHNOLOGY
1992	INDUSTRIAL INSTRUMENT TRAINING COURSE: SPONSORED BY LIEN-HO COLLEGE OF TECHNOLOGY
1991	COOPERATOR FOR DEVELOPING “SPECIAL PROCEDURES OF LATEX GLOVE QUALITY CONTROL
1990	LECTURER FOR EMPLOYEES OF COMPANY :BASIC COMPUTER LANGUAGE
1987	COURSE IN LASER TECHNIQUE: SPONSORED BY NATIONAL CENTRAL UNIVERSITY IN TAIWAN

TEACHING EXPERIENCE

1	DESIGN OF DIGITAL SYSTEM
2	MICROCOMPUTER SYSTEM DESIGN
3	INDUSTRIAL INSTRUMENT (INCLUDING EXPERIENCE)
4	CONCEPT OF DIGIAL PROCESS CONTROL
5	INDUSTRIAL ELECTRONIS
6	PNEUMATIC ENGINEERING
7	FUNDAMENTAL OF ELECTRICAL MACHINERY

PUBLICATIONS

1	BOOKS: INTRODUCTION OF LASER TECHNIQUE: LIN, M.K., CHANG, F.C. PUBLICHER: PAN EAST PUBLISHING HOUSE
2	ESTIMATION OF UNKNOWN TARGETS BY KARMAN FILTER. ANNUAL RESEARCH REPORT. 1987 . LIEN-HO COLLEGE OF TECHNOLOGY AND COMMERCE